1. INTRODUCTION

1.1 Background

The Las Vegas Valley is located within Clark County in the southern part of Nevada. The area of the valley is nearly 4000 km^2 and includes the cities of Las Vegas, North Las Vegas, and Henderson, as well as several unincorporated towns. Geographically, the Las Vegas Valley lies in the southwestern part of the Great Basin; extends in a northwest to southeast direction, draining toward the south through the Las Vegas Wash into Lake Mead; and ranges in elevation from 550 to 760 meters above mean sea level (m amsl). It is surrounded by sharp, rugged mountains with elevations up to 3,600 m amsl. The valley is bounded on the northeast by the Nellis Air Force Base Ground Gunnery Range, on the west by the Spring Mountains, on the south by the McCullough Mountains and Spring Mountains, and on the east by the River Mountains and Frenchman Mountain.

Clark County is the fastest-growing county in the nation with a population of ~ 1.5 million supported by an ever increasing network of roadways and vehicle traffic. Major industries of tourism, gaming, government/defense, chemical manufacturing, quarry operations, and construction are low polluting except for their encouragement of greater driving distances between home and work. Previous studies (Chow and Watson, 1997, Chow et al., 1999, Green et al., 2002) have shown large contributions from roadway related pollutants such as vehicle exhaust and road dust to excessive levels of PM_{10}, $PM_{2.5}$ (particles with aerodynamic diameters <10 and <2.5 μm in aerodynamic diameter, respectively), and urban haze. Potentially excessive ozone (O_3) concentrations have been measured at some air quality monitors in the Las Vegas Valley during summer. Wintertime hot spots for carbon monoxide (CO) still exist at certain locations.

Vehicle exhaust is the major source of CO in the Las Vegas Valley, and it is also a large emitter of nitrogen oxides (NO), hydrocarbons (HC), and suspended particulate matter (PM). NO and HC react in the atmosphere to form O_3. These same photochemical reactions also produce secondary PM in the form of nitrates, sulfates, and organic compounds. Accurate and representative emissions rates of these pollutants from on-road vehicle operation are essential to the development of emissions reduction strategies and air quality maintenance plans that will reduce ambient pollutant concentrations in the Las Vegas Valley.

Emissions are currently estimated using generic emissions models supplied by the U.S. Environmental Protection Agency (EPA). EPA's MOBILE6 model estimates on-road fleet-average emission rates for CO, HC and NO while the PART5 model provides PM emissions estimates. These models use empirically-derived data from vehicle types, fuels, and operating conditions that do not necessarily represent conditions in the Las Vegas Valley. Their results need to be verified against real-world, on-road emissions that are specific to the area.

On-road emissions require fast response instruments that can extract a portion of the exhaust plume for real-time analysis near the road side, or that can quantify integrated concentrations of a pollutant by remote sensing across the plume. Remote sensors use the attenuation of light over small wavelength intervals that correspond to CO, NO, HC, and carbon dioxide (CO_2) absorption bands. Light absorption is related to gas concentration by calibration with known gas concentrations in absorption cells. Ratios of each pollutant concentration to total gaseous carbon (i.e. CO_2, CO, and HC) in excess of background levels in the plume

provides a relationship to the amount of carbon consumed in fuel combustion. With appropriate accounting for the carbon in the gasoline or diesel fuel, these ratios can be related to the amount of pollutant emitted per unit of fuel consumed. Using reasonable estimates of vehicle fuel economy (i.e. miles per gallon), emissions can also be related to vehicle miles traveled (VMT). Light absorption instrumentation can also measure directly emitted particles, but only if these contain a large fraction of black carbon (BC) and are sufficiently dense as to be visible to the naked eye. Most modern vehicles do not have visible PM emissions under normal operating conditions, even though they may have widely varying PM emission rates. A new approach that measures the light scattered from particles in a backwards direction is more sensitive to PM emissions than the path length absorption measurements.

1.2 Goals and Objectives

The goal of this project is to measure and interpret on-road vehicle exhaust emissions for CO, NO, HC, and PM that are specific to the Las Vegas area and that represent a larger fraction of the vehicle fleet than has been evaluated in previous tests. Specific study objectives are:

- Develop emissions distributions for light and heavy duty gasoline and light and heavy duty diesel vehicles.
- Independently evaluate fleet average emissions factors derived from generic EPA emissions models.
- Evaluate on-road exhaust sensing methods for potential use in clean screen and supplemental inspection and maintenance programs.
- Define additional on-road tests and emissions model sensitivity studies that will improve vehicle exhaust emissions inventories for the Las Vegas Valley.

1.3 Guide to Report

This introduction has defined the problem and specified the study goals and objectives. Section 2 describes the measurement approach, including the instrumentation used, the sampling locations, the exhaust measurement conditions, and data acquisition. Although on-road measurement systems for gases have been used to evaluate emissions inventories and determine compliance in other states, this report represents the first application of the LIDAR-based backscatter measurements of PM. A more detailed description of this system, its limitations, and its results is given in Section 2. Section 3 describes the data base of emissions and linkages with vehicle-specific data obtained by joining Department of Motor Vehicle (DMV) registration information with each test via the vehicle license plate. Data validation criteria and flags are defined, as are the algorithms used to estimate concentration ratios to excess CO_2 and to convert between fuel consumption and vehicle miles traveled. Section 4 evaluates the precision, accuracy, and detection limits for CO, NO, HC, and PM emissions from more than 60,000 vehicles tested at different times and locations in the Las Vegas Valley. Section 5 analyzes the test data with respect to attaining the above-stated objectives. Section 6 summarizes the conclusions and formulates recommendations based on the results of this project.

2. EXPERIMENTAL SETUP

This section describes siting considerations associated with vehicle emissions remote sensing and the commercial exhaust gas measurement systems used during this study. The theory and operation of the LIDAR particle measurement system developed at DRI is also presented here.

2.1 Instrument Siting

Remote sensing of vehicle emissions is optimally efficient for a single lane of traffic, 5-7 meters wide, on dry pavement. Rain, snow, and vehicle spray from very wet pavement cause interference with the optical beams, ultimately to the point that data are rejected as being contaminated by too much noise. At suitable locations, exhaust can be monitored from over one thousand vehicles per hour. Experience indicates that cars should be under light to moderate load, traveling approximately 25 - 60 kph with sufficient spacing in-between to minimize exhaust plume overlap. The wake of vehicles traveling faster than 80 kph rapidly dissipates the exhaust plume, causing many measurements to fall below detectable limits. Vehicles under load burn more fuel and in turn emit a more concentrated plume that is easier to measure. An uphill slope is a good attribute for a remote sensing site since vehicles must be under load to maintain their speed in the test section. Adequate shoulder space is also an essential attribute for safety and to minimize interference with traffic flow in the lane.

Remote sensing locations were selected at multiple sites in the Las Vegas Valley to maximize the number of vehicles tested and to collect a sample set of vehicles representative of the on-road fleet in Clark County, NV. To achieve these objectives, freeway onramps were chosen as the principle group of sampling sites. The onramps selected typically had an average daily travel (ADT) of 5,000 to 15,000 vehicles per lane under moderate load. The Gowan site between Rancho and Decatur (GOWAN) is a collector street and was selected to measure vehicles on surface streets. The number of vehicles sampled at this location was quite small (<700 in 5 hours). After evaluating the data collected at that location, it was decided that freeway onramps were the most productive locations based on traffic density.

Placement of the remote sensing equipment on the onramp proved to be an important factor in the fraction of valid measurements collected at the site. Most drivers exercise caution and reduce speed when traveling through the remote sensing test section. Only when drivers can see that they are not required to stop do they accelerate to merge on the freeway. If the remote sensing equipment is placed too close to the beginning of the on ramp, drivers will coast through the section and accelerate after the test section. If the test section is placed too close to the freeway merge area, drivers may already have accelerated to merging speed prior to the measurement area.

All sites were visually surveyed prior to testing to select optimal placement of the equipment on the on ramp. Once the site was determined to meet the criteria mentioned above, DRI requested temporary occupancy permits from either the Traffic Management Division of the Clark County Department of Public Works or the Nevada Department of Transportation. Traffic control plans were assembled for each sampling site and submitted to the appropriate agency for review. These plans are included in Appendix A of this report. Sampling took place once the permits had been granted.

Table 2-1 lists the locations of each of the remote sampling sites. A map of these sites is shown in Figure 2-1. The table shows the number of vehicles measured at each site on each day as well as the number of vehicles with sufficient plume to measure CO_2 (a requirement for measuring fuel based emissions factors). Sites with road slopes greater than 2 degrees had CO_2 validity rates in the range of 73% to 87% in contrast to sites with road slopes less than or equal to 0 degrees that had CO_2 validity rates of 41% to 49%.

Table 2-1. List of DRI vehicle remote sensing locations for the period 04/04/00 to 05/16/02.

Date	*SiteID*	*Site Description*	*Latitude (deg)*	*Longitude (deg)*	*Number of Vehicles*	*Fraction of Vehicles with Valid CO_2*	*Road Slope (deg)*	*Average Measured Speed (kph)*	*Average Measured Accel. (kph/s)*
04/04/00	SUNS515	Sunset onramp to I-15 westbound	36.0660	-115.0313	7165	90%	1.2	51	1.5
04/05/00	MEADI15	Lake Mead Blvd onramp to I-15 southbound	36.1969	-115.1390	5200	87%	2.7	49	0.3
04/06/00	CHRL515	Charleston to I-515 westbound	36.1617	-115.0917	1263	67%	0.4	68	0.6
04/17/00	CHRL515	Charleston to I-515 westbound	36.1617	-115.0917	656	58%	0.4	70	0.9
04/19/00	CHRL515	Charleston to I-515 westbound	36.1617	-115.0917	7848	57%	0.4	70	0.9
04/20/00	SUNS515	Sunset onramp to I-15 westbound	36.0660	-115.0313	6155	82%	1.2	56	1.8
04/21/00	CHRL515	Charleston to I-515 westbound	36.1617	-115.0917	6322	57%	0.4	71	1.0
07/18/00	MEADI15	Leak Mead Blvd onramp to I-15 southbound	36.1969	-115.1390	3520	77%	2.7	52	0.1
07/19/00	CHRL515	Charleston to I-515 westbound	36.1617	-115.0917	5599	53%	0.4	71	0.9
07/20/00	CHRL515	Charleston to I-515 westbound	36.1617	-115.0917	7250	45%	0.4	70	1.0
07/21/00	MEADI15	Lake Mead Blvd onramp to I-15 southbound	36.1969	-115.1390	6175	78%	2.7	50	0.3
07/24/00	MEAD515	Lake Mead Drive onramp to I-515 northbound	36.0358	-115.0157	5602	51%	0.4	67	0.8
07/25/00	MEAD515	Lake Mead Drive onramp to I-515 northbound	36.0358	-115.0157	7097	44%	0.4	72	0.5
08/17/01	GOWAN	Gowan westbound between Decatur and Rancho	36.2252	-115.2092	559	83%	0.7	46	0.9
08/21/01	MEADI15	Lake Mead Blvd onramp to I-15 southbound	36.1969	-115.1390	5544	74%	3.3	44	0.2
08/22/01	MEADI15	Lake Mead Blvd onramp to I-15 southbound	36.1969	-115.1390	6428	77%	3.3	46	0.2
08/23/01	EASTERN	Eastern onramp to US-95 westbound	36.1684	-115.1172	9413	74%	2.2	49	0.7
08/24/01	EASTERN	Eastern onramp to US-95 westbound	36.1684	-115.1172	6027	73%	2.2	51	0.5
04/29/02	GVI215	Green Valley onramp to I-215 westbound	36.0243	-115.0860	2893	48%	0.0	69	0.9
04/30/02	GVI215	Green Valley onramp to I-215 westbound	36.0243	-115.0860	6123	49%	0.0	67	1.2
05/03/02	SUMMRAM	Rampart onramp to Summerlin Pkwy eastbound	36.1776	-115.2868	10073	41%	-0.7	71	1.4
05/08/02	EASTERN	Eastern onramp to US-95 westbound	36.1684	-115.1172	13134	73%	2.2	50	0.8
05/14/02	CRAIG95	Craig onramp to US-95 southbound	36.2392	-115.2487	9137	41%	0.2	65	0.5
05/16/02	CRAIGI15	Craig eastbound onramp to I-15 southbound	36.2395	-115.1045	9064	47%	0.0	71	0.9

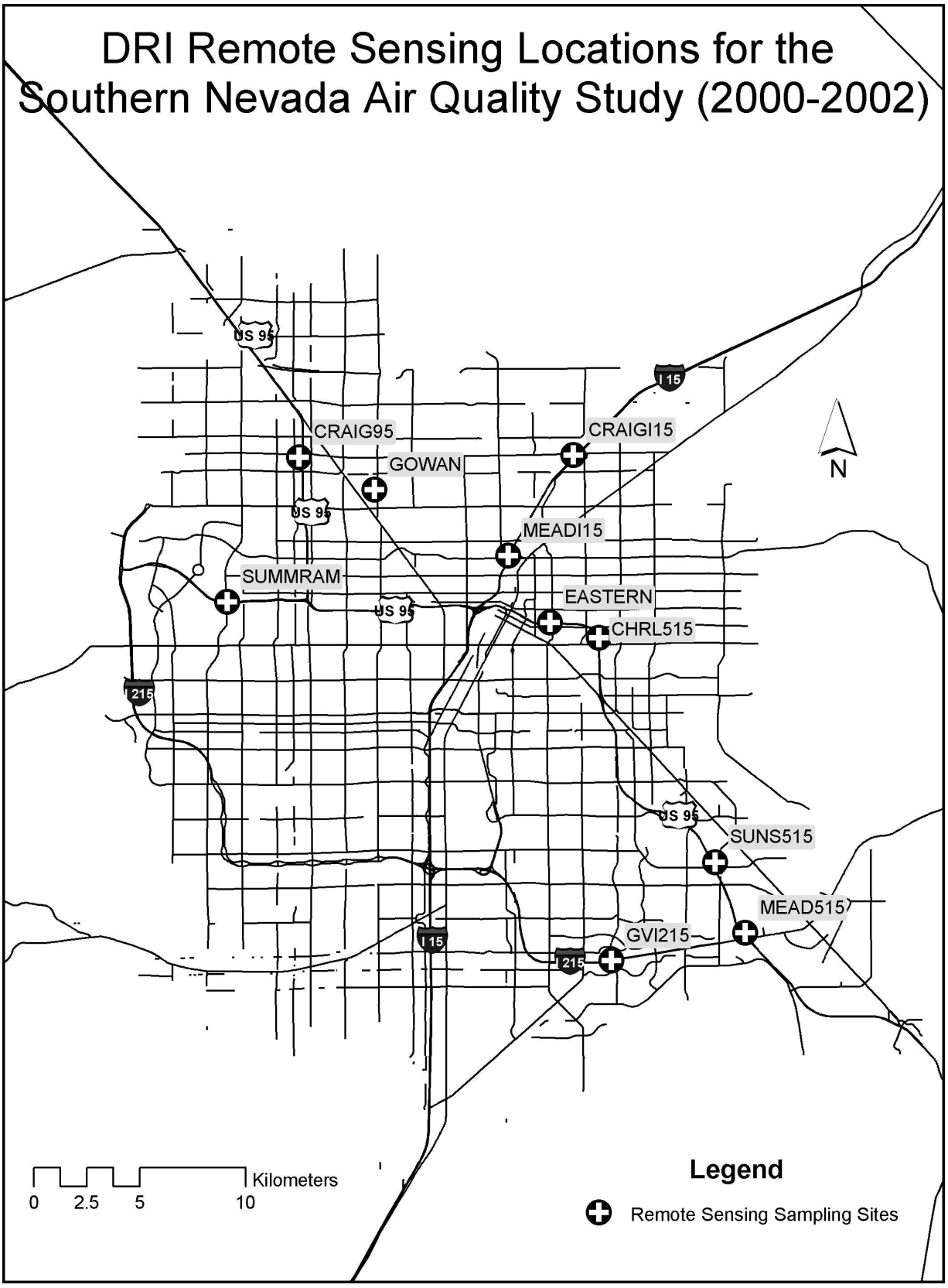

Figure 2-1. Map of DRI's remote sensing location in the Las Vegas Valley (04/04/00 to 05/16/02).

2.2 RSD

In 1987, the University of Denver (DU) developed an infra-red remote monitoring system for automobile carbon monoxide (CO) exhaust emissions, called a remote sensing device (RSD). A hydrocarbon (HC) channel was soon added. Significant improvements in fuel economy result if rich-burning (high CO emissions) or misfiring (high HC emissions) vehicles are tuned to a more stoichiometric and more efficient air/fuel (A/F) ratio. Therefore, the University of Denver remote sensor was named Fuel Efficiency Automobile Test (FEAT). In 1991, Sun Electric was licensed to develop the FEAT patent into an off-the-shelf commercial product. In 1993, EnviroTest bought Sun Electric, and the patent was licensed to Remote Sensing Technologies, Inc., a subsidiary of EnviroTest. Finally, in 1998, Environmental Systems Products, Inc. (ESPi) bought EnviroTest. The current ESPi instrument, the RSD3000, measures CO, HC, CO_2, and NO. NO is not presently monitored in the Nevada Emissions Inspection Program.

Because of remote sensing, the highly skewed gamma-distribution of vehicle emissions is better understood (Zhang et al. 1994). Relatively few vehicles, called high-emitters, account for a disproportionately large amount of the fleet emissions. Remote sensing has been used in numerous studies to identify these high emitters (e.g., Lawson et al. 1990; Stephans et al. 1994; Lawson et al. 1996; Cadle et al. 1997; McClintock 1999). In a report prepared by the California Inspection and Maintenance Review Committee (Schwartz 1998), remote sensing errors of omission (false pass) and errors of commission (false fail) are reported to be on the order of a few percent. This is an acceptable level since most of these cars are found to be marginal emitters anyway, i.e., cars with emissions near (just above or just below) the pass/fail cut-points for HC and CO. For example, remote sensing readings were used in California to immediately pull over apparently gross polluting vehicles. A team of Smog-Check engineers tested these cars and performed EPA IM240 dynamometer tests (Knapp 1992). Of 79 vehicles tested on IM240, 76 failed and the three which passed had all failed the previous Smog-Check. In a comprehensive high-emitter study in Orange County California, repair costs and emissions reductions were tracked from initial RSD identification through pre- and post-repair dynamometer tests. Lawson et al (1996) found that remote sensing is the most cost effective method of reducing automotive emissions. The fact that a remote sensor can be used to directly measure the on-road tailpipe emissions is also a considerable advantage over other tests, particularly if there are ways that individuals or manufacturers can circumvent other tests, thus rendering those results unrepresentative of the on-road fleet.

2.2.1 Gas Measurement

Automobile exhaust remote sensors, e.g., the RSD3000, emulate the results one would obtain using a conventional non-dispersive infra-red exhaust gas analyzer, such as the NV94 Analyzer used by emissions test stations to conduct State emissions tests. Non-dispersive ultra-violet light is used for the NO channel on the remote sensor. An interference filter is placed in front of a detector to transmit light of a wavelength known to be absorbed by a molecule of interest. Reduction in the detector's voltage output is caused by absorption of light by the molecules of interest. Because the effective plume path length and amount of plume seen depends on turbulence and wind, one can only look at ratios of CO, HC, and NO to CO_2. These ratios are termed Q for CO/CO_2, Q' for HC/CO_2, and Q" for NO/CO_2, and are approximately constant for a given exhaust plume.

These ratios are useful parameters for describing the combustion system. With the aid of a fundamental knowledge of combustion chemistry, many parameters of the vehicle's operating characteristics can be determined including: the instantaneous air/fuel ratio, the %CO, %HC, or %NO which would be read by a tailpipe probe, and the grams CO, HC, or NO emitted per gallon of gasoline (Bishop and Stedman 1996). Since most new gasoline powered vehicles emit little CO or HC, they show a Q and Q' near zero, and often below the detection limit of the remote sensor. To observe a substantially larger Q, the engine must have a fuel-rich air/fuel ratio and the emission control system, if present, must not be fully operational. A high Q' can be associated with either fuel-rich or fuel-lean air/fuel ratios coupled with a missing or malfunctioning emission control system. A lean air/fuel ratio, while impairing driveability, produces very little CO in the engine. If the air/fuel ratio is lean enough to induce misfire then a large amount of unburned fuel (HC) is present in the exhaust manifold. If a catalyst is absent or non-functional, then high HC can be observed in the exhaust without the presence of high CO. To the extent that the exhaust system of this misfiring vehicle contains some residual catalytic activity, the HC may be partially or totally converted to a CO/CO_2 mixture.

The height of the sensing beam is typically set at 20-30 cm above the road surface to observe exhaust plumes from light duty vehicles, provided the exhaust plume exits the vehicle within a few feet of the ground. The remote sensor is accompanied by a video system for vehicle identification information. The video camera is coupled directly into the data analysis computer so that the image of each passing vehicle is displayed on the video screen.

2.2.2 Speed and Acceleration

The speed and acceleration strips provided with the RSD3000 consist of two bars approximately 2 meters in length, placed parallel to the fogline on either side of the lane. One is equipped with two diode lasers at either end, and the other with two photodetectors at either end. These are aligned such that each diode laser hits the corresponding photodetector. As the front and back tires sequentially break the upstream and downstream beams, the speed and acceleration can be computed for the vehicle.

2.2.3 License Plate Picture

DRI has extracted license plate images from each legible video record and appended that information to the remote sensing emissions database. Each complete remote sensing record in the RSD3000 files contains the information for Unit Code (i.e. serial number of RSD3000), Site Code, Date, Time, Vehicle Sequence Number, CO, CO_2, HC, NO, License Plate, Plate Flag, Plate Description, Speed, and Acceleration.

2.3 LIDAR

2.3.1 Theory

The light detection and ranging system (LIDAR) developed by the Desert Research Institute is designed to measure particle mass (PM) in a column defined by the laser beam through an exhaust plume. Simultaneously, an infrared source is used to detect the CO_2 in a similar column through the exhaust plume. The ratio of PM to CO_2 gives a relative measure of the pollution being generated by the vehicle in grams of PM per unit of fuel carbon consumed. This section of the report will focus on the LIDAR measurement of PM.

When light illuminates a small particle such as a pollution particle in an exhaust plume, the light is both scattered in all directions and absorbed by the particle. For a particular incident light beam, the nature of the scattering and absorption interaction is determined by the physical characteristics of the particle – its size, shape, and material characteristics as well as by the size and shape distribution of a suspension of particles. If the characteristics of the incident light are known, specifically its direction of propagation, polarization, wavelength, and intensity, then this knowledge, coupled with the nature of the scattered light and a laboratory calibration, can be used to determine some features of an unknown small particle or size distribution of particles.

The light scattered by a particle or suspension of particles back in the direction of the incident light is known to be particularly sensitive to the physical characteristics of the particle. Analysis of this "backscattered" light to determine particle characteristics is analogous to what is done with radar, whereby microwave radiation is "bounced" back from an unknown airborne target to determine its location. The sensitivity of detection of the backscattered light can be maximized by choosing a light source at a wavelength that is comparable to the size of the particles being measured. Soot in vehicle exhaust generally falls in the size range of 0.05 to 0.5 μm.

In the remote sensing system utilized here, a narrow pulse (nominally 1 ns in duration) at an ultraviolet wavelength of 0.266 μm leaves the transmitting laser at one side of the road and is partially reflected back toward the transmitter by particles in the exhaust plume. The received signal is the output of a photo-multiplier tube (a voltage) vs time. The dimensions of the typical roadside configuration are such that the 1 ns pulse (traveling at the speed of light) interacts with the exhaust plume and the beam termination and is returned in less than 100 ns. For the given pulse repetition frequency of 6.8 KHz, a pulse is transmitted approximately every 150 μs, ensuring that only a single 1 ns transmitted pulse interacts with the exhaust plume at a time. The remote sensing configuration is shown in Figure 2-2.

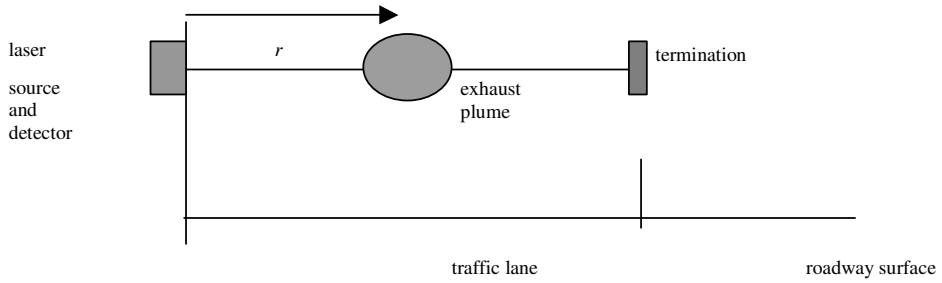

Figure 2-2. LIDAR configuration. The range variable is *r*.

The calculated single-particle differential scattering cross section in the backscatter direction and the single-particle extinction cross section provide the particle information that is required to predict the received power that can be measured by a LIDAR system.

The basic operation of the system is defined by the LIDAR equation,

$$P(r) = P_L O(r) \frac{c\tau}{2} \frac{A}{r^2} \sum_i [N_i(r)\sigma_{d,i}(r,\pi)] e^{-2\sum_i \int_o^r N_i(r')\sigma_{e,i}(r')dr'} \qquad (2\text{-}1)$$

where

$P(r)$ = scattered laser power (Watts) received at the detector at a time corresponding to the leading edge of the laser pulse propagating to a range r, meters.

$O(r)$= characterizes the overlap of the receiving telescope field of view with the UV-laser illuminated particulate path.

P_L = average power (Watts) of the incident laser beam.

c = speed of light, 3×10^8 m/s.

τ = incident pulse width, s.

A = area of receiver telescope aperture, m^2.

$N_i(r)$ = number density of scatterer species i, #/m^3, at range r.

$\sigma_{d,i}(r,\pi)$ = differential scattering cross section of species i in the backscatter (π) direction, m^2/steradian, at range r.

$\sigma_{e,i}(r)$ = extinction cross section of species i, m^2, at range r.

i = an index denoting a particle that has a specific size, shape, and composition. Eq. (2-1) includes a summation over all of the different particles that may be present.

The term $N_i(r)\ \sigma_{d,i}\ (r,\pi)$ in (2-1) quantifies the backscattering from particles of species i. The term $N_i\ (r')\ \sigma_{e,i}(r')$ in the exponent quantifies the extinction from particles of species i, where the factor of 2 accounts for the roundtrip two-way extinction experienced by the LIDAR pulse. Therefore, the initial amplitude of the backscattered pulse diminishes at later times during the two-way attenuation of the pulse by the scattering and absorption (the sum is the extinction) of the intervening particles.

In general, three species i are of interest: (1) the PM in the exhaust plume of the vehicle being measured, (2) the background molecular gases in the atmosphere, and (3) the ambient PM. This latter quantity may include multiple components, such as the background PM from regional sources, PM from vehicles that immediately preceded the vehicle currently being measured, and dust particles raised from the road surface by vehicle motion and roadway tire contact. For purposes of the present analysis, species (2) and (3) will be incorporated in a single ambient term.

This form of the LIDAR equation incorporates a number of assumptions that simplify the analysis. However, none of these assumptions detract from our ability to use (2-1) to understand the factors that determine the received laser power. Some of the assumptions are that the incident laser signal is a rectangular pulse (in time) and monochromatic (single wavelength) and the spatial distribution of PM in the exhaust plume is homogeneous.

The LIDAR equation will be analyzed by first considering the combined effect of the scattering from two species of particulates – PM in an exhaust plume and an ambient background consisting of only atmospheric molecular scattering. Once this situation is illustrated, then it is straightforward to incrementally add additional ambient terms, including background regional PM, PM from preceding vehicles, and dust.

For a homogeneous particulate distribution within the plume, the exponential term in (2-1) can be simplified, since $N(r')$ and $\sigma_e(r')$ are constant with r. For a system consisting of two species of particles, background molecular gases and PM in the exhaust plume, the term in the exponent in (2-1) becomes,

$$-2\{N_a\ \sigma_{e,a}\ r + N_{PM}\ \sigma_{e,PM}\ [r-r_o]\}, \qquad (2\text{-}2)$$

where the quantities with the subscript *m* are associated with molecular gases and variables with the subscript *PM* are associated with the exhaust plume. Then (2-1) becomes

$$P(r) = P_L O(r) \frac{c\tau}{2} \frac{A}{r^2} \sum_i [N_i \sigma_{d,i}(\pi)] e^{-2\{N_a \sigma_{e,a} r + N_{PM} \sigma_{e,PM} [r - r_o]\}}. \quad (2\text{-}3)$$

Here it is important to remember that $\sigma_d(\pi)$ and σ_e associated with the exhaust plume only have value within the plume and are zero when the range variable *r* is not within the plume.

It is useful to consider the special case when the quantity in (2-2) can be approximated as zero. This assumes that the extinction by both the ambient particles and the PM in the exhaust plume are negligible. The extinction by molecular gases (the first term) over the limited range of the system will be quite small. In the case of the exhaust plume (the second term), this would be small when the product $N_{PM}\,\sigma_{e,PM}$ is small, either because the particle density N_{PM} in the plume is low or the particles in the plume have low extinction coefficients, or the thickness of the plume is small, or some combination of all three factors. When the quantity in (2-2) is negligibly small, $e^o = 1$ and (2-3) becomes

$$P(r) = P_L O(r) \frac{c\tau}{2} \frac{A}{r^2} \sum_i [N_i(r) \sigma_{d,i}(\pi)]. \quad (2\text{-}4)$$

Except for the $O(r)$ and $1/r^2$ terms, the term preceding the summation is a system constant that can be represented by C_o. Making this substitution and expanding the summation in (4) gives,

$$P(r) = \frac{C_o O(r)}{r^2} [N_a \sigma_{d,a}(\pi) + N_{PM} \sigma_{d,PM}(\pi)]. \quad (2\text{-}5)$$

The first term in brackets, the backscatter from molecular gases, includes no range dependence – it exists across the entire range. The second term, as mentioned earlier, is zero outside the plume and has value only when the range variable *r* is within the plume. Both terms decrease as $1/r^2$ with range *r*.

Eq. (2-5) also describes the temporal behavior since $r = ct/2$. If the leading edge of the laser pulse leaves the source at time $t = 0$, then the scattered power is received at the detector as some later time $t = 2\,r/c$, where the factor of 2 accounts for the round trip transit time. Scattered power from the exhaust plume is only received when the pulse overlaps the plume. There are three distinct regions of overlap – when the pulse is entering the plume, when the pulse is entirely within the plume, and when the pulse is exiting the plume.

As an example, consider an arrangement where the total path length is 11 m with a 1 m thick exhaust plume located at the center. The first signal to arrive back at the receiver is from the leading edge of the incident pulse entering the exhaust plume at a distance of 5 m. This occurs when $t = (2)(5\text{ m})/3 \times 10^8$ m/s = 33.3 ns. Scattered power from the pulse interaction with the leading edge of the plume will continue to be received until the trailing edge of the pulse is at 5 m, which occurs 1 ns later, so the last signal from the leading edge of the exhaust plume arrives at 34.3 ns. The last signal from the exhaust plume arrives at the receiver when the trailing edge of the pulse is leaving the trailing edge of the plume at a distance of 6 m. The leading edge of the pulse is at 6 m when $t = (2)(6\text{ m})/3 \times 10^8 = 40$ ns. Signal will continue to be received until the trailing edge of the pulse is at 6 m, which occurs 1 ns later, so the last signal from the trailing

edge of the exhaust plume arrives at 41 ns. The reflected signal from the beam termination is received when $t = (2)(11\text{ m})/3 \times 10^8 = 73.3$ ns. The duration of the beam termination signal is 1 ns.

The received LIDAR power for the two-species system defined by (2-5), background molecular gases and exhaust PM, is qualitatively described, for this example, by Figure 2-3.

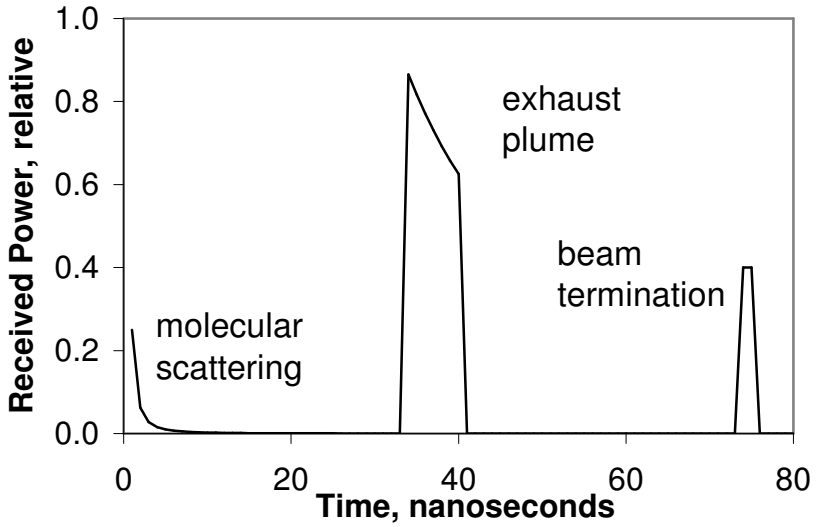

Figure 2-3. LIDAR signal for a 1 ns pulse transmitted at $t = 0$.

Note that the received power from the exhaust plume increases between 33.3 and 34.3 ns as the incident 1 ns pulse enters the plume, decreases as $1/r^2$ as the pulse transits the plume, and then decreases between 40 and 41 ns as the incident 1 ns pulse exits the plume. The received power from the background molecular scattering is only observable at early times, when the transmitted pulse is close to the source. At later times the molecular scattering is significantly reduced by the $1/r^2$ term in (2-5). The returned power from the beam termination has been given an arbitrary amplitude for purposes of this example.

This has been a qualitative example. A quantitative simulation of the LIDAR process defined by (2-5) requires specific knowledge of the exhaust PM and its scattering and extinction characteristics.

For vehicle (gasoline and diesel) exhaust, it is necessary to determine the physical characteristics of the particles contained within the plumes, i.e., their size, shape and index of refraction (related to composition), so that the quantities $\sigma_d(\pi)$ and σ_e may be approximated or calculated, thereby enabling backscattering and extinction calculations. This information requires some knowledge of the form in which elemental carbon and organic carbon are present in the particulate distributions as separate particles, homogeneous spherical mixtures, agglomerations, or in layered configurations. In addition to the characteristics of individual particles, we need to know the particle size and shape distributions that may be expected for vehicle exhaust. A number of studies have considered the above factors.

2.3.1.1 Vehicle Exhaust Characteristics

Horvath, (1993) focuses on the properties of black carbon and its (exclusive) role in absorption in the atmosphere. He indicates that for atmospheric particles, only elemental carbon, the main constituent of black carbon, is highly absorbing. His Table 1 summarizes 15 refractive indices that have been used for elemental carbon. Real parts of the refractive index vary from 1.5 to 2.0 and imaginary parts vary from 0.1 to 1.0. He indicates that light-absorbing particles are only formed by combustion processes, where the majority are of anthropogenic origin. Incomplete oxidation of the carbon-containing fuel causes the formation of black carbon. Major sources of elemental carbon in the atmosphere are diesel motors and small furnaces, as well as biomass burning. For vehicles, black carbon emissions from pre-1992 diesel engines are about 100 times those of a hot stabilized gasoline engine for an equivalent driving distance. A specific example for a particular pre-1992 diesel engine shows that the emitted particulates can contain both elemental and organic carbon, with the fraction of each varying from 10% to 90% depending upon the quality and the operating conditions of the engine.

Völger et al. (1996) give a table of refractive indices of aerosol components at different wavelengths. Specifically, the refractive index of soot at wavelengths of 250 nm and 300 nm, is given as 1.62- i0.45 and 1.74-i0.47, respectively.

Kittelson, (1998) indicates that particulate mass emissions from pre-1992 heavy duty diesel engines typically are 10-100 times higher than those from spark ignition engines. The structure of unaged diesel exhaust particles is shown in his Fig. 1 as agglomerated solid carbonaceous material, ash, and volatile organic and sulfur compounds. His Fig. 3 shows a typical engine exhaust size distribution, for both mass and number weighting. Most of the particle mass exists in the 0.1-0.3 μm diameter range. This is where the carbonaceous agglomerates and associated adsorbed materials reside. The nuclei mode typically consists of particles in the 0.005-0.05 μm diameter range. This mode usually consists of volatile organic and sulfur compounds that form during exhaust dilution and cooling, and may also contain solid carbon and metal compounds. His Figs. 10 and 11 show number-weighted size distributions for two specific diesel engines.

Martins et al. (1998) use a layered-sphere configuration to model biomass burning particles. The model consists of a highly-absorbing black-carbon core surrounded by a much lower absorbing shell. They indicate that this low-absorbing shell is likely formed by gas-to-particle conversion and condensation of volatile compounds. At a wavelength of 0.55 μm, the refractive index of the black carbon is assumed to be 2.0-i1.0 and that of the low-absorbing shell is assumed to be $1.5 - i10^{-6}$.

Shi et al. (2000) have determined the physical properties (size distribution, number, volume, mass concentrations, and density), chemical properties (organic and elemental carbon, PAH, sulfate, and nitrate), and morphology of particles of a particular diesel engine. They found wide variations in particle size distributions and number concentrations depending upon dilution conditions and humidity. They found that combustion particles are largely present in the form of clusters. Large particles were found to be clusters of small basic particles that ranged from 10 to 40 nm. Their measurements provide some confirmation that emitted particles consist of a nonvolatile core covered by a volatile liquid material.

Bessagnet and Rosset (2001) focus on the plume emitted by diesel vehicles. They indicate that recent studies have shown that particles exist as aggregates of carbon spherules

displaying linear to quasi-spherical structures. Fresh combustion particles, presumably elemental carbon spheres, each about 20-30 nm in diameter, are emitted together with sulfuric acid, water vapor and a number of other species, including volatile organic species, at vehicle exhaust pipes. These nucleate, condense and are absorbed on the carbonaceous particles. Their Fig. 1 is a schematic drawing that depicts the evolutionary processes that occur immediately at the exit of the vehicle exhaust system. They indicate that emissions from vehicle exhaust occur under different meteorological conditions that can influence the composition of the plume. This pertains particularly to humidity. Furthermore, the makeup of the emission depends strongly upon vehicle type and operating conditions. One example shows that the mass fraction of dry aerosol emitted in the exhaust of a diesel vehicle is 15.8% elemental carbon and 83.7% organic carbon, with much smaller percentages of other components. The size distribution of particles has been simulated in the immediate area of the exhaust pipe. A nucleation burst occurs at the exit of the exhaust pipe and intense coagulation follows, such that in only a few meters a bimodal particle spectra with peaks at 5 and 60 nm occurs (their Fig. 3a).

The selection of particulate models to use in the mathematical simulation of the LIDAR interaction with vehicle exhaust involves a tradeoff. The particulate systems are so complex and variable that it is unlikely that exact particle models can be formulated. Furthermore, even if an exact model could be formulated, the ability of available electromagnetic scattering and absorption computer programs to obtain numerical results is restricted to a small class of particle configurations. In the end, the goal is to obtain numerical results that will indicate the semi-quantitative behavior of the real-world light scattering and absorption interactions. For purposes of the present LIDAR simulation, the above considerations and information contained in the literature indicate that the use of a layered sphere model may be the best compromise between reality and our ability to obtain numerical results.

Furthermore, for purposes of this simulation, we will use an index of refraction for elemental carbon of $1.5+i0.5$ and for organic carbon of $1.5+i0.0$. Presumably these two components can appear together in the same particle – the most commonly assumed configuration is a layer of organic carbon condensed upon an elemental carbon base particle.

The literature shows wide agreement that the number distribution of the particles in vehicle exhaust is a log-normal size distribution. The rough diameter of pollution particles in vehicle exhaust peaks around the 0.1 to 0.2 μm range. The paper by Bassagnet and Roset (2001) for diesel engines probably is the most useful in defining number distributions for different cases.

2.3.1.2 Light Scattering Calculations

It is clear from the previous discussion that the quantities of interest are the particle differential scattering cross section in the backscatter direction, $\sigma_d(\pi)$, and the particle extinction cross section, σ_e. These calculations have been made for particle diameters from 0.01μm to 10μm, encompassing the expected size range of vehicle exhaust particles. Results have been obtained for solid spheres with an index of refraction characteristic of organic carbon as well as for two-layer spheres consisting of an elemental carbon core and an organic carbon shell. The calculated quantities, $\sigma_d(\pi)$ and σ_e, have been normalized by particle volume. Calculations have been made for a wavelength of 0.266 μm, the ultraviolet wavelength of the LIDAR system.

Figure 2-4 shows the results of a calculation of $\sigma_d(\pi)$ and σ_e for a homogeneous spherical particle with an index of refraction of $m = 1.5 + i0.0$, representing a sphere of solid organic

carbon. This particle is nonabsorbing (the imaginary part of the index of refraction is 0.0), so the extinction cross section σ_e is equal to the scattering cross section and, like the backscatter cross section $\sigma_d(\pi)$, exhibits a straight-line log-log behavior in the range 0.01 to 0.1 μm, indicative of the scattering behavior of particles that are small relative to a wavelength.

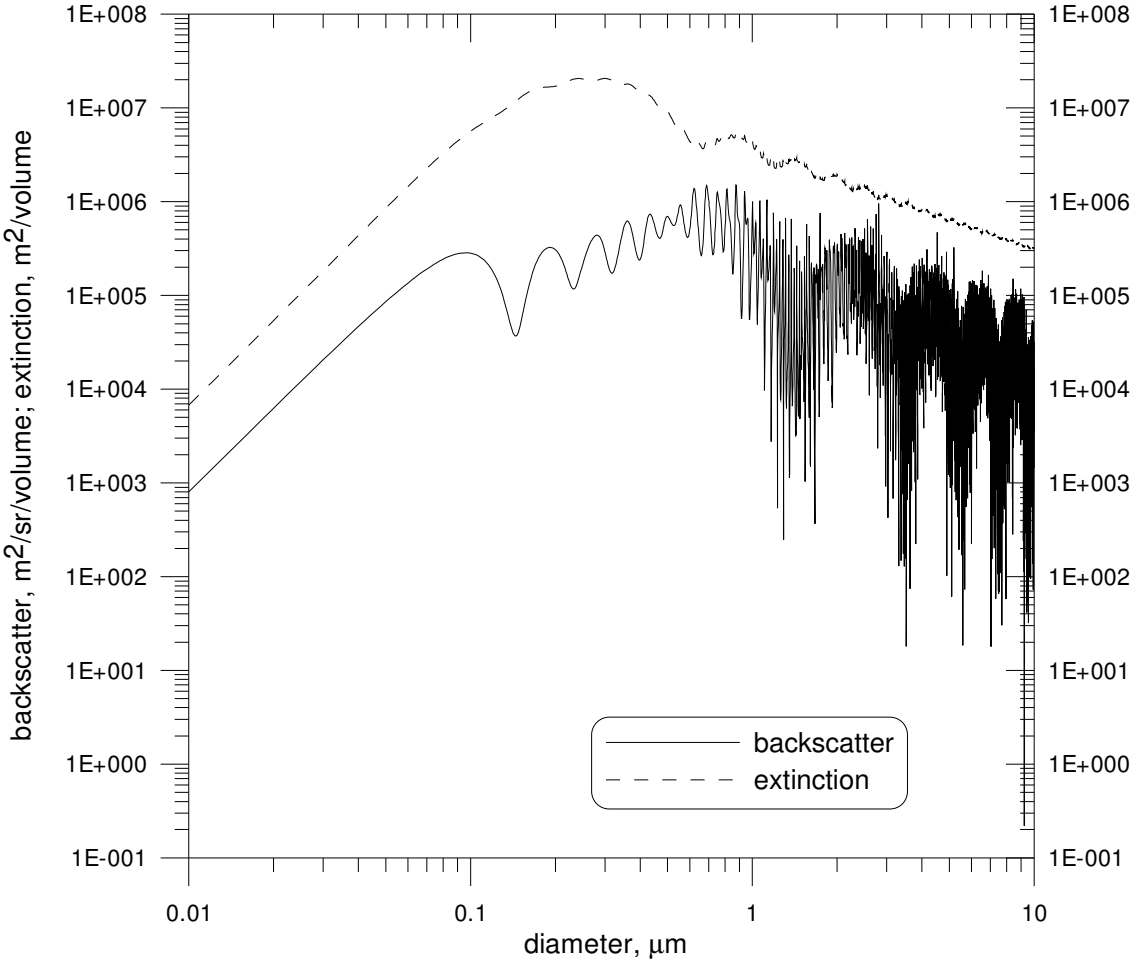

Figure 2-4. Backscatter and extinction (normalized by particle volume) for a homogeneous spherical particle with an index of refraction of m = 1.5 +i0.0 at λ = 0.266 μm.

A well-known layered sphere program[9] has been obtained and the program has been successfully tested for a variety of core and shell configurations representative of the particle distributions that we expect to use.

Figure 2-5 shows the result of a calculation for a layered spherical model consisting of an elemental carbon core surrounded by an organic carbon shell.

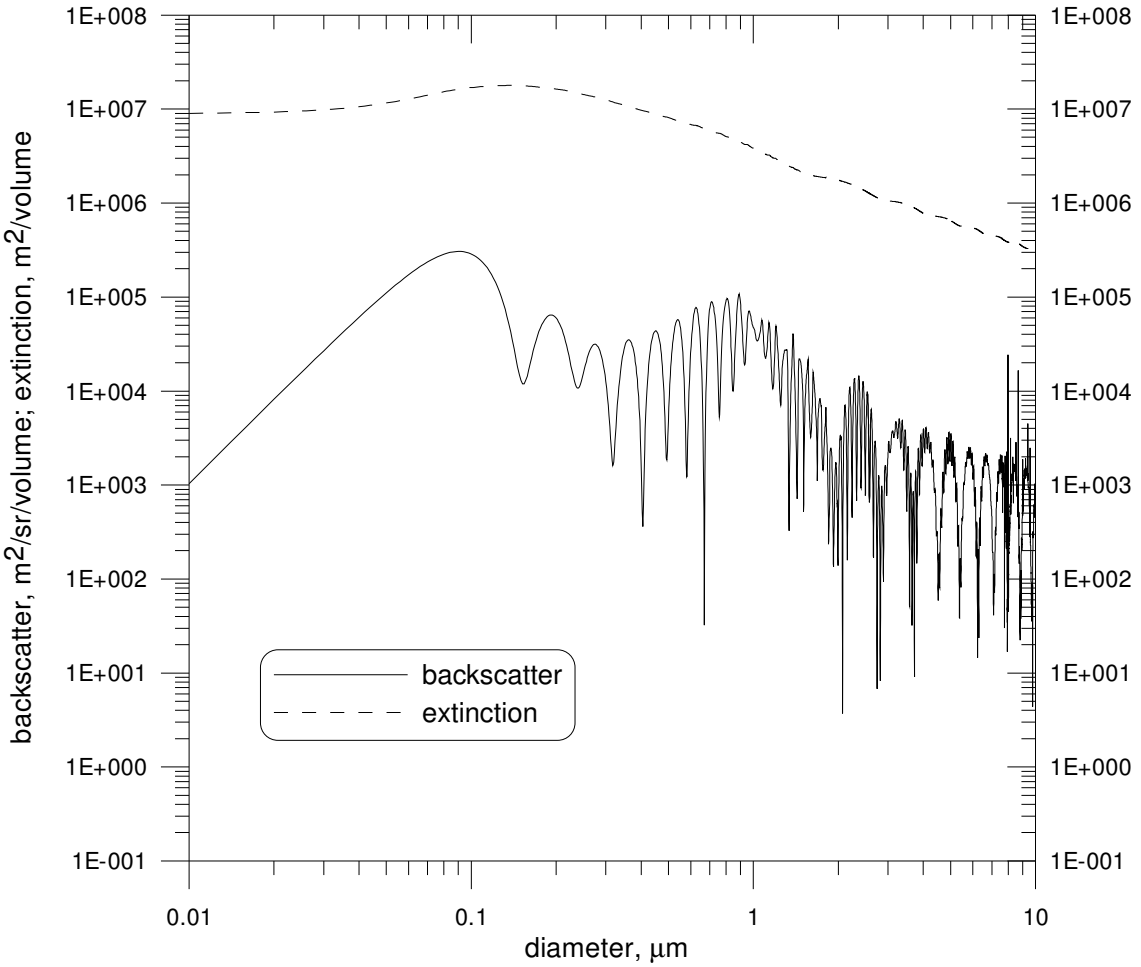

Figure 2-5. Backscatter and extinction (normalized by particle volume) for a layered spherical particle with an index of refraction of mcore = 1.5 +i0.5 and mshell = 1.5 +i0.0 at λ = 0.266 µm. Fractional core volume is 0.5.

2.3.2 Particle Emissions Factor Estimation

The LIDAR return in an exhaust plume remote sensing application when the path extinction is assumed to be negligible is given by (2-5), where N and σ_d (π) are generally functions of the range variable r, i.e., the particulate matter in the path changes in both number density and particle characteristics along the range.

In general, the ambient term includes the scattering from atmospheric molecules as well as the scattering from background particles, such as dust, particulate matter that may exist in the atmosphere on a regional basis, as well as lingering PM from a previous vehicle that may have transited the LIDAR remote sensing system. Two LIDAR measurements are made in the field, a pre-vehicle measurement and a post-vehicle measurement. We assume that the ambient term measured in the pre-vehicle measurement accurately describes the background when the post-vehicle measurement of vehicle exhaust is measured. Therefore, we subtract the ambient background from the vehicle exhaust measurement and obtain the scattered power from the particulates in the exhaust plume as

$$P(r) = \frac{C_o O(r)}{r^2}[N_{PM}\sigma_{d,PM}(\pi)]. \quad (2\text{-}6)$$

Before field measurements are made, laboratory calibration of the system is necessary. This calibration includes a range correction to compensate for the nonuniform overlap of the receiving telescope field of view with the UV-laser illuminated particulate path and also to take out the $1/r^2$ dependence of the LIDAR returned signal. For purposes of the LIDAR measurement then, the general form of (2-6) is

$$P(r)\frac{r^2}{C_o O(r)} = N\sigma_d(\pi), \quad (2\text{-}7)$$

where the units are 1/(m-sr). This signal is registered as a voltage (mV) at the terminals of the detecting photo multiplier tube (PMT) that converts the LIDAR optical signal to a voltage.

The range along the path can alternatively be described in terms of distance or time. For this application, the range correction is applied in the time domain at 0.25 ns intervals. In the laboratory we separately measure HEPA-filtered air and CO_2 with the LIDAR system. For both of these gases, the right hand side of (2-7) is known (Measures, 1984). The value for the normal atmosphere at sea level under standard conditions of temperature (0 ˚C) and pressure (1013mb) and a wavelength of 266 nm is 2.55×10^{-5} 1/(m-sr). This is sometimes referred to as 1 Rayleigh unit to signify that the scattered return from molecules in the standard atmosphere is calculated using the Rayleigh approximation in scattering theory. The scattering return for CO_2 for the same conditions is 2.96 Rayleigh units.

In the laboratory measurements of HEPA-filtered air and CO_2, we know that the scattering should be uniformly constant across all range gates. The process of range correction is to make a laboratory measurement of the LIDAR received signal (in mV) at each range gate and then develop a procedure so that later field measurements can be related back to the absolute measurements that were made in the laboratory. We take measurements for both HEPA-filtered air and CO_2 in the laboratory because the signal correction at each range gate is assumed to be linear, i.e., following the equation $y = mx + b$, and we need to determine the slope m and y-intercept b at each range gate – two measurements will give us the two unknowns.

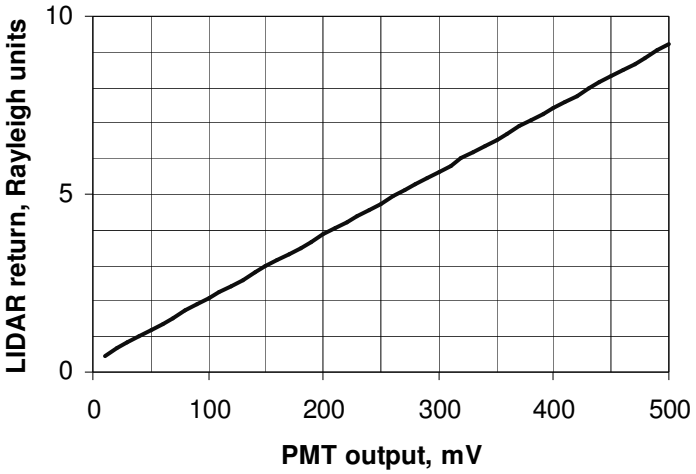

Figure 2-6. LIDAR Calibration Curve.

The procedure can be illustrated by reference to Figure 2-6, the laboratory-derived calibration curve for a particular range gate. Assume that for this range gate, a laboratory measurement for HEPA-filtered air has produced a PMT output of 40 mV. This is known to correspond to a LIDAR scattering amplitude of 1 Rayleigh unit (2.55×10^{-5} 1/(m-sr)). A similar measurement for CO_2 has produced a PMT output of 150 mV and this is known to correspond to a LIDAR scattering amplitude of 2.96 Rayleigh units. Then the linear calibration curve can be drawn. A later field measurement of the PMT output for the LIDAR return from an exhaust plume can then be related back to the laboratory calibration. For example, a field measurement of 376 mV from an exhaust plume corresponds to a LIDAR return of 7 Rayleigh units or $7 \times 2.55 \times 10^{-5}$ 1/(m-sr) = 0.178×10^{-3} 1/(m-sr).

2.3.2.1 Field Measurements

The laboratory calibration provides us with a procedure for converting the field measurements of PMT voltage to absolute LIDAR return in terms of Rayleigh units. Specifically, with reference to (2-7), we can write the unknown PM scattering as,

$$N_{PM}\,\overline{\sigma}_{d,PM}(\pi) = R_{PM}\,N_{cal}\,\sigma_{cal}(\pi), \tag{2-8}$$

where $N_{cal}\,\sigma_{cal}(\pi)$ is 2.55×10^{-5} 1/(m-sr) and R_{PM} is the LIDAR return from the exhaust plume in dimensionless Rayleigh units as determined from a field measurement (mV) and Figure 2-6. Note that we use the mean differential scattering cross section in the backscatter direction, $\overline{\sigma}_{d,PM}(\pi)$. The quantities on the right hand side of (2-8) are all known from the laboratory calibration and a field measurement.

2.3.2.2 Mass Density Calculation

We now have a prescription, with some assumptions, for finding the mass density of particulate matter in the exhaust plume. N_{PM} in 2-8 is the number of particles per unit volume, #/m^3. If this quantity can be determined and if the mean mass of the exhaust particles is $\overline{m}$ kg, then the PM mass density M_{PM} is

$$M_{PM} = N_{PM}\ \overline{m}\ \text{, kg/m}^3. \tag{2-9}$$

To obtain N_{PM} it is necessary to determine the quantity $\overline{\sigma}_{d,PM}(\pi)$ on the left hand side of (2-8), the differential scattering cross section in the backscatter direction. We can calculate $\overline{\sigma}_{d,PM}(\pi)$ for a size distribution of solid spheres of organic carbon to represent the exhaust particles from spark-ignition vehicles and for a size distribution of layered spheres consisting of a core of elemental carbon surrounded by a shell of organic carbon to represent the exhaust particles from diesel-powered vehicles.

We make the further assumption that the particles in the exhaust can be represented by a normalized (to N) log-normal distribution $n_N(D)$,

$$n_N(D) = \frac{1}{(2\pi)^{1/2} D \ln \sigma_g} \exp[-\frac{(\ln D - \ln \overline{D}_g)^2}{2\ln^2 \sigma_g}], \tag{2-10}$$

where D is the particle diameter and the log-normal distribution is defined by the particle median diameter $\overline{D}_g$ and the geometric standard deviation σ_g. For our purposes it is more convenient to define the particle mass median diameter $\overline{D}_{gm}$ than $\overline{D}_g$, but these two quantities are related as

$$\ln \overline{D}_g = \ln \overline{D}_{gm} - 3\ln^2 \sigma_g, \tag{2-11}$$

so

$$\overline{D}_g = \exp(\ln \overline{D}_{gm} - 3\ln^2 \sigma_g). \tag{2-12}$$

Representative values for $\overline{D}_{gm}$ and σ_g can be found in the literature for spark and diesel exhaust plumes.

Then we can calculate the mean differential scattering cross section in the backscatter direction for defined particulate systems as

$$\overline{\sigma}_{d,PM}(\pi) = \frac{\int_o^\infty \sigma_{d,PM}(\pi, D) n_N(D) dD}{\int_o^\infty n_N(D) dD}, \tag{2-13}$$

where $\sigma_{d,PM}(\pi, D)$ is the differential scattering cross section in the backscatter direction for a particle of diameter D.

The mean mass is given by,

$$\overline{m} = \frac{\int_o^\infty m(D) n_N(D) dD}{\int_o^\infty n_N(D) dD}, \tag{2-14}$$

where $m(D)$ is the mass of a particle of diameter D.

The process of obtaining the mass density M_{PM} can then be summarized:

1. From a remote sensing field measurement for a particular vehicle, obtain the exhaust plume PMT backscatter signal in mV.

2. Convert the PMT mV signal to Rayleigh units R_{PM} from the calibration curve represented by Figure 2-6

3. Calculate $\overline{\sigma}_{d,PM}(\pi)$ and $\overline{m}$ from (2-13) and (2-14), respectively, for a defined particulate distribution, for a spark-ignition or diesel vehicle, as applicable.

4. Obtain NPM from (2-8) using $\overline{\sigma}_{d,PM}(\pi)$ and then solve (2-9) for M_{PM}, using $\overline{m}$.

The final form for M_{PM} is

$$M_{PM} = R_{PM} N_{cal} \sigma_{cal}(\pi) \frac{\int_o^\infty m(D) n_N(D) dD}{\int_o^\infty \sigma_{d,PM}(\pi, D) n_N(D) dD} \text{ kg/m}^3. \qquad (2\text{-}15)$$

We evaluate the two integrals in 2-15 using a numerical technique, then take the ratio as indicated. Multiplying by $N_{cal}\ \sigma_{cal}(\pi)$ then gives the constant that relates mass density M_{PM} to Rayleigh units R_{PM}. The constant, which can be denoted as C_{PM}, can be written explicitly as,

$$C_{PM} = N_{cal} \sigma_{cal}(\pi) \frac{\int_o^\infty m(D) n_N(D) dD}{\int_o^\infty \sigma_{d,PM}(\pi, D) n_N(D) dD} \text{ kg/m}^3. \qquad (2\text{-}16)$$

Before giving calculated results for C_{PM}, it is important to summarize the assumptions that have been made.

$N_{cal}\ \sigma_{cal}(\pi)$ represents the backscattering by the calibration gases in the laboratory. One value from the literature at standard temperature and pressure for air is 2.55 x 10-5 1/(m-sr). New more precise measurements could provide a more accurate value for this constant. Furthermore, a recalibration that takes into account nonstandard temperature and pressure in the laboratory would result in a small change to this constant. The calibration curve represented by Figure 2-6 assumes that the backscattering by CO_2 is 2.96 greater than that for air. Finally, the calibration curve in Figure 2-6 is assumed to be linear and was obtained by taking two measurements, one for air and one for CO_2. Measurements for other calibration gases, or for one or both of these gases at other temperatures and/or pressures may show that the calibration curve deviates from a straight line. So there are at least four assumptions in the use of $N_{cal}\ \sigma_{cal}(\pi)$.

The evaluation of the integrals in (2-16) is based on the assumption that the PM particles are spherical in shape. Furthermore, the size distribution of the particles is assumed to be lognormal with a specific geometric standard deviation σ_g and mass median diameter $\overline{D}_{gm}$. The calculations here assume a value of 1.5 μm and 0.1 μm for these two quantities, respectively. We assume a particle mass density of 1250 kg/m^3. Selection of other values will result in a change in the calculated C_{PM}.

The calculation of $\sigma_{d,PM}(\pi, D)$ inside the integral in the denominator of (2-16) assumes that the PM of spark-ignition vehicles can be represented by a solid sphere of organic carbon with an index of refraction of m = 1.5+i0.0. Calculations for diesel vehicles assume that the PM can be represented by a layered sphere consisting of a spherical core of elemental carbon surrounded by a shell of organic carbon. The index of refraction of the elemental carbon core is

assumed to be m = 1.5+i0.5. The volume fraction of the layered particles is assumed to be 50/50, i.e., the core and shell are of equal volume.

It is known that PM particles are not spherical, but rather consist of coagulated aggregates of possibly spherical building blocks. Nevertheless, the spherical particles assumed here do incorporate many of the know features of these particles, including the known optically non-absorbing characteristics of organic carbon and the absorbing characteristics of elemental carbon. Furthermore, the size range of the particles is in the known size range of PM particles from spark-ignition and diesel vehicles.

There are also complex assumptions in replacing $\sigma_{d,PM}(\pi)$ with $\overline{\sigma}_{d,PM}(\pi)$ in (2-8) and in asserting the relationship in (2-9).

All of these assumptions enter into the calculation of C_{PM} in (2-16). Therefore, the conversion of Rayleigh units to PM mass density resulting from the use of this constant should be viewed as a best estimate at this time, given what is currently known. However, as new information is obtained and incorporated, some of the assumptions may be refined or eliminated. When this occurs, revised values of C_{PM} may be calculated and used to linearly scale previous field measurements.

Finally, we should note that the scale factor C_{PM} is calculated at each range gate, but is assumed to be the same for all range gates. The major assumption in this is that the size distribution of the PM particles is been assumed to be the same at all range gates, although the number density of particles may be different at each range gate (as represented by the spatial variation of R_{PM}). The data reduction process obtains a value for R_{PM} at each range gate, then obtains an average value across all range gates for a particular vehicle. This linear process of data reduction does not invalidate the use of C_{PM} for converting the R_{PM} for each vehicle.

Given these assumptions we have calculated C_{PM} values of 0.16 mg/m^3 for spark-ignition vehicles and 0.18 mg/m^3 for diesel vehicles. These values can be used with a measurement of the PM backscatter in Rayleigh units and the exhaust CO_2 in kg/m^3 for each vehicle to obtain vehicle emission factors in units of mg of PM per kg of fuel burned. With suitable assumptions for vehicle average mileage, an emission factor can be obtained in units of mg of PM per mile.

2.3.3 LIDAR Design and Operation

DRI has designed and built a LIDAR remote sensing device temporarily called the Lidar On-Road Aerosol EXperiment (LORAX) (Keislar et al. 1999). The device measures on-road particulate matter emissions from passing cars. With suitable assumptions regarding size distribution and particle composition, the LIDAR backscatter signal can be used to estimate particle mass emissions (as discussed in the preceding theory section). With an approximately collocated measurement of CO_2 across the plume, the particulate mass emission factor (per fuel consumption) can be obtained.

Figure 2-7 shows a functional schematic of the LIDAR system. Three main subsystems comprise LIDAR: 1) the transmitter, which includes an UV laser and guiding optics; 2) the receiver, which includes a refracting telescope and a photomultiplier tube; and 3) the data acquisition subsystem, which includes a 1.5 GHz, 8 Gigasample s^{-1} oscilloscope and an acquisition computer. In addition, there are three auxiliary subsystems: 1) an extinction measurement subsystem, which includes a photodectector for a UV extinction measurement, 2) a

triggering/safety subsystem, which includes optical gates and a mechanical shutter on the UV laser, and 3) an alignment system comprised of three guide lasers and appropriate targets.

Figure 2-8 shows a top view of the on-road setup, where the main LIDAR (and the RSD3000) system can be placed on either the right or the left shoulder of a single lane of traffic. Passive components, i.e., mirrors, absorbing plates, and retro-reflectors, are placed in the LIDAR Beam Terminus on the opposite side of the road (and the Vertical Transfer Mirror for the RSD3000).

Figure 2-9 shows a layout of the LIDAR instrument box, and Figure 2-10 shows the layout of the Beam Terminus, which sits across the traffic lane. The transmitter is a Nd:YAG laser (λ=1.034 μm), frequency-quadrupled to yield 266-nm ultraviolet light (Nanolase, Model 00211-150, Meyllan, France, distributed by JDS Uniphase Corp., Sunnyvale, CA). The laser has an average power of 1 milliwatt, pulse duration of approximately 1 ns, and a pulse repetition frequency of 6.8 kHz. A fused silica beam splitter directs a signal into a high-speed silicon detector (ThorLabs DET210, 0.8 mm^2, Newton, NJ) for an oscilloscope trigger. A spatial filter helps remove fringes by focusing laser light onto a 75 μm aperture, then collimates the beam which also acts as a 2x beam-expander. Two bounce mirrors (Mirror 1 and the outgoing Mirror 2) direct the beam out across the lane of traffic where it scatters off particles in the beam path.

The receiver is a 2" refracting telescope. Backscattered light in the field of view of the telescope is focused onto a photomultiplier tube (PMT, Hamamatsu H6780-06, Tokyo, Japan). A solar-blind filter and a notch filter are added to reduce background light. The PMT current is dropped across a 50 Ω load into the oscilloscope (Infinium 54845A, Agilent Technologies, Sunnyvale, CA). With a laser pulse duration of one ns, range gates would be 15 cm wide. Actual range resolution through the electronics is approximately 25 cm. An acquisition computer receives the waveforms from the oscilloscope where a single shot is recorded approximately every 5 ms.

Like the RSD3000 system, LIDAR is triggered by a beam unblock signal which follows a beam block signal after 0.2-0.4 second, indicative of a passing vehicle. The optical gates provide this triggering as well as a safety cut-off which closes the mechanical shutter. The average gasoline-powered vehicle is from 1.5-1.8 m wide, giving approximately 10-12 range gates across the back of a car. If the exhaust stream exits at the side of the car, more range gates of interest are possible. Scattering from the terminus plate indicates the end of each pulse after approximately 40-50 ns, depending on the distance from the transmitter to the terminus plate. With an approximate pulse repetition rate of 6.8 KHz, backscatter from 3400 pulses, with 20-25 range gates each, could be collected in the half-second following the passage of the car. However, with the present data acquisition system, only 100 waveforms are collected. The time-evolution of the LIDAR returns over this period together with the range result signal may permit discrimination of road dust thrown up by the tires from particulate matter in the exhaust plume.

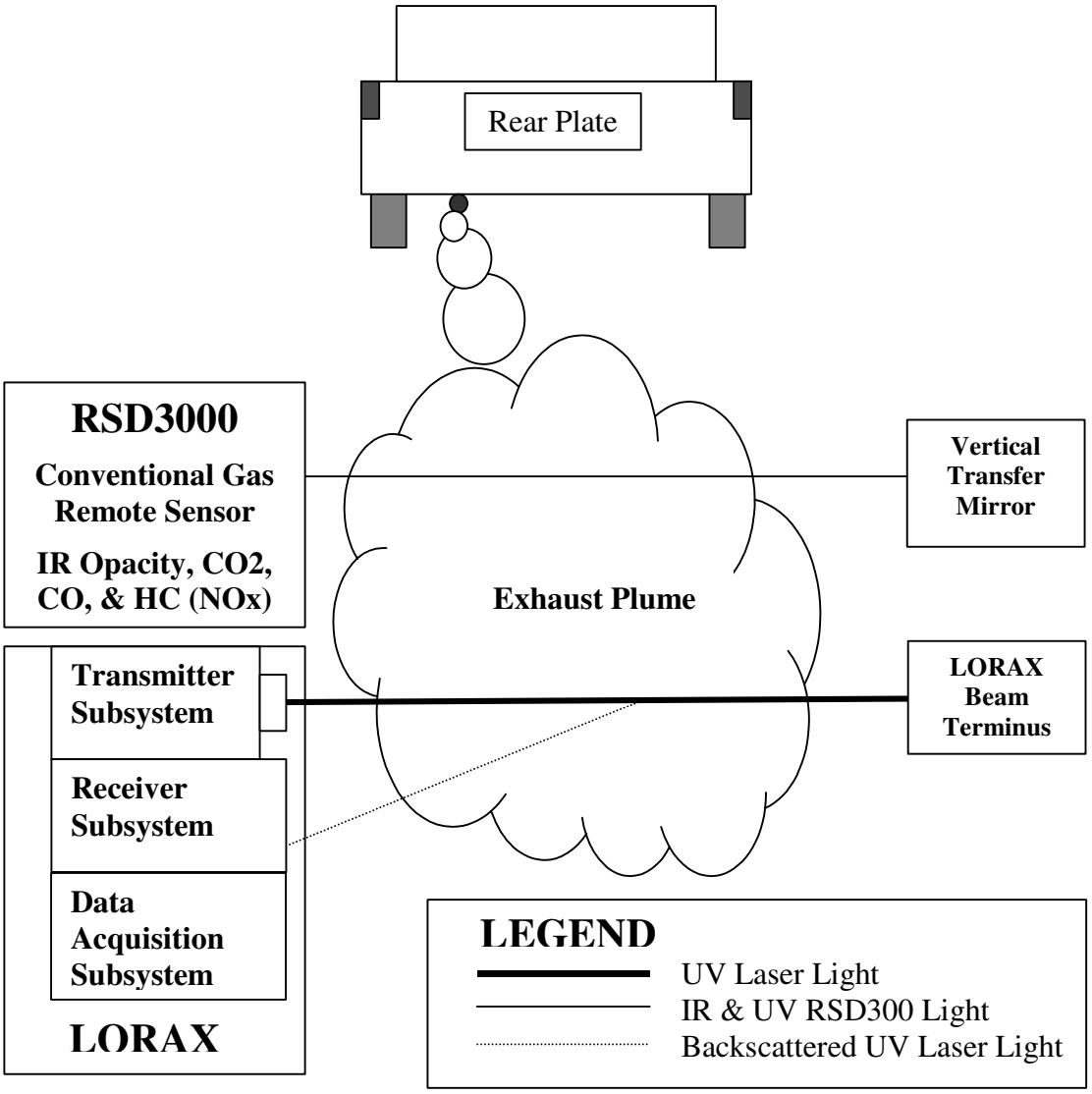

Figure 2-7. Functional schematic drawing of the LIDAR System with the RSD3000 exhaust gas analyzer shown.

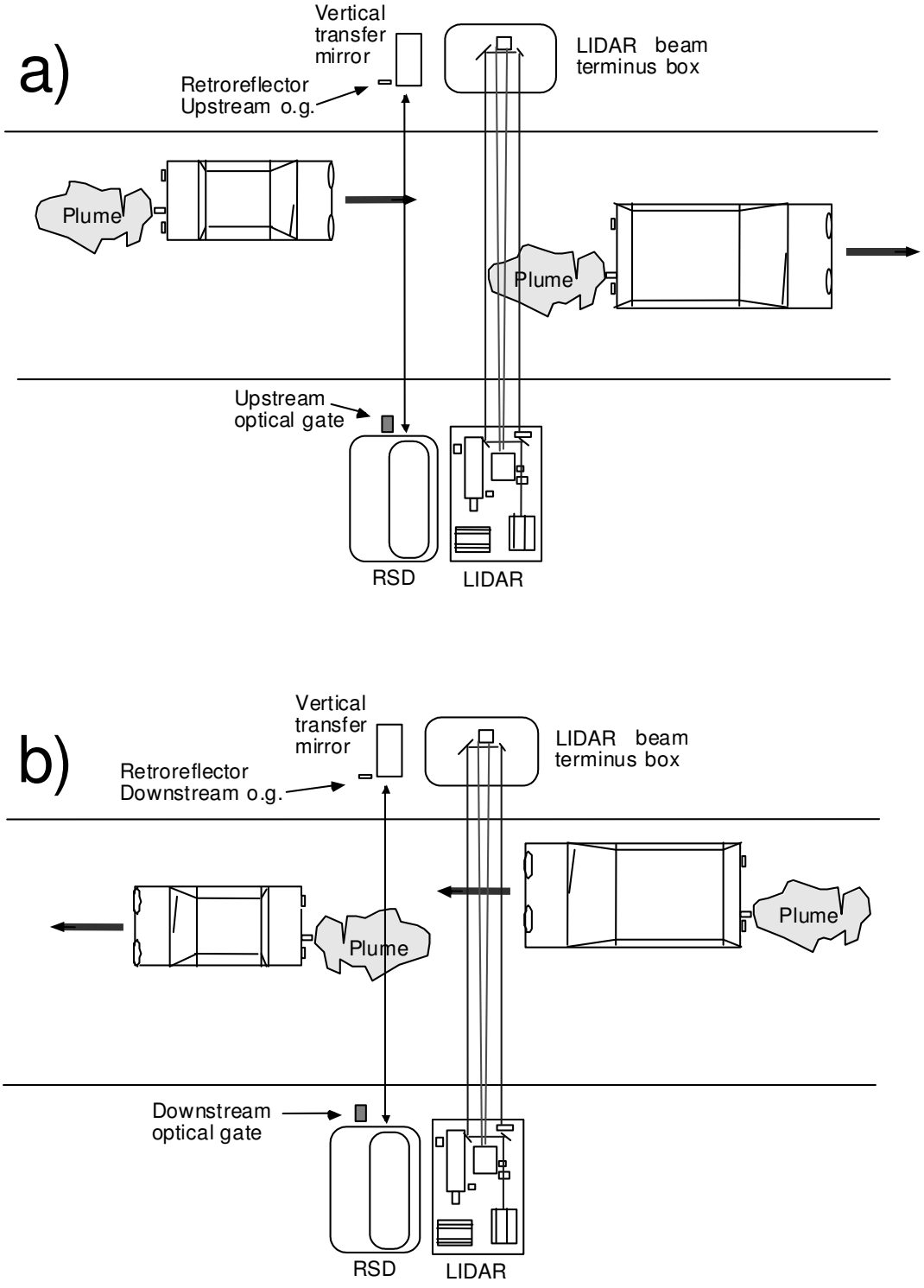

Figure 2-8. Top view of LIDAR and RSD3000 setup on a) the right side of the traffic lane and b) the left side of the traffic lane. Processing is slightly different for the two scenarios, and the operator must enter either "Left" or "Right" in the initiation of the acquisition program.

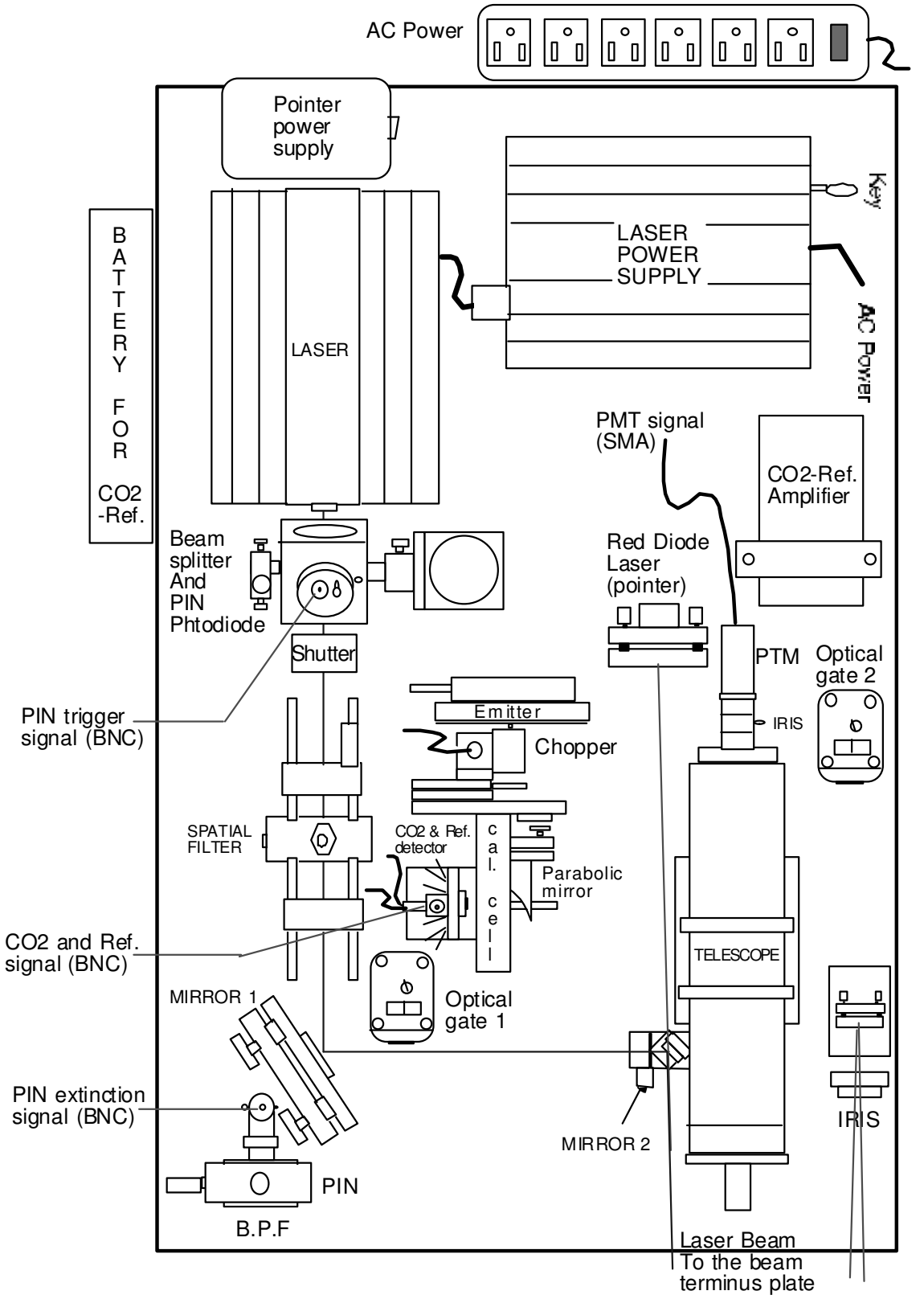

Figure 2-9. Layout of LIDAR box.

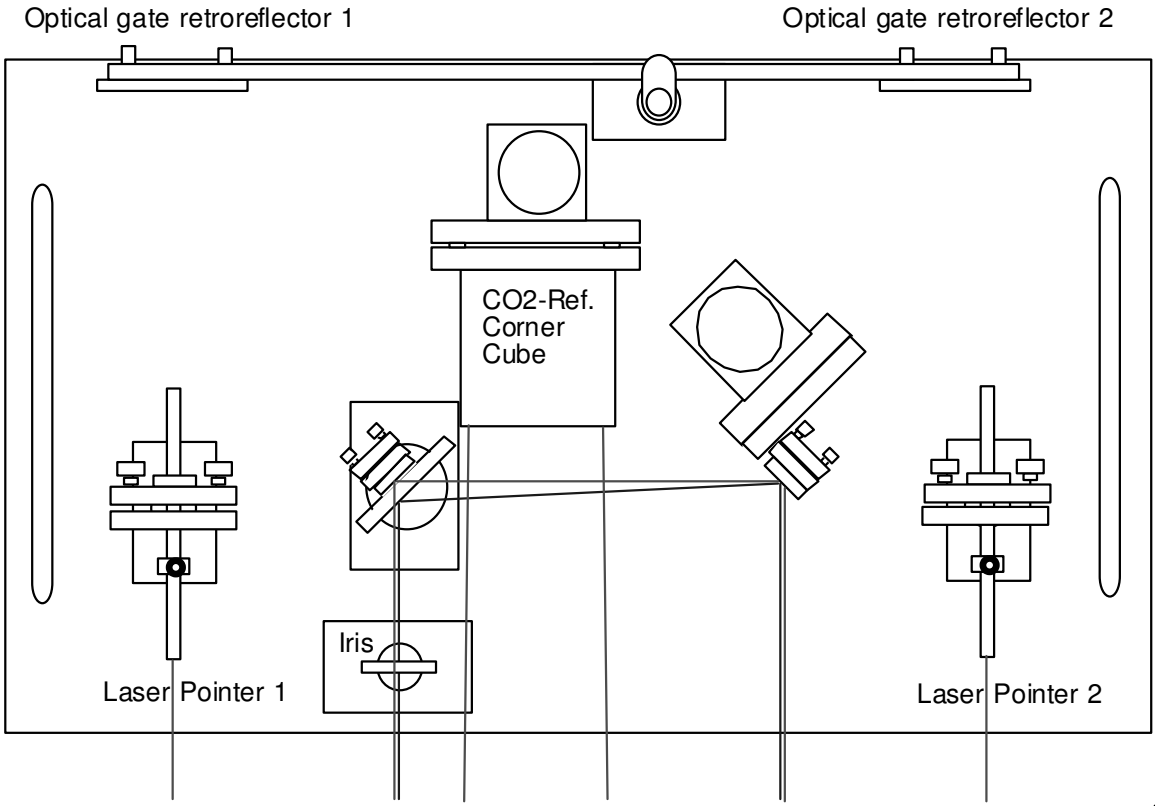

Figure 2-10. Layout of beam terminus.

Computer processing includes selecting the background LIDAR return and cataloging of sufficient time-stamps or other signals to link the LIDAR data with the RSD3000 data.

The Beam Terminus box has two laser pointers for alignment, the beam terminus plate, which absorbs 99.99% of the laser energy, and three bounce mirrors to return the remaining laser light for the extinction measurement, and the third alignment laser in the LIDAR box. Figure 2-10 also shows a corner cube used for the independent CO_2 channel. At the time of writing this report, the independent CO_2 channel is in the developmental stage. No measurements from this CO_2 system are presented in this report. Retroreflectors for the optical gates are also housed in the Beam Terminus.

3. DATA ACQUISITION AND PROCESSING

Remote sensing of vehicle exhaust produces very large data sets that must be managed in a systematic manor. In one day, it is possible to produce more than 2 GB of raw data. Data is reduced using custom computer programs and database applications. Because it is not possible to review each data point collected, data validation criteria are applied to eliminate invalid data. This chapter documents the programmatic steps that record the raw voltage data from the remote sensing instrumentation, process the data into physical quantities related to vehicle emissions, and store the data in a relational database.

3.1 Remote Sensing Data Acquisition System

All the control of the instrumentation, data acquisition and preliminary processing and display are performed by using a National Instruments LabView 6.0 program developed at DRI specifically for this application. The acquisition of the LIDAR return signal, DRI UV extinction and DRI CO_2 data follows the steps listed below:

1. The acquisition system is switched on and ambient data are collected continuously in circular buffers.
2. When a vehicle intercepts and blocks the beam of the downstream optical gate (DOG) the previous 60 data points, corresponding to approximately 300 milliseconds of LIDAR return, CO_2, IR reference, and UV extinction signals are stored. These data will serve as pre-vehicle or "ambient" values.
3. The UV extinction channel is continuously interrogated during the passage of the vehicle, to estimate the background due to ambient light, electrical offsets and instrumental drift.
4. When the DOG is unblocked (i.e. the vehicle just passed through the beam) the system is immediately instructed to start the new post-vehicle or "exhaust" data acquisition.
5. About 500 milliseconds (approximately 100 data points) of post-vehicle data are acquired and stored.
6. At the end of the 500 milliseconds the acquisition system starts again to acquire ambient data continuously in the circular buffers until a new vehicle pass through the DOG beam. At this point the process is repeated from step 2 above until the end of the data collection.

The data acquisition system (DAQS) is schematically represented in Figure 3-1. The hardware comprises a fast Hewlett Packard Infinum oscilloscope (Bandwidth 1.5 GHz, sampling rate up to 8GS/s), a Stanford Research Systems gated integrator & boxcar averager SR250, two Stanford Research Systems digital Lock-in amplifiers SR830, a Pentium III PC with a National Instruments PCI GPIB 488.2 bus card and a National Instruments PCI data acquisition board (DAQ 6023E with 8 Input/Output digital lines and 16 12 bit analog channels at a sampling rate of 200 KS/s).

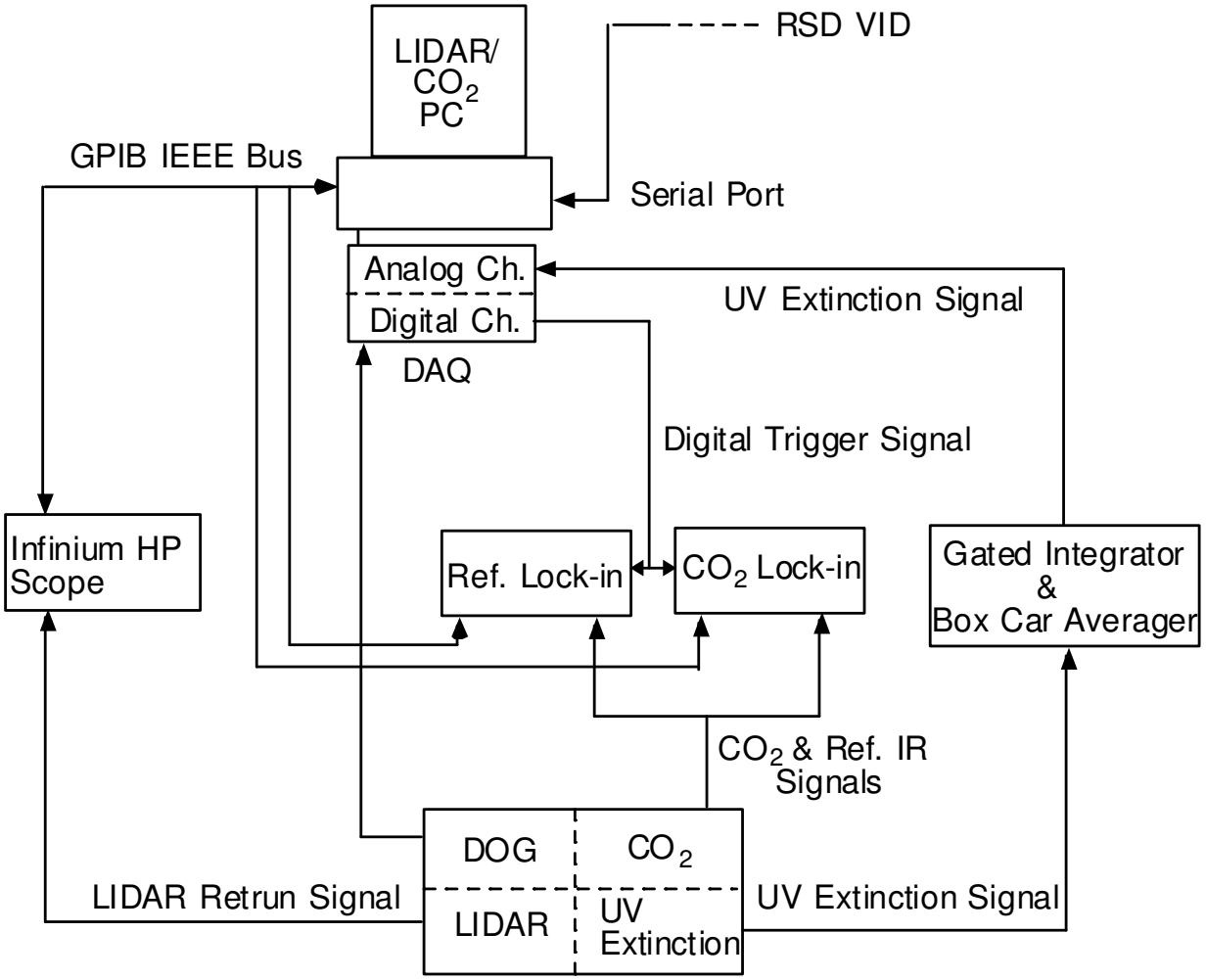

Figure 3-1. Data Acquisition System diagram.

After initialization by the PC via the GPIB bus, the oscilloscope first acquires and stores in its memory the LIDAR range resolved backscattering signal (waveform). Second, at the PC request, the acquired waveform is transferred from the oscilloscope to the PC over the GPIB bus.

Synchronously with the LIDAR waveform acquisition, a value of the UV extinction data is acquired from the box car, by one of the analog channels on the DAQ card and stored in the computer memory. Also a digital signal is placed, by the computer, on a digital output of the DAQ card to trigger both the CO_2 and Reference lock-in amplifiers. This trigger instructs the lock-in amplifiers to acquire an average data value and store it in the internal circular buffer. When 500 milliseconds elapse, after the vehicle unblock, the PC interrogates both the lock-in amplifiers requesting via the GPIB bus the data collected for approximately 800 milliseconds (500 ms of post-vehicle and 300 ms of pre-vehicle data). In the case in which another vehicle blocks the DOG before 300 milliseconds have elapsed after the previous vehicle, the data stored in the buffer from the previous pre-vehicle set are used to fill the empty array elements for the actual pre-vehicle data set of this new vehicle.

The data set, covering the 800 milliseconds, for any vehicle constitutes a one-dimensional array for the UV extinction data, a one-dimensional array for the IR CO_2 data channel, a one-dimensional array for the IR Reference channel and finally a two-dimensional array of backscattering data. The two dimensions of the backscattering array represent respectively the time elapsed from the vehicle passage and the LIDAR range resolved signal across the lane (see Figure 3-2).

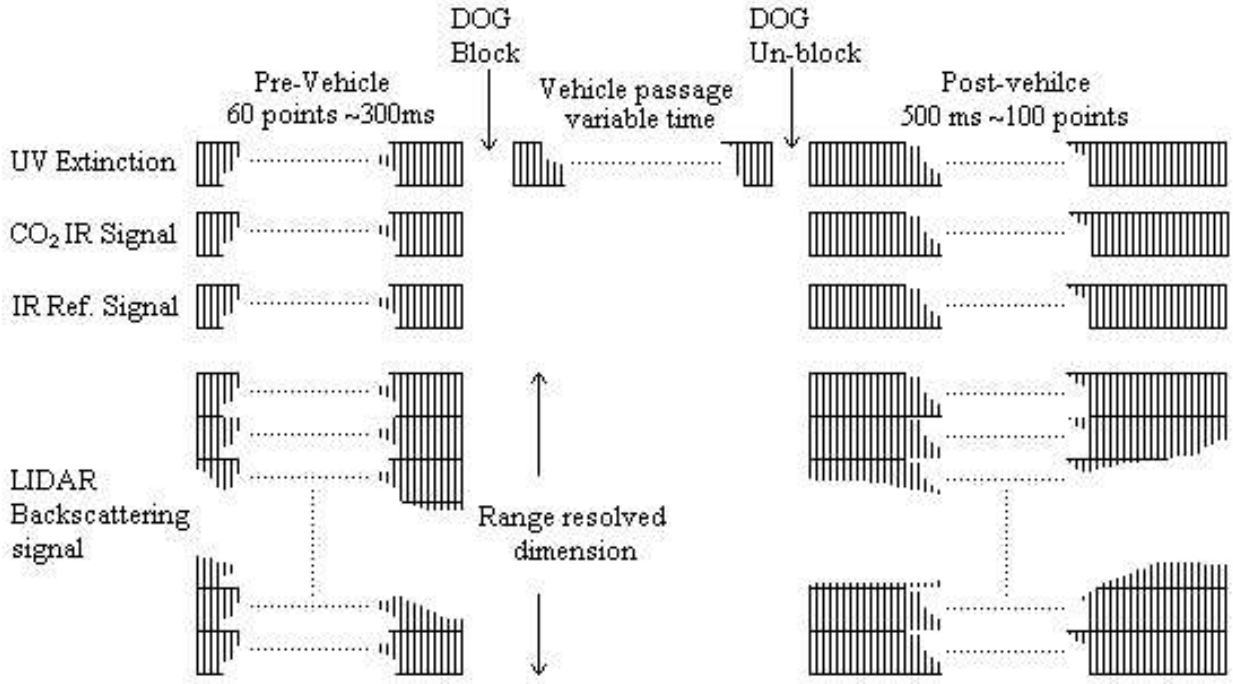

Figure 3-2. Data flow diagram.

Table 3-1 describes a hypothetical time sequence of events during the acquisition of vehicle emissions. The timing is also compared with the RSD timing.

Table 3-1. Time sequence of measurement and data acquisition steps.

TIME (ms)	*LIDAR*	*RSD*
-20	External OG blocked**	
-17		IR beam blocked Pre-vehicle sampling ends*
0	Upstream OG blocked Shutter blocks UV beam	
14	Downstream OG blocked Shutter blocks UV beam Pre-vehicle sampling ends*	
20		IR beam block signal arrives at DAQS** (avg. 37 ms delay in RSD)
230	External OG unblocked**	
233		IR beam unblocked License plate photo acquired Exhaust sampling begins
250	Upstream OG unblocked	
264	Downstream OG unblocked Shutter unblocks UV beam Exhaust sampling begins	
533		VID sent to LIDAR
733		Exhaust sampling ends (500 ms after beginning)
733+		Pre-vehicle sampling begins
764	Exhaust sampling ends (500 ms after beginning)	
764+	Pre-vehicle sampling begins	

*Pre-vehicle (ambient) data is collected in a circular buffer. The LIDAR utilizes 300 ms of ambient data preceding upstream OG blockage at 0 ms. The RSD utilizes 200 ms of ambient data preceding IR beam blockage at -17 ms.
** Optional functions for time synchronizing LIDAR and RSD systems- not used in current configuration.
Assumptions:
1.Remote sensing trailer on right hand side of roadway (Lane configuration A).
2.Vehicle length = 5 m and velocity = 20 m/s.
3.Distances: external OG to RSD IR beam = 6 cm; external OG to upstream OG = 40 cm; upstream OG to downstream OG = 29 cm.
Definitions:
OG = Optical Gate, DAQS = Data Acquisition System, IR = InfraRed, UV = UltraViolet, VID = Vehicle IDentification number.

All the data are saved in real time on the computer's hard drive. For consistency between the RSD data and the DRI LIDAR data, the name of each vehicles LIDAR file is determined by the RSD VID (vehicle identification number) passed to the LIDAR PC from the RSD computer by the serial port. A real-time simplified data analysis and graphical display is performed during the acquisition as a diagnostic tool for on-site performance evaluation. This feature permits the

field operators to check and debug any instrument problems and provides real-time feedback of the vehicle emissions.

The display reports a real-time backscattering graph, a time series graph of excess CO_2, integrated backscattering, UV extinction, and IR extinction. In addition, a table reports continuously a statistical summary describing the particle emissions measurements for the last three vehicles measured. These parameters are also stored on the hard drive for post processing analysis. Finally a data set recording of the output intensity of the UV laser is acquired and stored in the hard drive at intervals of approximately thirty minutes. This data is useful for monitoring the laser performance and stability over the entire data acquisition period in the field.

3.2 Data Processing

Data acquired by the LIDAR and the RSD3000 data acquisition systems are written to ASCII text files by their respective data acquisition computers. The LIDAR system writes one set of files – one for each VID – for the backscatter data and another set for the extinction data. The RSD3000 system writes three files incorporating extinction measurements for all VIDs. Data are transferred from the field computers to processing computers using CD-ROMs or portable hard drives. In the lab, the ASCII files are imported into an Access database using a custom VBA (Visual Basic for Applications) procedure within the Access database. This procedure is described in detail in Appendix B.

Using the VBA procedure, individual shot concentrations of RSD3000 CO_2, CO, and HC are calculated using proprietary algorithms from RSTI. Other calculations involve averages, standard deviation, quadrature for backscatter values, and correlation statistics.

3.2.1 Access Tool Data Processing Method

The following data processing steps are applied with the Access database.

3.2.1.1 LIDAR backscatter data importation

1. The ASCII files header records are subjected to format consistency checks. Files failing these checks are excluded from the analysis, and an error message is recorded. Numerical data contained within the header are also subjected to minimum and maximum tests for physical reasonableness. Data failing these checks are flagged.

2. After the reading of header information the remaining files are read for backscatter data. At this stage individual shot records are invalidated or flagged. Each record contains data for an individual backscatter pulse train or “shot”.

3. File formatting inconsistencies result in the VID being flagged or excluded from the backscatter analysis depending on the severity of the inconsistency.

4. Nonnumeric time values (milliseconds) for shots are invalidated.

5. The first 4 records for both ambient and vehicle data are invalidated, due to instabilities in these initial measurements.

6. Time values out of strict chronological order are invalidated.

7. Time values less than zero or greater than 10 minutes are invalidated.

8. Ambient data time values greater than 700 milliseconds are flagged.

3.2.1.2 LIDAR extinction data importation

1. File formatting inconsistencies result in the VID being flagged or excluded from the extinction analysis depending on the severity of the inconsistency.

2. Time values out of strict chronological order are invalidated.

3. Extinction background data are subjected to the following filters:

   - Data less than or equal to -5 V are invalidated.

   - The median and interquartile range are calculated and data falling below the median minus three times the interquartile range are invalidated.

   - The last two surviving extinction data points are invalidated as a precaution to assure that no bad points from the occultation of the beam are included as the car passes through.

3.2.1.3 RSD data importation

1. File formatting inconsistencies result in termination of RSD data importing or invalidation of individual records depending on the severity of the inconsistency.

2. RSD CO_2 individual shot data falling outside a three sigma filter are invalidated.

3.2.1.4 Data processing procedures and QA

1. Correlation statistics are invalidated for sample sizes smaller than 10 points.

2. LIDAR shot traces are examined and traces divided into classifications of good, flat, or clipped, and flagged as such. Flat traces are traces falling between -5 and 10 mv. Clipped traces are traces with 4 consecutive data points falling below

   ½ * VR – VO,

   where VR and VO are the voltage range and voltage offset read from the ASCII header. Good traces are those not flagged as flat or clipped, and only good traces are used in backscatter calculations.

3. Before quadrature to obtain backscatter values, trace data are subjected to range correction factors to correct for optical differences over the different path lengths. Quadrature limits are determined by user input at the beginning of data processing.

4. Various averages are subjected to the following tests and filters. All calculations exclude data flagged as invalid.

- Backscatter records with time values falling outside a user defined "region of interest" are not used.

- Extinction records with time values falling outside the aforementioned user defined "region of interest" are not used.

- Extinction records with DRI CO_2 values falling below a user specified limit are not used.

- If the number of data points in the average of the ambient backscatter trace (uncorrected) averages for a VID fall below 10, the backscatter record is invalidated. Otherwise, if the number of data points fall below 30, the backscatter record is flagged.

- If the number of data points in the ambient backscatter average for a VID fall below 10, the backscatter record is invalidated. Otherwise, if the number of data points fall below 30, the backscatter record is flagged

- If the number of data points in the exhaust backscatter average for a VID fall below 10, the backscatter record is invalidated. Otherwise, if the number of data points fall below 30, the backscatter record is flagged

- If the number of data points in the ambient UV average for a VID fall below 10, the extinction record is invalidated. Otherwise, if the number of data points fall below 30, the extinction record is flagged.

3.2.1.5 Data processing using additional queries

Exhaust particle concentration content is calculated from the regression slope of integrated LIDAR backscatter with RSD3000 CO_2 (BKCO2M). The equation used fo the calculation follows:

$$Exhaust\ Concentration\left(\frac{mg}{m^3}\right) = \left(0.002 \cdot BKCO2M\left(\frac{Rayleigh}{ppm\ CO_2 \cdot m}\right)\right)(L\ m)\left(X\ \frac{ppm\ CO_2}{ppm\ C_T}\right)\left(0.15\ \frac{ppm\ C_T}{ppm\ Exhaust}\right)\left(\frac{10^6\ ppm}{1}\right)\left(C_{PM}\ \frac{mg\ particles}{m^3 \cdot Rayleigh}\right) \quad (3-1)$$
$$= 300 \cdot L \cdot X \cdot C_{PM} \cdot BKCO2M$$

where L = LIDAR path length (m), X = mixing ration of CO_2 to C_T, C_{PM} = mass density constant (see Chapter 2), and BKCO2M is the slope of integrated LIDAR backscatter to RSD CO_2 signal. BKCO2M is based on the CO_2 signal output from the RSD instrument that is not reported in standardized units. BKCO2M is be converted into units of Rayleigh/ppm CO_2 m in the first term on the right hand side of (3-1) by multiplying the value by 0.002.

3.2.2 Conversion of Pure Exhaust Content to Fuel Based Emissions Factors

The RSD3000 and the LIDAR instrumentation report pollutant measurements in terms of a atmospheric mixing ratio (i.e. % or ppm) for gases or a mass concentration (i.e., mg/m^3) for particles. These values represent the concentration of a pollutant in the pure exhaust from the engine. For the purpose of emissions inventories, a fuel based emissions factor with units of g pollutant per kg fuel burned is preferred. The assumptions and calculations used to convert pollutant concentration to fuel based emissions factors are presented here.

Gasoline is composed of a wide variety of hydrocarbons. Fuel combustion can be simplified to the following chemical equation assuming a H:C fuel ratio of 2 for non oxygenated fuels:

$$CH_2 + m(0.21O_2 + 0.79N_2) \rightarrow aCO + bH_2O + c(C_3H_6 + invisible\ C_3H_6) + dCO_2 + eNO + \left(0.79m - \frac{e}{2}\right)N_2 \quad (3-2)$$

Note the *invisible C_3H_6* refers to the unseen exhaust hydrocarbons associated with remote sensing measurements of hydrocarbons using filtered infrared light (Singer et al., 1998). Using the assumptions and derivation shown in Appendix C (Gary Bishop, personal communication), the fuel based emissions factor can be calculated as:

$$EF_{CO}\left(\frac{g\ CO}{kg\ fuel}\right) = \frac{28 \cdot 860 \cdot \frac{CO}{CO_2}}{\left(1 + \frac{CO}{CO_2} + 6\frac{HC}{CO_2}\right) \cdot 12} = 2007\left(\frac{CO}{CO_2 + CO + 6HC}\right) \quad (4-3)$$

$$EF_{HC}\left(\frac{g\ HC}{kg\ fuel}\right) = \frac{2 \cdot 44 \cdot 860 \cdot \frac{HC}{CO_2}}{\left(1 + \frac{CO}{CO_2} + 6\frac{HC}{CO_2}\right) \cdot 12} = 6306\left(\frac{HC}{CO_2 + CO + 6HC}\right) \quad (4-4)$$

$$EF_{NO}\left(\frac{g\ NO}{kg\ fuel}\right) = \frac{30 \cdot 860 \cdot \frac{NO}{CO_2}}{\left(1 + \frac{CO}{CO_2} + 6\frac{HC}{CO_2}\right) \cdot 12} = 2150\left(\frac{NO}{CO_2 + CO + 6HC}\right) \quad (4-5)$$

$$EF_{PM}\left(\frac{g\ PM}{kg\ fuel}\right) = \frac{\left(\frac{1\,g}{1000\,mg}\right)\left(860\frac{g\ C}{kg\ fuel}\right)\cdot PM}{\left(CO_2 + CO + 6HC\right)\left(12\frac{g\ C}{mole}\right)\left(41\frac{mole}{m^3}\right)} = 0.00175\left(\frac{PM\left(\frac{mg}{m^3}\right)}{CO_2 + CO + 6HC}\right) \quad (4-6)$$

Where the gas concentrations CO_2, CO, HC, NO have units of atmospheres and PM has units of mg/m^3. The highest measured emissions of NO and HC were 0.6% while typical emissions of CO_2 + CO are 15%. The fuel based emissions factors were calculated only if valid measurements were available for CO and CO_2. If HC was also valid, its concentration was included in the emissions factor calculation.

3.2.3 License Plate Transcription

In order to relate emissions measurements to the vehicle types measured, a camera was used to take digital pictures of the vehicle's license plate as it passes the emissions test area. The RSD program stores these images to a file that is later converted into a smaller JPG format file for subsequent license plate transcription. The JPG files usually contain images of five to ten thousand vehicle license plates collected during a day. The information about each car's emissions, speed, acceleration, and time of measurement was stored on a separate VDF file.

The JTAGEDIT program was used for transcribing the license plate records. JTAGEDIT requires the VDF file and the JPG file in order to link the license plate data to the emissions record. Students from UNLV manually entered the license plate data by examining the digital images. The license plate information entered by the reader was automatically added to the VDF file by the JTAGEDIT program.

The JTAGEDIT program manual defined the procedures for license plate transcription (ESPI, 1999). The first attribute assigned while reading the license plate was the vehicle type (i.e. light duty vehicle, trailer, motorcycle, big tractor trailer, etc). This step permitted the identification of heavy duty diesel tractors when they were pulling a trailer. The license plate on the trailer is not associated with the haul vehicle and thus would yield a useful record when the license plate number was linked to the vehicle registration database. The second step in the transcription process was to read the license plate and identify the state where the vehicle was registered.

A booklet with images of different license plates from each state was used to identify appropriate states for out of state vehicles. The majority of out of state vehicles were from California, Arizona, Oregon, Utah, Texas, and Colorado. More specific categories existed for Nevada vehicles, and JTAGEDIT permitted the user to mark special plates including affinity (i.e. university and different organizations), disabled, dealer, state exempt, and veterans.

A substantial number of images were unreadable. In some of the images cars would be out of view because the camera did not trigger at the right time, cars were unusual size, or cars would pass close to one side of the test area. Data flags were assigned to the records when the license plate could not be read or when there was an obstruction (e.g. a trailer hitch, that prevented an accurate transcription of the plate).

When license plate transcription was completed, the VDF files were processed to produce ASCII text files. These files were then imported into a MS Access relational database for linking with Department of Motor Vehicles registration records.

3.2.4 Joining Remote Sensing Data with DMV Database

A database of all registered vehicles in Clark County spanning the period 01/01/00 to 04/20/02 was obtained from the Nevada Department of Motor Vehicles (DMV). The data contained 2.2 million records of following data fields: license plate number, vehicle identification number (VIN), fuel type, gross vehicle weight (GVW), and date of registration. The DMV assigned a new record to vehicles whenever the vehicle was reregistered.

License plates transcribed using the JTAGEDIT program and supplied by the DMV occasionally had spaces mixed in with their alphanumeric characters. To maximize the number of successful matches between the emissions and registration databases, non-alphanumeric characters were removed from license plate fields. The emissions and registration databases were joined on the license plate field when the date of measurement was later than the date of registration. For joins, with more than one registration record corresponding to an emissions record, the most recent registration record was used. The results of this query produced a table with one record for each emissions measurement and the corresponding registration data when a license plate match was successful.

3.3 Secondary Data Validation Steps

Upon examination of the original validated remote sensing data set, numerous records were found to be physically inconsistent with known exhaust measurements. A secondary set of data validation criteria were developed to eliminate these measurements. Special care was taken to ensure that the criteria would not introduce a bias into the remaining set of valid measurements.

3.3.1 RSD3000

The validation criteria for the RSD3000 emissions measurements have been developed over many years of testing. These criteria are applied to the data as it is collected. The data acquisition program flags invalid data, but the original raw data is stored in the database for subsequent analysis.

Table 3-2 summarizes the criteria that the RSD3000 uses to validate a CO_2 measurement. The first criteria in the table ensures that a minimum number of the CO_2 readings in the post vehicle signal are within the detectable range. The second criteria are selected to

ensure that a measurable plume is detected immediately after the vehicle and that that plume dissipates after more than 250 milliseconds. The last criteria ensures that reasonable numbers are obtained for the composition of the exhaust.

Table 3-2. RSD3000 data validation criteria for exhaust gases measure with the IR channel.

Variable	*Description*	*Criteria*
CO2/REF Voltage	Normalized voltage used to measure CO_2 in pre-vehicle and post-vehicle air.	• At least 10 post vehicle readings must have a relative change from the pre vehicle readings within –0.25% and 12% • In the first 25 readings post vehicle at least 8must have a change from the pre car average by more than 0.5% • In the last 25 readings post vehicle, at least 4 must not change from the pre vehicle average by more than 0.2% • The sum of the calibrated CO_2 plume content must be greater than 6% and less than 16%
CO/REF Voltage	Normalized voltage used to measure CO and pre vehicle and post vehicle air	• The sum of the calibrated CO_2 + CO plume content must be less than 21%

3.3.2 LIDAR Validation

This project is the first field deployment of the LIDAR particle sensor for vehicle remote sensing. The data validation algorithms are being formulated and evaluated as experience is gained with the instrument. The LIDAR particle sensor makes measurements at approximately 200 Hz. Post processing analysis of the data indicated that erratic readings were observed under certain circumstances. Table 3-3 summarizes the criteria used to filter out these erratic readings. Criteria are limited to the number of data points collected and the pre car ambient backscatter. These criteria should not bias the resulting particle measurements because they are not based on the magnitude of the post vehicle backscatter signal.

Table 3-3. Criteria used to validate LIDAR remote sensing data.

Variable	*Description*	*Criteria*
numxsBkAvg	Number of LIDAR backscatter returns in post vehicle measurement	≥ 60
numbkAmbAvg	Number of LIDAR backscatter returns in pre vehicle measurement	≥ 30
bkAmbAvg	Average of LIDAR backscatter returns (Rayleighs)	< 5

4. QUALITY ASSURANCE

Emissions factors measured by remote sensing are reported in units of pollutant mass per mass of fuel burned. These factors are derived from the slope of the concentration of the pollutant of interest versus the total concentration of carbonaceous species (i.e. CO_2, CO, and HC) that are used to scale plume dilution. The assumption is made that the correlation between the pollutant of interest and the plume dilution species is due solely to the exhaust of the tested vehicle. Thus the quality of the remotely sensed emissions factor is dependent on the quality of the measurements of the pollutant of interest (i.e. particles, CO, NO_x, etc) and the quality of the measurements used to scale the plume dilution.

The remote sensing optical measurements are based on either light transmittance or light reflectance. These measurements are calibrated by introducing a gas of known concentration into all or part of the instruments optical path and measuring the resultant transmittance or reflectance. The basis for the calibration is the integrated path concentration of the pollutant of interest with units of $\mu g/m^2$ or ppm m. Since the optical path of the transmittance measurements for CO_2, CO, NO_x, and HC are all the same for a given measurement setup, the path length terms in the numerator and denominator cancel out of the emissions factor calculation. The reflectance measured by the LIDAR particle remote sensing system is not path length dependent but measurements of the plume dilution species are path length dependent. Thus, in order to calculate a particle emissions factor from the LIDAR and gas measurement, optical path length must be factored into the calculation. Whenever possible, data quality will be addressed in terms of the fundamental measurement (i.e. transmittance, reflectance, and path length), however in some cases only the slope relating two species is known.

4.1 Measurement Accuracy

4.1.1 RSD

With the exception of HC, each pollutant (CO, CO_2, and NO) is a specific gas, which can be unambiguously measured and calibrated by comparison of RSD response to a known concentration. The HC from tailpipe exhaust is a very complex mixture of oxygenated and unoxygenated hydrocarbons. The particular wavelength chosen measures carbon-hydrogen (C-H) stretching vibrations that are present, but it cannot do so equally for all HC compounds due to variations in the C-H bond strength for different species (Singer et al., 1998). Thus, the results on an individual vehicle cannot be expected to correlate perfectly with a flame ionization detector, or with ozone forming reactivity, or with air toxicity, since the three are not perfectly correlated among themselves. However, for gross polluter detection, the HC channel of this remote sensing system is entirely adequate.

There are two separate calibration procedures performed on every remote sensing unit. The first consists of exposure in the laboratory at a path length of about 22 feet to known absolute concentrations of NO, CO, CO_2, and propane (surrogate HC) in an 8 cm flow cell. The calibration curves generated are used to establish the fundamental sensitivity of each detector/filter combination absorbed by the gas of interest, and to derive an equation relating the reduced voltages to gas concentrations. As expected, CO and CO_2 curves are non-linear. Because of the small amount of HC and NO to which the instrument is exposed, the HC and NO curves are closer to linear and are approximated by a linear equation. The equations for the calibration lines become an empirical component of the instrument data analysis algorithm.

Before, during and after each day's operation in the field, the instrument undergoes field calibrations performed on location. A puff of gas designed to simulate all measured components of the exhaust is released into the instrument's path from a cylinder containing certified amounts of NO, CO, CO_2, and propane. The ratio readings from the instrument are compared to those certified by the cylinder manufacturer. Because of the curvature of the response functions, particularly for CO_2, the field calibrations usually show higher ratios to CO_2 than those derived from the laboratory tests. The field data are adjusted by that day's correction factors.

The remote sensing technique has been shown to give accurate readings for CO by means of double-blind studies of vehicles both on the road and on dynamometers (Lawson et al., 1990; Stedman and Bishop, 1990). EPA has shown that the readings are comparable to laboratory readings from a vehicle on a dynamometer (Knapp, 1992). Lawson and coworkers used a vehicle with variable emissions under passenger control to show the correctness of the on-road readings (Lawson et al. 1990). Independent studies (Ashbaugh et al., 1992) show that the CO readings are correct within ±5% and HC within ±15%.

4.1.2 LIDAR

Accuracy of a measurement method is typically determined by comparison with data acquired by an alternate and proven measurement method. The LIDAR is the first method of its kind to remotely measure particle emissions from in use vehicles. Although the light scattering measurement is calibrated with gases in the laboratory (see chapter 2), the LIDAR measurement has yet to be compared with extractive particle measurement techniques (e.g. filter based sampling methods). Exhaust emissions factors generated by the LIDAR instrument are based on theoretical assumptions about the scattering properties of the vehicle exhaust aerosol.

Future experiments are planned as part of SNAQS phase 3 to collocate the LIDAR with standardized particle and gas measurement methods. These experiments are intended to evaluate the accuracy of the theoretical assumptions used to estimate the particle emissions factors.

4.2 Measurement Precision

The precision of an analytical instrument is the repeatability of its response under otherwise identical input conditions. The difficulty in ascertaining repeatability for remote sensing is that vehicle emissions are inherently variable under seemingly similar conditions. With large numbers of vehicles, or with several individual passes of a single vehicle, repeatability can be investigated. These results will be included in the final report. However, laboratory tests provide the only truly repeatable input conditions and are discussed here.

4.2.1 Instrument Repeatability

This subsection describes the precision of the RSD and LIDAR instruments operating in controlled laboratory conditions.

4.2.1.1 RSD Repeatability

Figure 4-1 through Figure 4-3 show the results for CO, HC, and NO_x respectively. Coefficients of variation (standard deviation divided by the mean) run between 1.5 and 2.4% for CO, 1.5 and 2.1% for HC, and 2.1 and 4.2% for NO_x, with absolute zero-level variability of 0.8% CO exhaust content, 44 ppm HC, and 33 ppm NO_x.

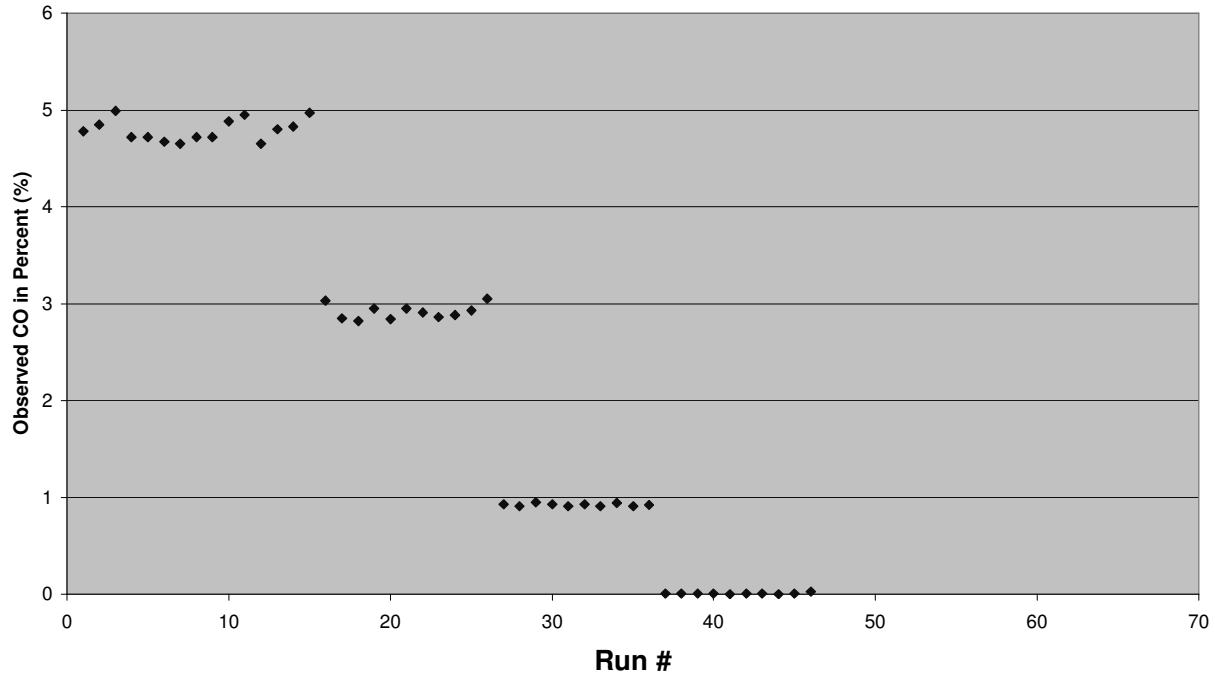

Figure 4-1. CO certification results for Unit R523 conducted in 10-August-2000.

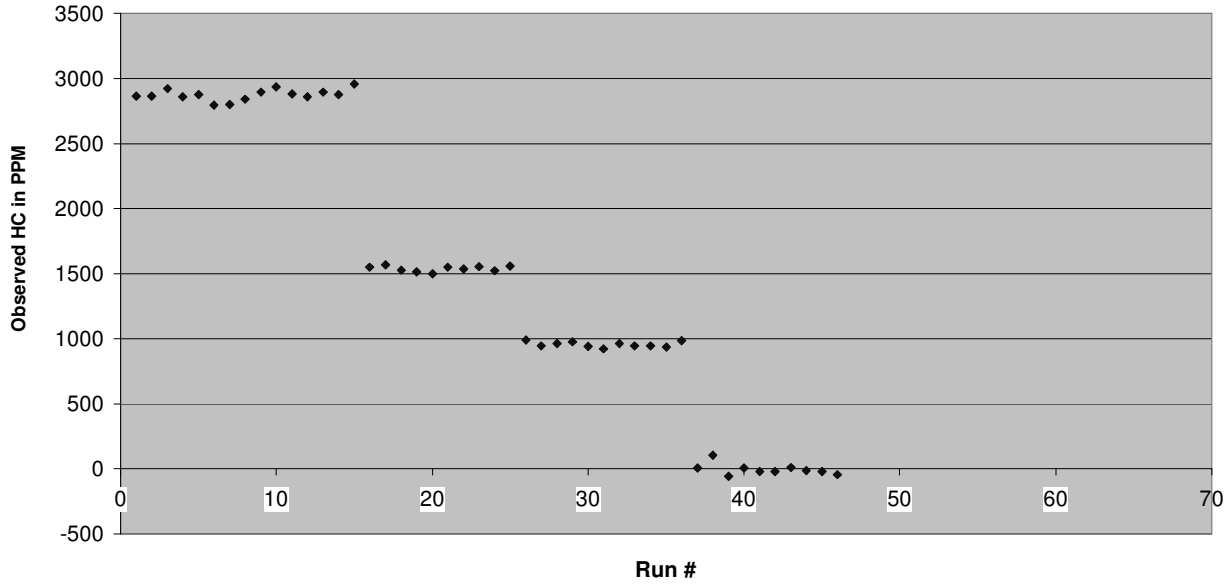

Figure 4-2. HC certification results for Unit R523 conducted in 10-August-2000.

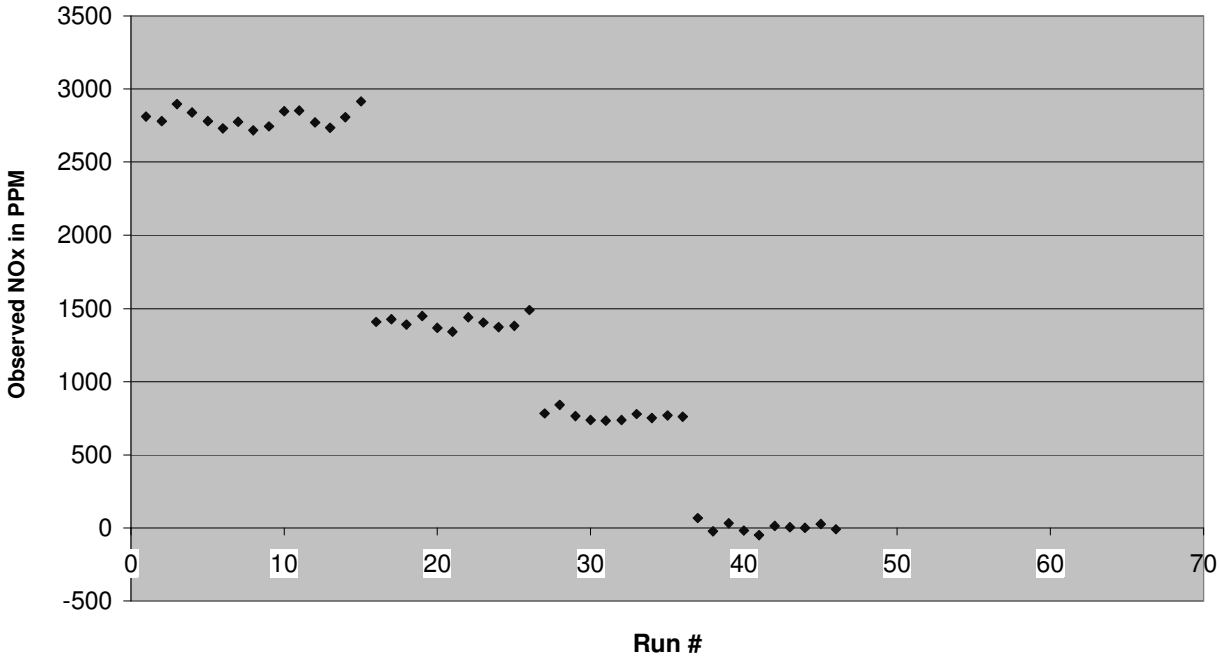

Figure 4-3. NO_x Certification Results for Unit R523 conducted in 10-August-2000.

4.2.1.2 LIDAR Repeatability

LIDAR calibration and repeatability measurements are performed by use of a calibration tube. Figure 4-4 shows a schematic diagram of the calibration tube. The tube fits over the telescope and has an entry hole for the laser. Gases can be introduced from the far end of the tube and fill toward the front. Particle free air (HEPA filtered) is introduced and should have a backscatter of 1 Rayleigh. A tube/no-tube correction is performed by using lab ambient air before, during and after the calibration tube is in place. A range correction is developed as described in Section 2.3.2.

Figure 4-5 shows the results for the range corrected values. Note that air, which should be exactly one for all range gates, varies between 1.09 and 0.97 along the range (right-hand axis). Thus, any one shot has a range correction error of ±10%. Air comes back slightly higher than one on average because the CO_2 values are generally lower than the 2.96 Rayleigh value (see Section 2.3.2).

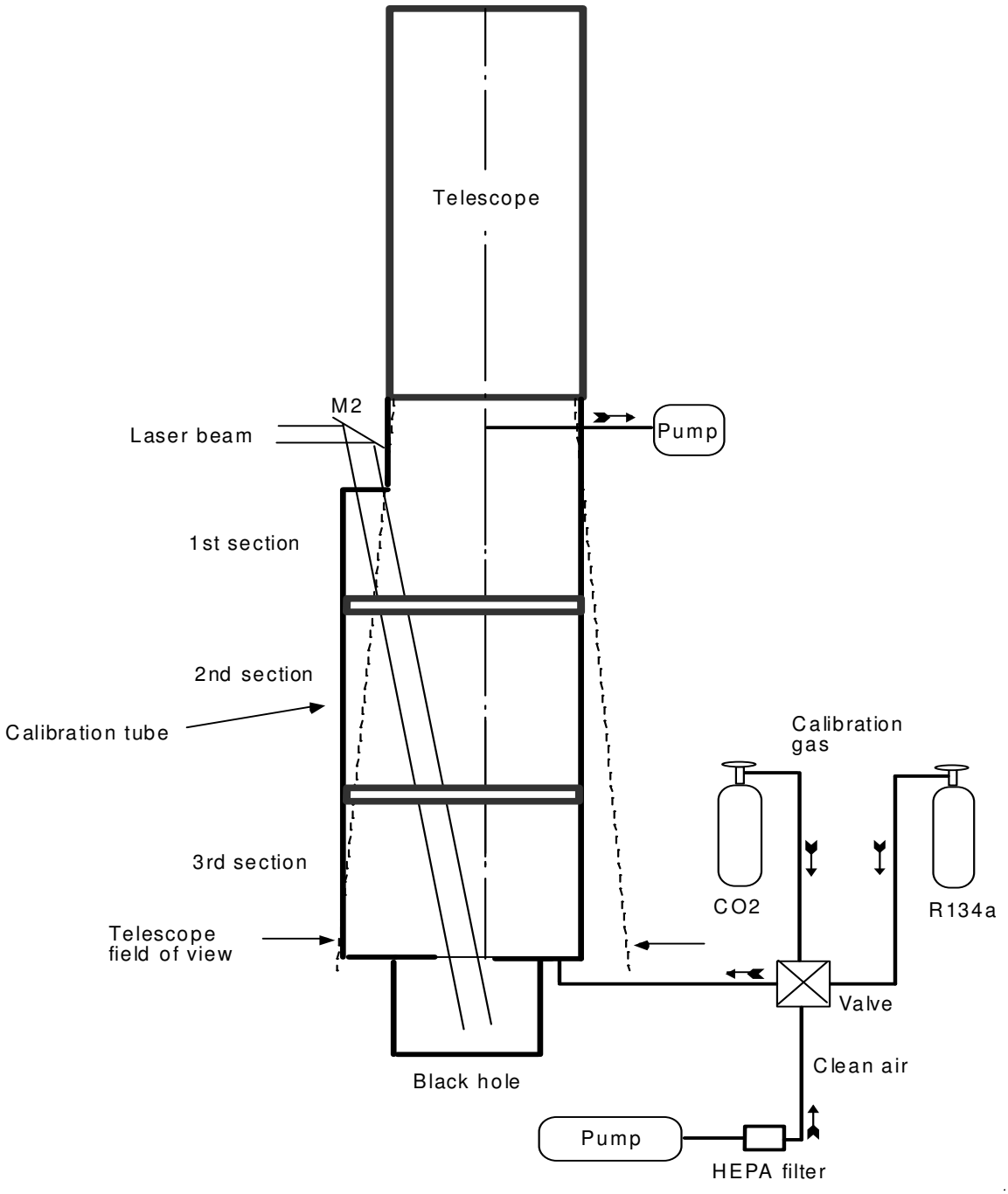

Figure 4-4. LIDAR calibration tube.

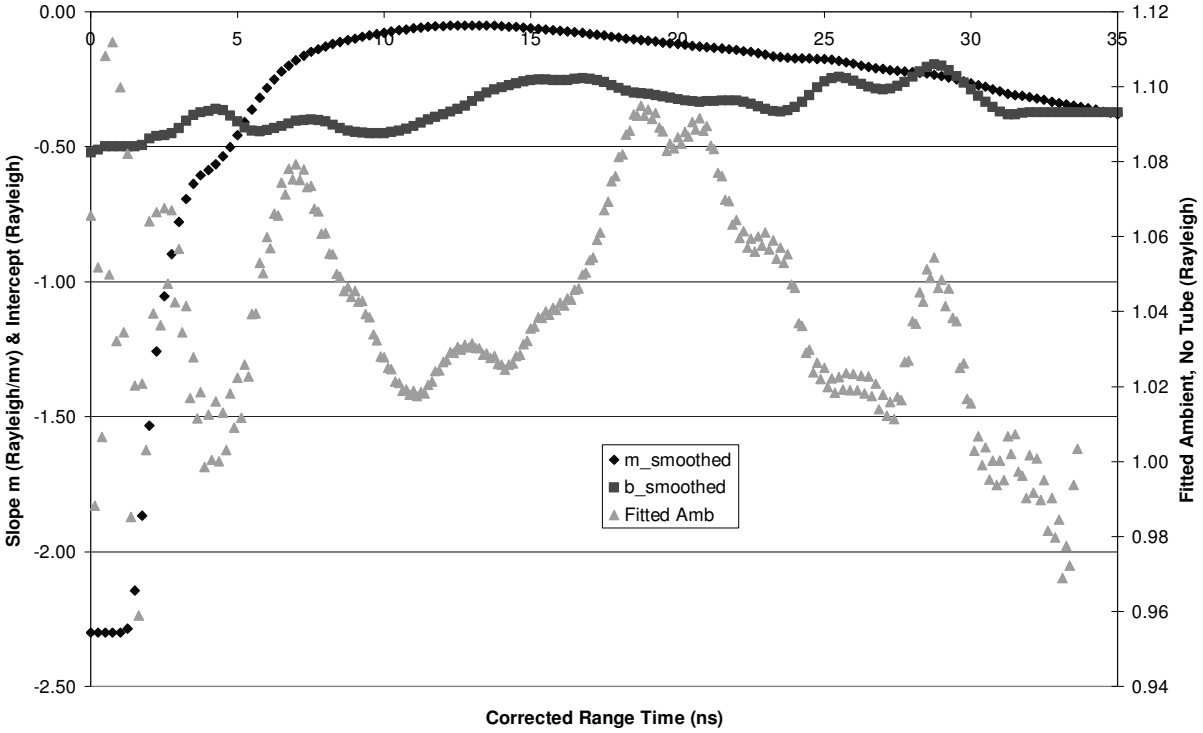

Figure 4-5. LIDAR Range Correction.

4.2.2 Emissions Factor Repeatability

The definitive measure of remote sensing instrument repeatability is the comparison of calculated emissions factors for vehicles that are repeatedly driven through the test section. Because operating mode can cause substantial differences in instantaneous emissions from vehicles, criteria are applied to speed and acceleration measurements to ensure that the vehicles tested are operating under comparable modes.

A subset of vehicles was selected from the validated emissions factor database using the following criteria: (1) more than one measurement of a vehicle on the same date, (2) valid CO, HC, NO, and PM emissions factors, (3) range of vehicle speed < 5 kph, and (4) range of vehicle acceleration < 1 kph/s. A total of 49 vehicles met these criteria out of more than 50,000 measurements. The correlation of these repetitive measurements is shown in Figure 4-6. The results of the first emissions factor measurement for a vehicle are shown on the x-axis and the results of the last measurement from the same vehicle on the same day are shown on the y-axis. (Only 2 vehicles of the 49 met the set criteria with 3 or more measurements.) The error bars on the figure are based on the propagated standard error of the slopes of the pollutant of interest with CO_2. No error bars are shown for NO because the calculation of the NO plume content by the RSD3000 is a proprietary algorithm with RSTI and the regression parameters were not available for analysis. A line of unit slope and intercept of 0 is shown in the figures to demonstrate how the measurements differ from each other. Several points on the CO comparison panel are far removed from the 1:1 line with respect to the size of the error bars. These points represent vehicles that had very different measured emissions factors although the operating mode (based of VSP) were similar.

The operating mode of an engine may vary substantially within a given range of VSPs. Depending on the transmission gear, a vehicle may be operating with high RPMs or low RPMs and produce the same power output. These differences in modes may account for the inconsistencies observed with some of the CO measurements. The scatter of the HC and PM emissions factors appear to be more dependent on the precision of the measurement itself since the points are not as far from the 1:1 line with respect to the size of the error bars.

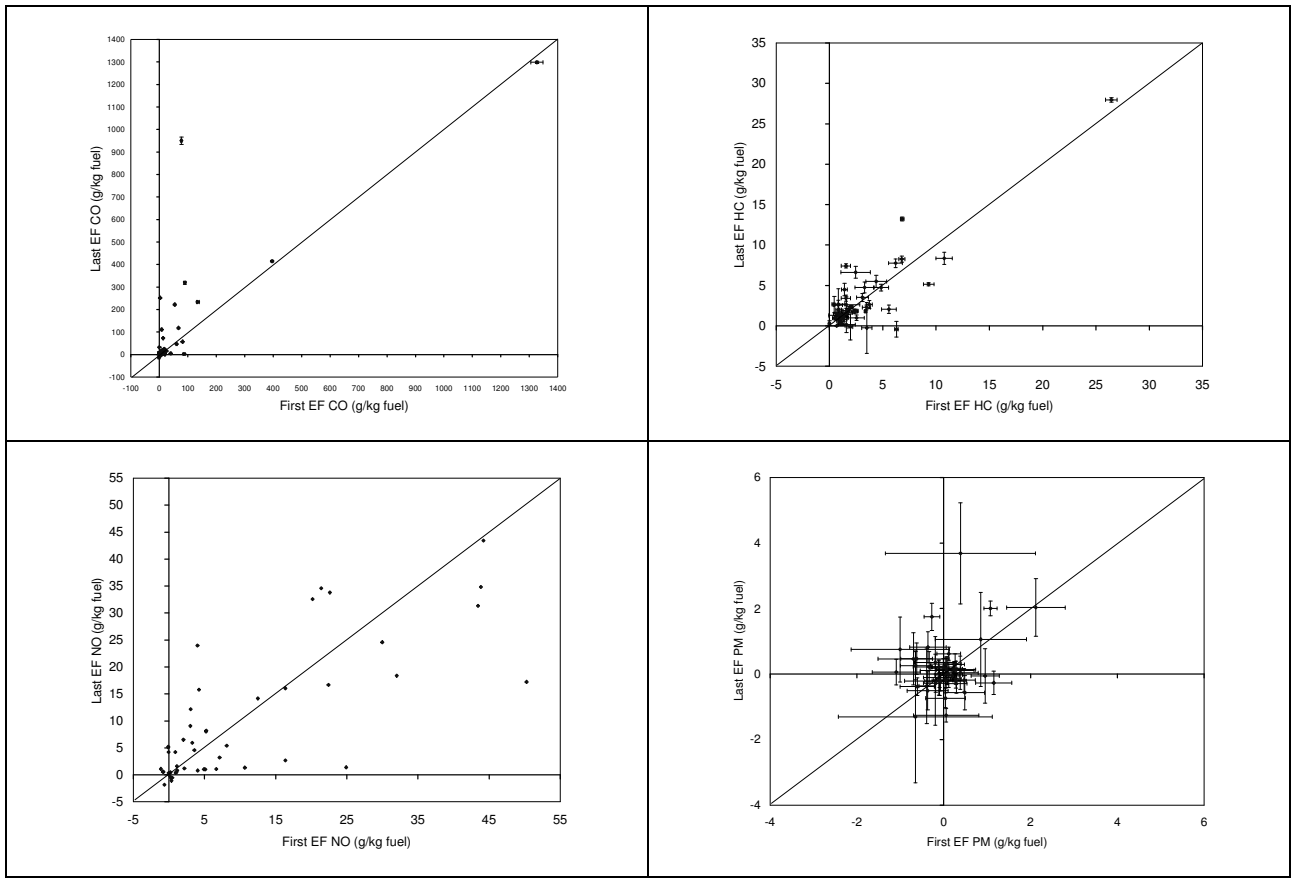

Figure 4-6. Correlations of replicate emissions factors from 49 vehicles measured on the same day with similar operating conditions.

A quantitative measure of the uncertainty of a single RSD measurement can be inferred from the regression of the repeated measurements. The standard error of the predicted y value in the regression represents the uncertainty of one measurement with respect to a repeated measurement. Using the data in the figures above the standard error of the y values are 110 CO g/kg fuel, 2 g HC/kg fuel, 7 g NO/kg fuel, and 0.7 g PM/kg fuel.

4.3 Minimum Limits of Detection (MDL)

Detection limits are defined as the lowest value of a measurement that can be distinguished from 0 with some confidence. Typically, the detection limit is calculated by measuring the standard deviation of a measurement with a value known to be 0. The MDL is equal to two times the standard deviation (i.e. 95 percent confidence that the measurement is > 0) or three times the standard deviation (i.e. 99 percent confidence that the measurement is > 0). Because the remote sensing emissions measurements are calculated from the ratio of the

pollutant of interest (i.e., CO, HC, NO_x, or particles) to the total of the fuel combustion products (CO_2, CO, and HC), the limit of detection for the emissions measurement depends on the precision of all of the measurements used in the calculation. For example, the emissions measurement detection limit of a pollutant measured in a dense plume will be less than the emissions factor detection limit when there is very little plume present to measure. By controlling for the range of the integrated CO_2 absorbance measured in the exhaust plume, the precision of the measurement of the species of interest can be quantified.

For each vehicle measured, the slope and its standard error are calculated for the regression of CO, HC, PM, and "smoke" with CO_2. (The parameter "smoke" is calculated from the RSD3000 3.9 μm wavelength absorbance channel and is considered to be a qualitative indicator of particle emissions.) Emissions factors are calculated as a function of the regression slope. When no statistical relationship is measured between the pollutant of interest and CO_2, the standard error of the slope provides useful information about the uncertainty of the emissions factor measurement. To calculate the MDL, the group of points ranging from the 45^{th} percentile CO_2 Volume (375 ppm m CO_2) to the 55^{th} percentile CO_2 Volume (432 ppm m CO_2) (i.e. 0.5 second average column CO_2 post vehicle above background) was selected from the set of exhaust measurements. These 9,202 measurements represent the median measurable plume strength of all 148,247 vehicles passing the remote sensors. (Note: only 62% of vehicles passing the sensors had measurable CO_2 plumes.).

The lower panels of Figure 4-7 through Figure 4-10 are scatter plots of the standard error of the emissions factor on the y-axis versus the emissions factor on the x-axis for the pollutants CO, HC, PM, and smoke. Figure 4-7 shows that the standard error of the emissions factor for CO increases as the emissions factor rises. This behavior indicates that the uncertainty of the CO emissions factor has both an absolute and a relative component. The absolute uncertainty is the standard error of the emissions factor when the emissions factor is 0. The relative uncertainty is the slope of the standard error of the emissions factor vs. the emissions factor itself. The MDL for the remote sensing measurements is calculated as two times the y-intercept of the regressed line between the standard error of the emissions factor and the emissions factor.

The scatter plots for HC, PM, and smoke show a different trend than observed for CO. In these figures, the relationship between the standard error in the emissions factor is not as statistically significant ($R^2 \leq 0.02$). These results indicate that the absolute error overwhelms the relative error for the range of emissions factors measured in the vehicle fleet. For the case of smoke (Figure 4-10), an insignificant relationship is observed between the standard error and the emissions factor. All of the uncertainty in the smoke measurement can be explained with the absolute error.

The relative size of the standard errors to the measured emissions factors are shown in the upper panels of Figure 4-7 through Figure 4-10. For each pollutant, the emissions factors were rank ordered and the average of the decile values were calculated. The average standard error for each decile group was also calculated. The column charts show the distribution of emissions factors by decile with the average standard error of the corresponding emissions factors. The uncertainties of the CO and HC emissions factors are quite small relative to the emissions factors above the 40-percentile value. Below the 40-percentile level, most vehicles are very clean and below the detection limits for these measurements. The relative uncertainties of the PM and smoke emissions factors are substantially higher than those of CO and HC. PM emissions factors are greater than two times the average standard error only for the 95-percentile group.

Average smoke emissions factors are both significantly positive above the 50-percentile level and significantly negative below the 10-percentile level. The significantly negative values of the smoke parameter do not have a physical explanation with respect to vehicle emissions. One explanation for this behavior is that the wake of vehicles passing the RSD3000 will buffet the optical bench perturbing the CO_2 and IR absorbance signals simultaneously (Stedman, 2002). This interference would result in a correlation or anti-correlation between the CO_2 and IR absorbance in the post vehicle signal that is independent of the exhaust emissions.

The regression parameters from the lower panels of Figure 4-7 through Figure 4-10 are summarized in Table 4-1. Relative errors of less than 5 percent were observed for CO, HC, and PM emissions factors. The MDL's of each exhaust pollutant were calculated as two times the regressed y-intercept from the scatter plots. The fraction of vehicles with emissions factors greater than the MDL was calculated from the same subset of vehicles with 45 to 55 percentile CO_2 plumes strength. Although 74 percent of the CO emissions factors and 81 percent of the HC emissions factors were above the MDL, only 8 percent of the PM emissions factors were above the MDL. These results imply that refinements are needed on the LIDAR measurement to lower its MDL so that it may accurately measure a larger fraction of the vehicle fleet.

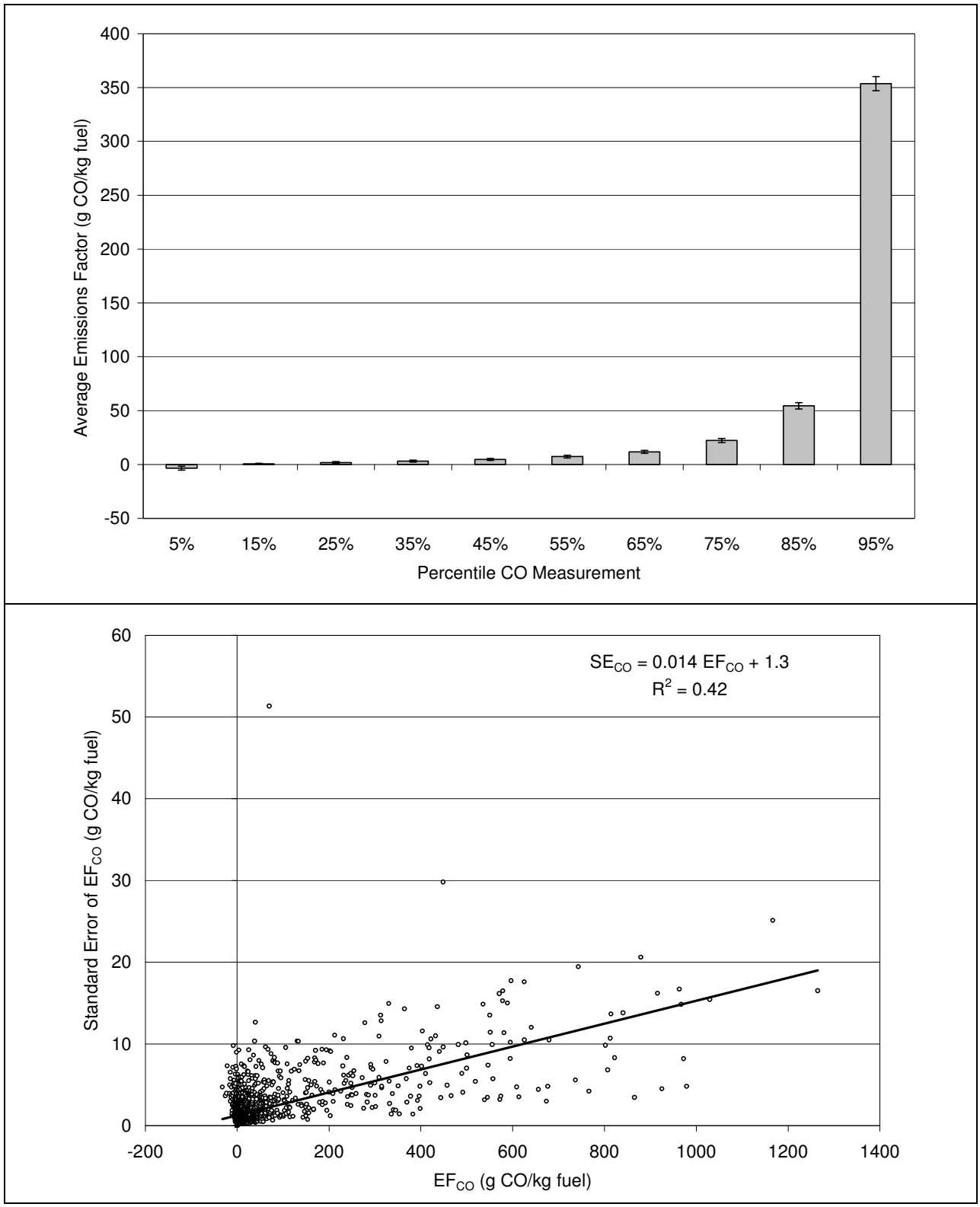

Figure 4-7. Comparison of standard error of CO versus CO2 slope versus absolute CO plume content.

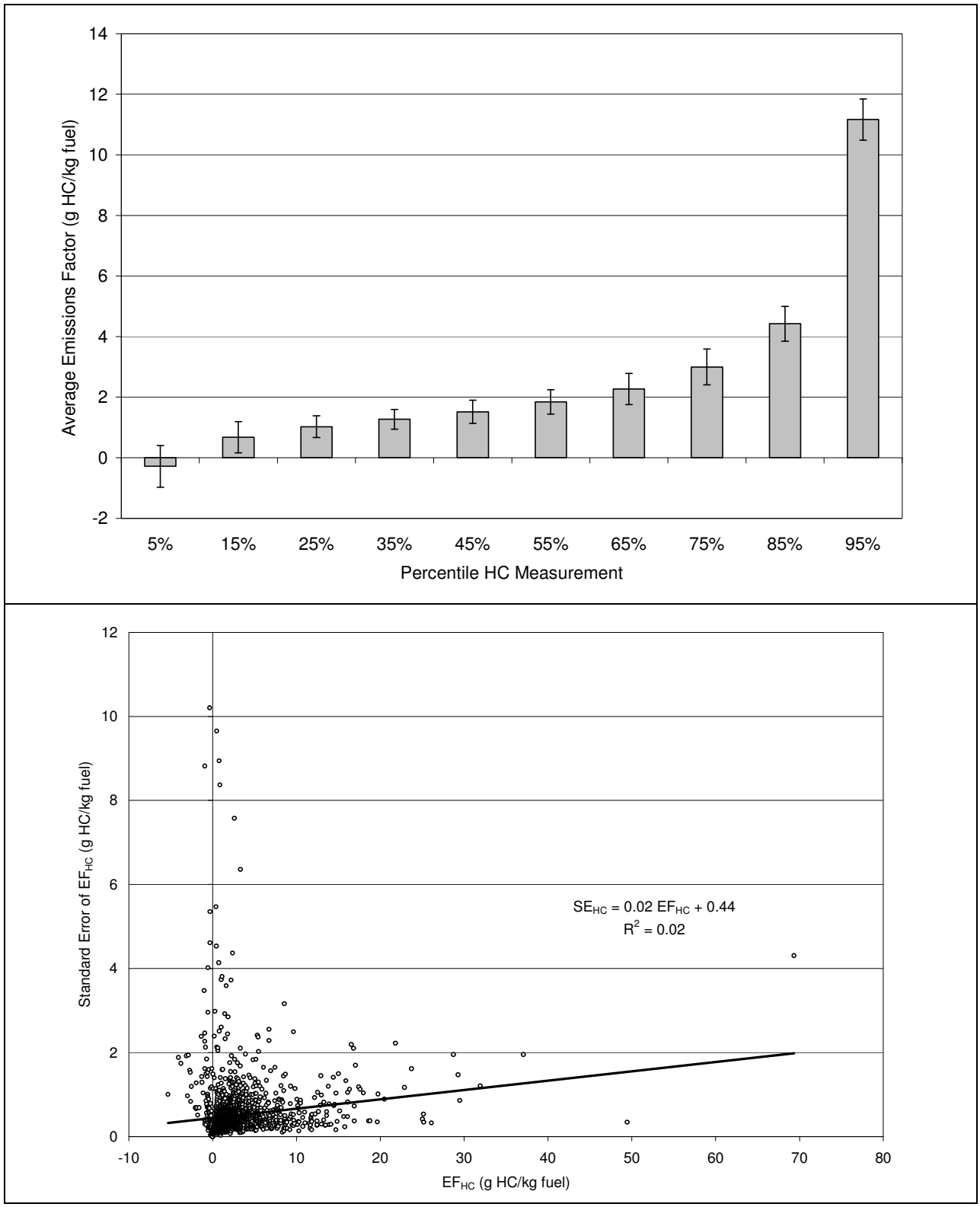

Figure 4-8. Comparison of standard error of HC emissions factor versus HC emissions factor.

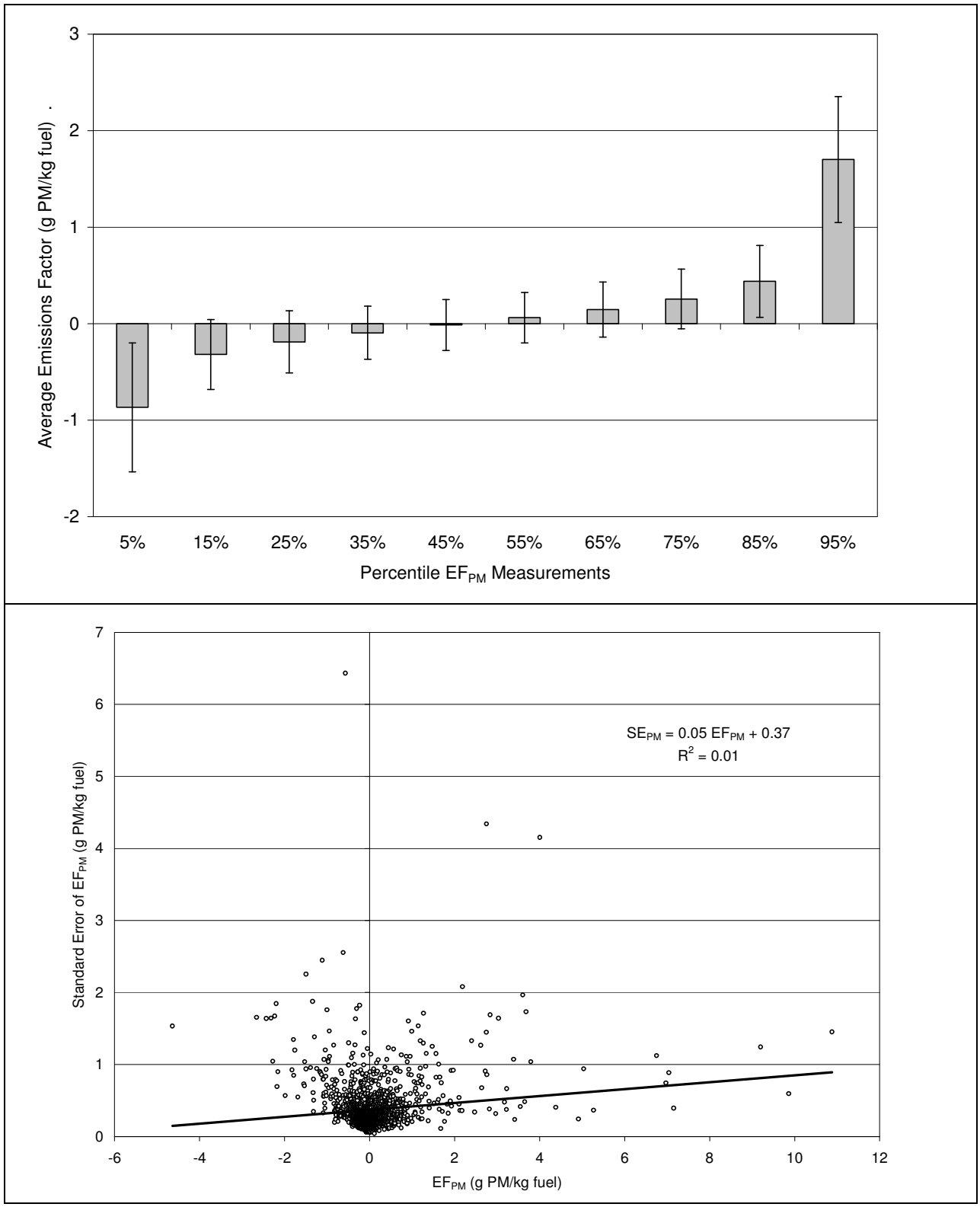

Figure 4-9. Comparison of standard error of PM emissions factor versus PM emissions factor.

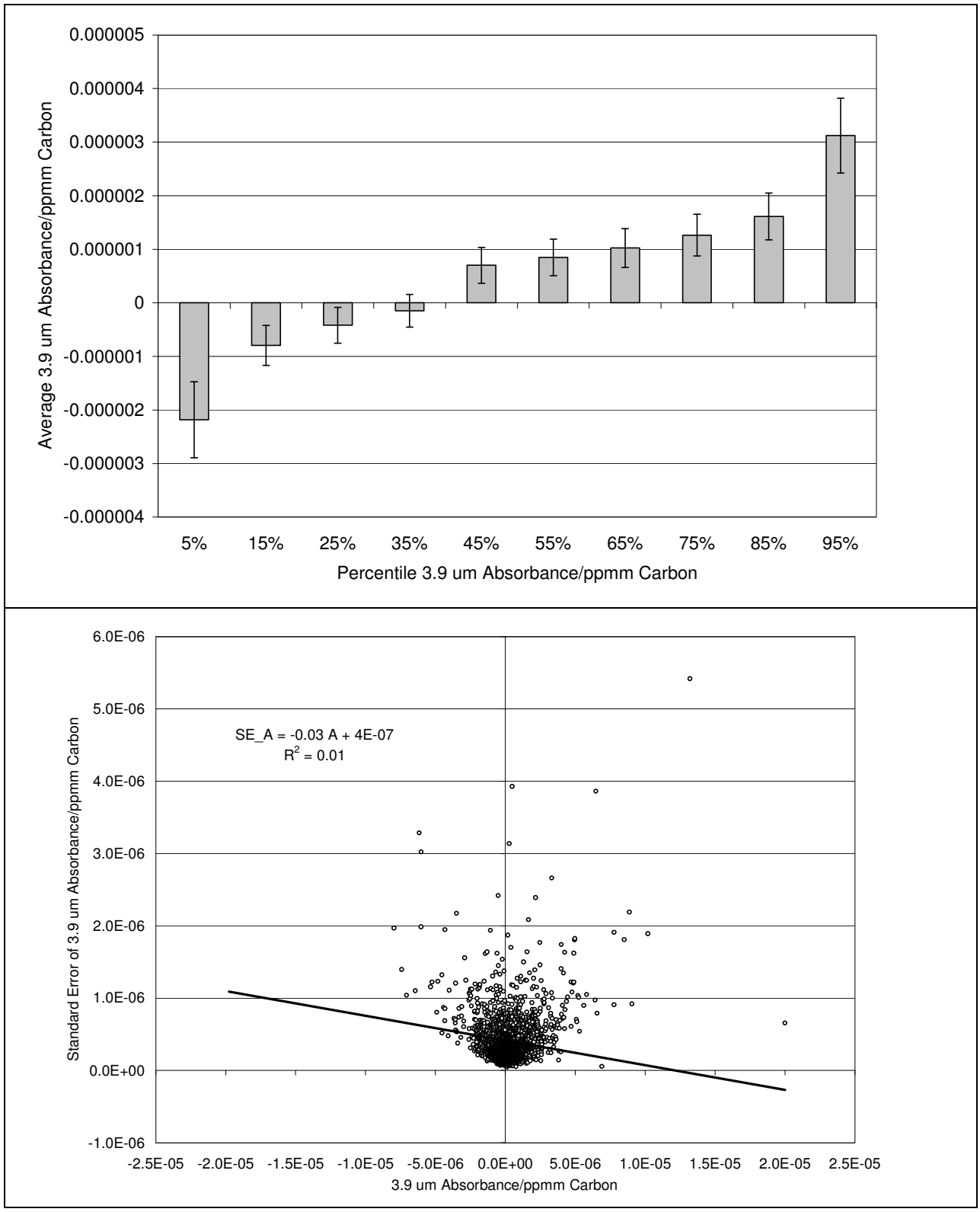

Figure 4-10. Comparison of standard error of 3.9 um Absorbance versus average values.

Table 4-1. Minimum detectable limits of CO, HC, PM, and 3.9 um Absorbance for median exhaust plume levels.

Pollutant	*Relative Error (%)*	*Absolute Error*	*Minimum Detectable Limit (2 * Absolute Error)*	*Percentage of vehicles with emissions greater than MDL*	*Percentage of vehicles with emissions less than -MDL*
CO	1.4	1.3 g/kg fuel	2.6 g/kg fuel	74%	5%
HC	2	0.44 g/kg fuel	0.9 g/kg fuel	81%	2%
PM	5	0.37 g/kg fuel	0.8 g/kg fuel	8%	4%
Opacity (3.9 μm Absorbance/ ppmm Carbon)	NA	4×10^{-7} Absorbance/ ppmm Carbon	8×10^{-7} Absorbance/ ppmm Carbon	28%	14%

4.4 Data Recovery

The number of valid measurements divided by the total number of measurements is defined as the data recovery and is expressed as a percentage. Data recovery statistics provide information on the success of the experiments and can be used to rapidly identify problems with measurements or sampling locations that have a low data yield. For vehicle remote sensing data, numerous measurements and data processing steps must be performed to produce a valid record. These steps include (1) capture image of license plate, (2) measure multiple exhaust species, speed, and acceleration of passing car, (3) read license plate from image, (4) match license plate to registration records, and (5) match registration record with address of registration. The success of one step generally precludes the success of subsequent steps. For example, if a license plate is not accurately transcribed and matched to registration information, the emissions record has no value for identification of high emitters or assembling inventories based on fuel and vehicle types. The data recovery rates of the remotely sensed exhaust measurements and vehicle registration information are described here in terms of the data processing steps.

4.4.1 License plate transcription

Table 4-2 summarizes data recovery statistics for the license plate transcription steps for each day and location surveyed with the remote sensing equipment. Overall, 57% of measurements had readable license plates.

The RSD3000 software used to acquire the license plate images uses the beam block and unblock trigger points to determine the proper timing to acquire the image of the vehicles license plate. It was observed in the field that a tailgating vehicle will reblock the beam before the picture has been processed. The image acquisition system may not have sufficient time to reset itself and acquire a new image of the tailgating vehicle. When this happens, two exhaust measurements are made, but no readable licence plate data is obtained. Other factors that

prevent successful license plate transcription include: camera out of adjustment, obscured license plate (i.e. too dark/bright or trailer hitch), and no license plate on vehicle.

For all measurements from 04/04/00 to 05/16/02, 42% (or 74% of license plates read) were matched to Nevada vehicle registration data. Potential causes for unmatched records include: vehicle registered outside of Clark County, inaccurately read license plate, and expired license plate.

Of all measurements, 0.8% (1.9% of vehicles with matched registration data) were registered diesel vehicles. In contrast, the average rate of "heavy truck/trailer" vehicles based on the captured image was almost twice as large at 1.4% of all measured vehicles. These two classifications are likely to represent different vehicles. Diesel engines are the preferred power source for on road heavy duty vehicles, yet when these vehicles are pulling trailers the license plate record will be associated with the trailer instead of the tractor. Thus the "heavy truck/trailer" classification may be a good indicator of heavy-duty diesel vehicles. However, the license plate reader may group non-diesel vehicles into this classification because the assignment of "heavy truck/trailer" is a subjective determination by the license plate reader. The vehicle registration determination of diesel vehicles may be a more accurate approach, but most tractors in operations are pulling trailers. Very few of these tractors can therefore be identified by their license plate number.

4.4.2 Remote sensing measurements

Exhaust measurements are made independent of the license plate and vehicles registration information. Table 4-3 shows the recovery statistics of the remote sensing speed, acceleration, and exhaust measurements. The speed and acceleration measurements had the highest overall data recovery of all measurements: 91%. Exhaust CO_2 is required for the success of all other exhaust measurements. Data recovery of CO_2 is related to the strength of the vehicles plume that in turn is dependent on the slope of the test section, average acceleration, and average speed. The CO_2 data recovery rates ranged from 41% at Rampart and Summerlin Parkway eastbound onramp (slope = -0.7 deg; avg speed = 71 kph; acceleration = 1.4) to 90% at the Sunset and I-515 westbound onramp (slope = 1.2 deg; avg. speed = 51 kph; acceleration = 1.5 kph/s). Although emissions data recovery was not the sole objective in choosing the sampling locations, the factor of 2 difference for CO_2 data recovery at these two sites emphasizes the importance of site selection with respect to emissions data recovery.

Overall data recovery rates for CO, HC, NO_x, and Opacity measurements were between 57% and 61% for all measurements and greater that 92% of measurements with valid CO_2. The particle LIDAR measurement yielded lower data recovery rates: 34% of all measurements and 57% of measurements with valid CO_2. The data acquisition and background light scattering criteria described in Chapter 3 eliminated additional points when the RSD was able to resolve gas concentrations.

Table 4-2. Date recovery statistics of vehicles emissions measurements match to license plate registration, fuel type, and address location.

Date	*Site Description*	*Total Vehicles*	*Plates Read (%)*	*Plates Matched to Registered Vehicles (%)*	*Registered Gasoline Vehicles (%)*	*Registered Diesel Vehicles (%)*	*Heavy Duty Tractor Trailers (%)**
04/04/00	Sunset onramp to I-515 westbound	7165	75	53	52	0.9	NA
04/05/00	Lake Mead Blvd onramp to I-15 southbound	5200	77	57	55	1.0	NA
04/06/00	Charleston to I-515 westbound	1263	46	34	33	0.4	NA
04/17/00	Charleston to I-515 westbound	656	31	21	21	0.5	NA
04/19/00	Charleston to I-515 westbound	7848	45	31	30	0.7	NA
04/20/00	Sunset onramp to I-15 westbound	6155	70	51	49	1.3	NA
04/21/00	Charleston to I-515 westbound	6322	45	28	28	0.7	NA
07/18/00	Lake Mead Blvd onramp to I-15 southbound	3520	41	28	28	0.7	NA
07/19/00	Charleston to I-515 westbound	5599	19	11	11	0.3	NA
07/20/00	Charleston to I-515 westbound	7250	27	18	18	0.6	NA
07/21/00	Lake Mead Blvd onramp to I-15 southbound	6175	53	38	38	0.5	NA
07/24/00	Lake Mead Drive onramp to I-515 northbound	5602	30	21	21	0.5	NA
07/25/00	Lake Mead Drive onramp to I-515 northbound	7097	30	23	22	0.7	NA
08/17/01	Gowan westbound between Decatur and Rancho	559	74	57	55	0.9	NA
08/21/01	Lake Mead Blvd onramp to I-15 southbound	5544	75	61	60	0.9	0.6
08/22/01	Lake Mead Blvd onramp to I-15 southbound	6428	78	65	64	1.1	0.3
08/23/01	Eastern onramp to US-95 westbound	9413	63	51	49	0.8	NA
08/24/01	Eastern onramp to US-95 westbound	6027	68	55	53	0.8	NA
04/29/02	Green Valley onramp to I-215 westbound	2893	62	49	48	0.4	0.4
04/30/02	Green Valley onramp to I-215 westbound	6123	55	39	38	0.6	2.2
05/03/02	Rampart onramp to Summerlin Pkwy eastbound	10073	67	55	54	0.8	1.7
05/08/02	Eastern onramp to US-95 westbound	13134	71	56	54	0.8	2.6
05/14/02	Craig onramp to US-95 southbound	9137	62	48	46	1.3	NA
05/16/02	Craig eastbound onramp to I-15 southbound	9064	56	35	33	0.8	NA
	TOTAL	**148247**	**57**	**42**	**41**	**0.8**	**1.4**

* Not all technicians noted the presence of tractor-trailer vehicles while transcribing license plates. The records marked with NA are periods no reported vehicle type information.

Table 4-3. Data recovery statistics for remotely sensed speed, acceleration, and emissions.

Date	*SiteDesc*	*Total Vehicles*	*Speed (%)*	*Accel. (%)*	*CO2 (%)*	*CO (%)*	*HC (%)*	*NOX (%)*	*Opacity (%)*	*Backscatter (%)*
04/04/00	Sunset onramp to I-515 westbound	7165	95	95	90	89	85	83	88	NA
04/05/00	Lake Mead Blvd onramp to I-15 southbound	5200	93	92	87	86	83	80	85	NA
04/06/00	Charleston to I-515 westbound	1263	58	58	67	66	64	60	65	NA
04/17/00	Charleston to I-515 westbound	656	49	49	58	56	56	52	55	NA
04/19/00	Charleston to I-515 westbound	7848	96	95	57	56	55	53	54	NA
04/20/00	Sunset onramp to I-15 westbound	6155	93	93	82	81	80	77	79	NA
04/21/00	Charleston to I-515 westbound	6322	93	93	57	57	55	55	56	NA
07/18/00	Leak Mead Blvd onramp to I-15 southbound	3520	65	64	77	75	74	71	76	NA
07/19/00	Charleston to I-515 westbound	5599	95	95	53	52	49	48	51	NA
07/20/00	Charleston to I-515 westbound	7250	92	91	45	45	43	41	44	NA
07/21/00	Lake Mead Blvd onramp to I-15 southbound	6175	89	88	78	77	75	73	78	NA
07/24/00	Lake Mead Drive onramp to I-515 northbound	5602	93	92	51	50	48	45	50	NA
07/25/00	Lake Mead Drive onramp to I-515 northbound	7097	89	89	44	43	42	38	43	NA
08/17/01	Gowan westbound between Decatur and Rancho	559	95	95	83	82	79	76	82	58
08/21/01	Lake Mead Blvd onramp to I-15 southbound	5544	94	94	74	72	71	70	73	18
08/22/01	Lake Mead Blvd onramp to I-15 southbound	6428	94	93	77	76	75	73	77	44
08/23/01	Eastern onramp to US-95 westbound	9413	96	96	74	73	72	70	74	29
08/24/01	Eastern onramp to US-95 westbound	6027	91	90	73	72	71	69	73	39
04/29/02	Green Valley onramp to I-215 westbound	2893	99	99	48	47	46	42	48	37
04/30/02	Green Valley onramp to I-215 westbound	6123	95	95	49	47	45	44	48	33
05/03/02	Rampart onramp to Summerlin Pkwy eastbound	10073	83	83	41	41	40	37	34	26
05/08/02	Eastern onramp to US-95 westbound	13134	96	96	73	71	71	67	66	49
05/14/02	Craig onramp to US-95 southbound	9137	97	97	41	40	39	36	40	24
05/16/02	Craig eastbound onramp to I-15 southbound	9064	79	79	47	46	45	43	46	33
	TOTAL	**148247**	**91**	**91**	**62**	**61**	**60**	**57**	**60**	**34**

5. DATA ANALYSIS AND INTERPRETATION

This section presents and discusses the validated remote sensing data, compares results with those from the MOBILE6 and PART5 emission models estimates, and compares remotely-sensed emissions from the Las Vegas area with similar measurements from other cities.

5.1 Relationship of remote sensing emission factors to vehicle specific power

Remote sensing of vehicle emissions for use as an enforcement tool has been questioned for compliance purposes owing to the short ~0.5 second measurement of exhaust from a passing vehicle. This concern is valid for evaluating emissions from a single vehicle because short-duration emissions may be higher or lower than average emissions over a longer operating period. During the cold start phase, prior to activation of the catalytic converter, emissions are generally higher than during hot stabilized driving (Singer et al., 1999). Catalytic converters do not activate until 2 to 8 minutes after ignition. Most vehicles have been driven for more than 5 minutes prior to being tested on a freeway on-ramp.

Vehicle specific power (VSP), defined as the power required to operate the vehicle at a given speed and acceleration divided by the mass of the vehicle (Jimenez, 1999), also causes short-duration deviations from average emissions. When vehicles are operating at high VSP, the engine computer may enter a command enrichment mode that provides maximum power at the expense of emissions control. The VSP in kW/Mg can be estimated by the speed and acceleration data acquired with the remotely-sensed as:

$$
\begin{aligned}
VSP &= \left(\frac{Power}{Mass} \right) \\
&= \left(\frac{P_{Kinetic} + P_{Potential} + P_{Rolling} + P_{Internal\,Friction} + P_{Aerodynamic}}{Mass} \right) \\
&= v \cdot a \cdot (1 + \varepsilon_i) + g \cdot grade \cdot v + g \cdot C_R \cdot v + C_{if} \cdot v + \tfrac{1}{2} \rho_a C_D \frac{A}{m} (v + v_W)^2 \cdot v \\
&\approx 1.1 \cdot v \cdot a + 9.81 \cdot grade \cdot v + 0.213 \cdot v + 0.000305 \cdot (v + v_W)^2 \cdot v
\end{aligned}
\qquad (5\text{-}1)
$$

The variables v and v_W are the vehicle speed and headwind speed in m/s, respectively. The variable a is the acceleration in m/s^2, and *grade* is the rise/run (i.e. arctan(slope in degrees)). The aerodynamic resistance, frontal area, and mass of a tractor-trailer or bus exceed that for a typical car or light truck resulting in a different specific aerodynamic power loss. Appropriate adjustments should be applied when calculating the VSP for these larger vehicles.

Table 5-1 shows VSP for several operating conditions. Acceleration from 0 to 60 miles per hour in 15 s with a VSP of 33 kW/Mg is typical for freeway on-ramps. In contrast, VSP of 5 to 8 kW/Mg is typical of a trip's driving cycle. For light-duty gasoline powered vehicles measured with the remote sensor during this study, the average VSP was 9.5 kW/Mg. These levels are approximately one-third of typical freeway on-ramp conditions and more consistent with level cruising conditions.

The relationships between VSP and remotely sensed emissions for light-duty gasoline vehicles are shown in Figure 5-1 and Figure 5-2. For each remotely sensed vehicle, the VSP was calculated using equation 5-1 and rounded to the nearest even number. Average, standard deviation, and number of valid emission factors were calculated for each even valued VSP. The standard error (the standard deviation divided by the square root of the number of measurements) was also calculated. The figures show the average and standard error of the emission factors for CO, HC, NO, and PM over a range of VSP's. Each point is the average of at least 100 valid measurements.

Table 5-1. Examples values of vehicle specific power (VSP) and typical vehicle activities. (Jimenez et al., 1999)

Activity	*VSP (kW/Mg)*
Max. Rated Power	44 – 112
0 to 60 mph in 15 seconds	33
60 mph up a 4% grade	23
Maximum in FTP/IM240	23
Rem. Sensing site averages	10 -15
Average in IM240	8
ASM 5015	6
ASM 2525	5

The top panel of Figure 5-1 shows that CO emissions initially decrease by approximately one-third from 60 g/kg fuel to 40 g/kg fuel over the VSP range of 0 to 8 kW/Mg. Emissions are generally stable between 8 kW/Mg and 18 kW/Mg. Above 18 kW/Mg, command enrichment begins and emissions rise from 50 g/kg fuel to approximately 100 g/kg fuel at a VSP of 26 kW/Mg. Similar results are reported in other remote sensing studies (Popp et al., 1998). Short-duration CO emissions are higher than average emissions when the VSP exceeds 20 kW/Mg. These are real emissions, but they do not represent longer duration averages implicit in vehicle emissions standards. When VSP is less than 20 kW/Mg, the short-duration emissions derived from remote sensing may be reasonable for determining compliance with these CO standards.

The lower panel of Figure 5-1 shows the relationship between HC and VSP. Contrary to the behavior of CO, the HC emission factor decreases from 3.5 to 2.5 g/kg fuel over a VSP range from 0 to 26 kW/Mg. Operating in the command enrichment mode does not have a large effect on HC emissions over this range. The lower HC emission factors at higher VSP may be due to higher temperatures and more complete combustion when the vehicle is under load. Other remote sensing studies have shown that increases in hydrocarbon emissions for periods of sudden deceleration are caused by unburned fuel remaining in the engine manifold (An and Scora, 1997). This mechanism is believed to cause 25 to 30% of HC emissions for the MEC01 and US06 test cycles.

The relationship of NO emissions to VSP is shown in the upper panel of Figure 5-2. For VSP less than 4 kW/Mg, NO emissions are ~25% lower than emissions at higher VSP. This is attributable to lower combustion temperatures when the engine is not under load (Jimenez, 1999). NO emissions are stable and independent of VSP in the range of 4 to 26 kW/Mg.

The bottom panel of Figure 5-2 shows the relationship between PM emissions and VSP. The standard error of PM emission factors is larger than that for other pollutants. PM emissions for gasoline vehicles range from 0.04 to 0.18 g/kg fuel over the VSP range of 0 to 26 kW/Mg. The large variability within each VSP range does not permit a relationship of PM emissions to VSP that is as precise as those observed for CO, HC, and NO.

The dependence of emission factor on VSP has several implications for the utilization of remote sensing data for clean screening, high emitter identification, and emissions inventory development.

5.1.1 Implications for Clean Screening

Clean screening is the remote sensing application in which vehicles determined to be in compliance with emissions regulations (based on remote sensing data) are exempt from periodic inspection and maintenance testing. Owners of clean vehicles are not inconvenienced with vehicle inspection and have the option of the standard I/M test. Effective clean screening emphasizes the accurate identification of low emitting vehicles. High emitting vehicles that pass clean screening will stay on the road and emit more pollutants over time. For NO, vehicles passing the test area with a VSP of less than 4 kW/Mg are more likely to show low NO emissions compared with vehicles passing the test section under a heavier load. Validation criteria should be applied to remote sensing measurements to ensure that vehicles are exempted from I/M testing only when VSP is greater than 4 kW/Mg. These criteria would reduce the number of "false negative" designations.

5.1.2 Implications for High Emitter Identification

High emitter identification programs notify vehicle owners of excessive emissions that were remotely sensed and request that additional testing be performed at I/M test facility for additional testing. This may inconvenience the owner if the vehicle is operating properly. Attempts to design and implement this type of program have been hampered by the lack of a reliable method to screen out the occasional high emissions of properly functioning vehicles, false positive" readings. The relationship between VSP and CO suggests that remote sensing measurements with a VSP greater than 20 kW/Mg should not be used for high emitter identification.

5.1.3 Implications for Emissions Inventory Development

The goal of emissions inventory development is to determine actual emissions for the vehicle fleet, fuels, and operating conditions. A representative sample of these variables is needed for an air quality control region, and remote sensing is suited to this purpose because it can test thousands of vehicles in a single day. Emissions per unit of fuel consumed are expected to vary from test to test, but random variations are attenuated by the large number of tests. The times and locations of on-road tests need to be selected to include the full range of vehicle types, fuels, and operations. As shown in Table 5-1, the operating conditions for the tests reported here have higher average VSP than some common test cycles. This is because remote sensing equipment operators select sampling sites where the vehicles will be under moderate load to increase the validity rate of the measurements.

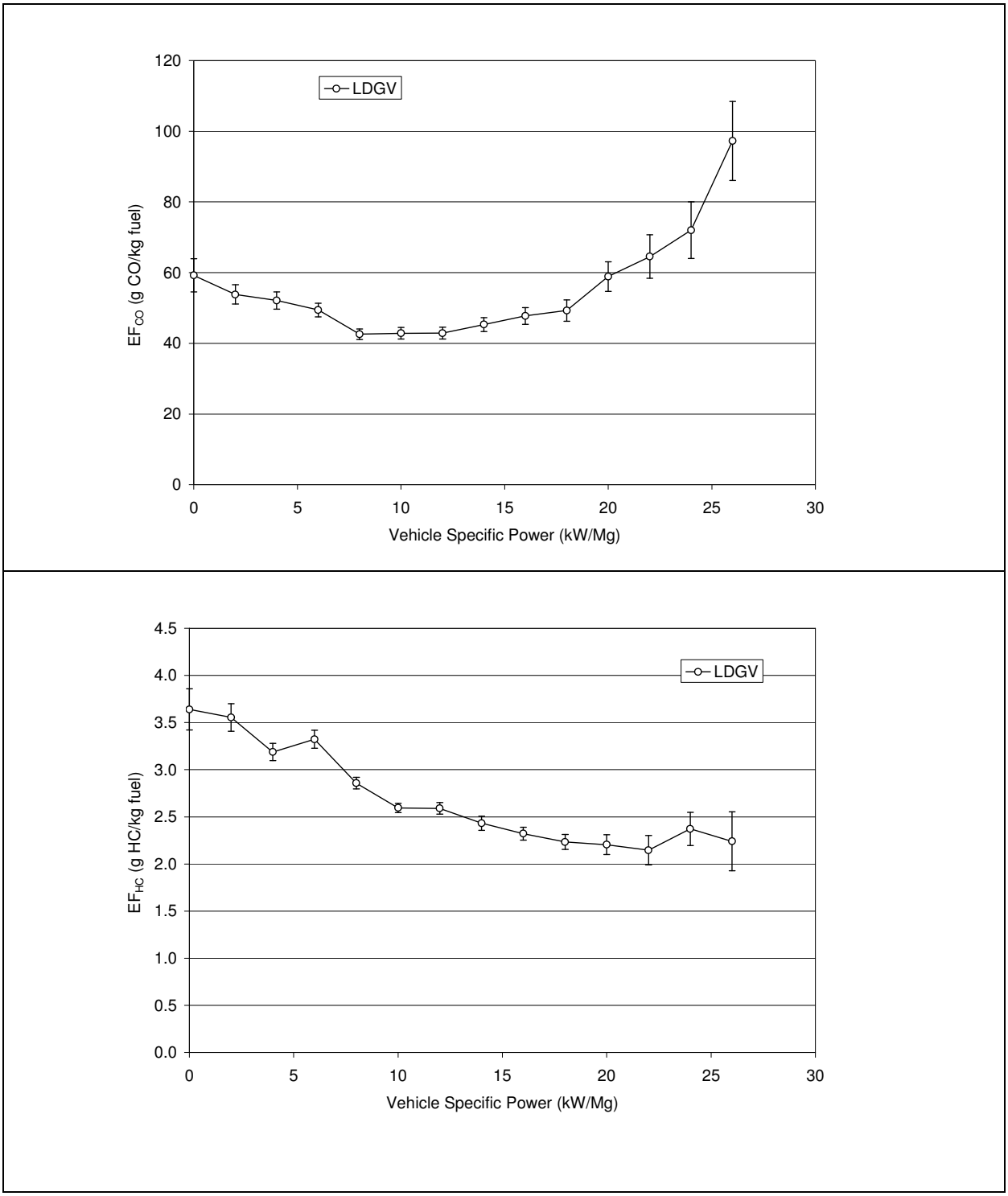

Figure 5-1. Relationship of the CO and HC emission factors for light-duty gasoline vehicles (all gasoline vehicles less than 8500 pounds GVW).

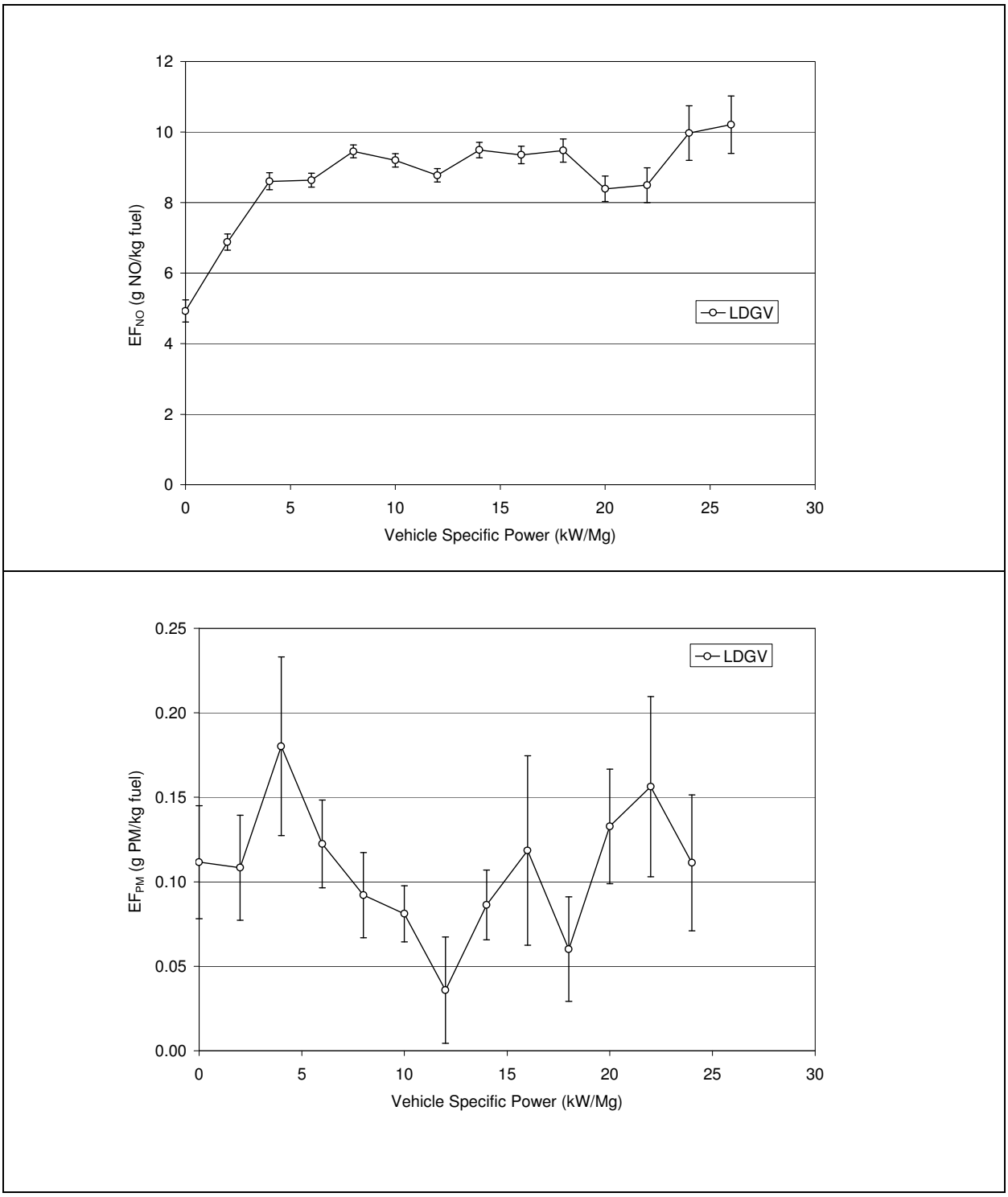

Figure 5-2. Relationship of the NO and PM emission factors for light-duty gasoline vehicles (all gasoline vehicles less than 8500 pounds GVW).

Jimenez (1999) proposed a method to estimate CO, HC, and NO emissions by mapping the distribution of on road VSP values to the VSP distribution of the federal test procedure using the Figure 5-1 and Figure 5-2 relationships. For this study, the average VSP from the on road measurements is 9.5 kW/Mg while the FTP has an average VSP of 8 kW/Mg. The data from Figure 5-1 and Figure 5-2 indicate that emission factors do not change substantially in this range of VSP and that the results of this study should be comparable to the driving cycles used in EPA's on road MOBILE6 emissions model that is based on the FTP cycle.

5.2 Emissions Factors Based on Model Year

Understanding how vehicle emissions change with model year is useful for developing cost-effective emissions reduction strategies that target high emitting vehicles. Tested vehicles with matched registration were subdivided into four categories based on the criteria in Table 5-2.

Table 5-2. Classification of remotely sensed vehicles in Clark County (2000-2002).

Vehicle Class	*Acronym*	*Fuel*	*Gross Vehicle Weight (lbs)*	*Number Measured with Registration Match*
Light Duty Gasoline Vehicle	LDGV	Gasoline	<8501	60,334
Light Duty Diesel Vehicle	LDDV	Diesel	<8501	277
Heavy Duty Gasoline Vehicle	HDGV	Gasoline	>8500	873
Heavy Duty Diesel Vehicle	HDDV	Diesel	>8500	903

Each on road measurement was grouped by vehicle age (measurement year minus model year) at the time of measurement. Average emissions were calculated for each age of each category when at least 10 or more valid measurements were available. Emissions factors are plotted against vehicle age in Figure 5-3 and Figure 5-4. In the upper panel of Figure 5-3, CO emission factors for LDGV increase smoothly as the age increases from 0 to 18 years. In contrast, the trend for HDGV CO emission factors is erratic, but there is a general increase with age from 0 to 12 years. The lower number of vehicles in the year-specific HDGV categories results in less year-to-year stability in the estimates; Table 5-2 shows that ~95% of the measured vehicles are LDGVs. Although averages of LDDV, HDGV, and HDDV are less certain, they are sufficient to show how emissions differ among the four vehicle types.

CO emissions for LDGV increased steadily with age from 20 g/kg fuel for a new vehicle to approximately 250 g/kg fuel for vehicles 20 years and older. When the vehicle fleet is new and the emission control system is functioning properly, typical emissions of CO are very low. As the fleet ages, the fraction of malfunctioning vehicles increases. These vehicles can emit hundreds of times the amount of CO that a properly functioning vehicle emits. This in turn increases the average emissions of older vehicles. CO emissions stop increasing after 20 years for a combination of reasons. By mass balance, vehicles cannot emit more molecules of CO than molecules of carbon in the fuel burned. Although few vehicles reached this point, a physical upper limit exists for the amount of CO that a car can emit for a given quantity of fuel. As

vehicles age, and more vehicles fall into disrepair, there is convergence on this upper limit. Vehicles older than 20 years have been better cared for by their owners, else they would have broken down earlier, and are more likely to be tuned to reduce emissions. Vehicles that are not maintained by their owners will more quickly reach a price point where the cost of repairs exceeds the value of the vehicle. At this point the vehicle is removed from service and no longer increases average emissions for that vehicle age. HDGVs also show increasing CO emissions with vehicle age. Both light-duty and heavy duty diesel vehicles emit the same amount of CO as gasoline vehicles when they are new. HDDV emissions do not increase with age as much as gasoline vehicles, so older diesel vehicles emit less CO than their gasoline counterparts.

Emissions trends with vehicle age for HC are very similar to those for CO. LDGV HC emissions increase from 1.5 to 9.0 g/kg fuel as the vehicle ages from 0 to 20 years. Beyond 20 years, HC emissions for LDGV level off. Average HC emissions levels for gas and diesel vehicles are very similar for vehicles less than five years old. HDDV older than five years emit less HC than same-year gasoline vehicles.

NO emissions LDGVs increase more with vehicle age than do CO and HC emissions. LDGV NO emissions rise from ~2 g/kg fuel for brand-new vehicles to ~19 g/kg fuel for vehicles 15 years and older. HDGV NO emissions increase at a faster rate from ~2 g/kg fuel when new to ~20 g/kg fuel for five-year-old vehicles. Diesel vehicles emit ~20 g/kg fuel when new but show little increase in NO emissions over time. Both gas and diesel vehicles emit similar amounts of NO after 10 to 15 years on the road.

PM emissions in Figure 5-4 follow the same pattern as HC and CO for LDGV. PM for new LDGV are near 0 g/kg fuel (within instrumental detection limits) but increase to ~0.8 g/kg fuel for 20 year old vehicles. Both LDDV and HDDV emit substantially more PM than gasoline vehicles. The average PM emissions of ~8.3 g/kg fuel for new (age = 0) HDDVs is heavily influenced by a single vehicle that was recorded to emit 35 g/kg fuel. Diesel PM emissions for other vehicle ages are in the range of 1 to 2 g/kg fuel.

5.2.1 Implications for Vehicle Profiling

The increase of emissions with vehicle age is a well-known feature of on road vehicle emissions tests. New vehicles are often exempted from annual I/M testing because they are unlikely to be high emitters; the first Nevada smog-test is require when a vehicle is three years old. Reduction in fleet emissions can be achieved by scrapping high emitting vehicles or banning them from operation within a polluted airshed. Based on the CO, HC, and PM emissions distributions with vehicle age, many vehicles older than fifteen to twenty years (i.e. model year 1987 and older) should be candidates for fleet removal.

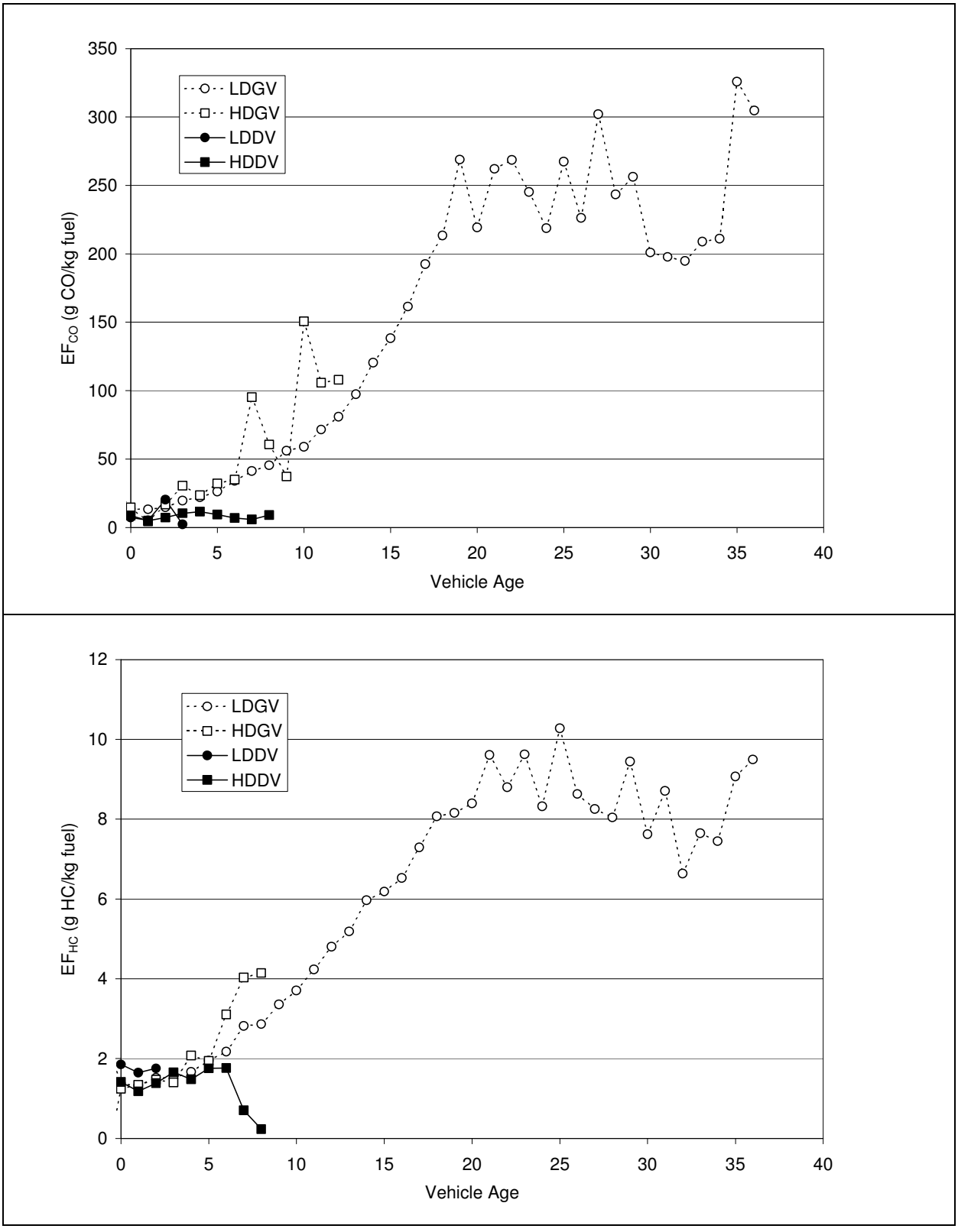

Figure 5-3. Average CO and HC emission factors by vehicle age from remote sensing tests.

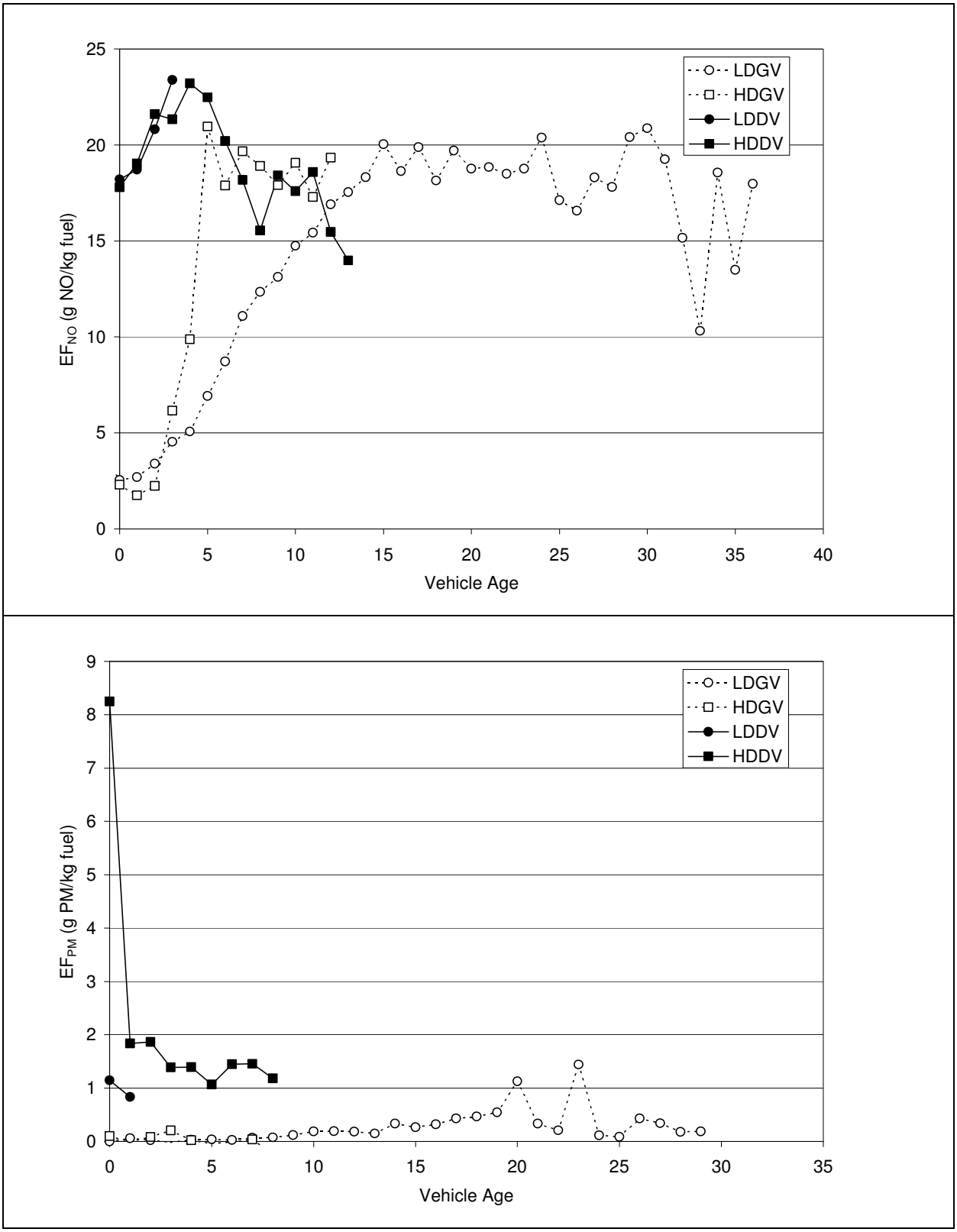

Figure 5-4. Average NO and PM emission factors by vehicle age from remote sensing tests.

5.3 Comparison of Remotely Sensed Emissions Factors with MOBILE6 Model

MOBILE6 is EPA's prescribed on road emission factor model. The model incorporates information about a region's on road fleet age distribution, meteorology, I/M program, use of reformulated or oxygenated fuel, road types, and operating conditions to estimate mileage based emission factors for 28 different vehicle classifications. MOBILE6 is used to estimate emission factors of CO, HC, and NO. PART5 is a module that estimates particulate matter emissions from mobile sources including exhaust, road dust, and brake and tire wear.

In this analysis, on road emission factors are compared with the MOBILE6 and PART5 estimates. The Las Vegas on road vehicle data contain information about model year, fuel type and gross vehicle weight. On-road emission factors are grouped into four vehicle-type categories as defined in Table 5-2: LDGV, LDDV, HDGV, and HDDV. MOBILE6 and PART5 estimates were consolidated into the same four categories by weighting the populations of the 28 vehicle sub classifications within each of the four vehicle classes. MOBILE6 emissions estimates for Clark County are based on a registration census maintained by the Nevada DMV (Li, 2002). The DMV distribution for LDGV is compared with the distribution from the ~60,000 on road tests in Figure 5-5. Vehicle age distributions are similar, indicating that the on road tests captured a representative sample of model years operating in Clark County.

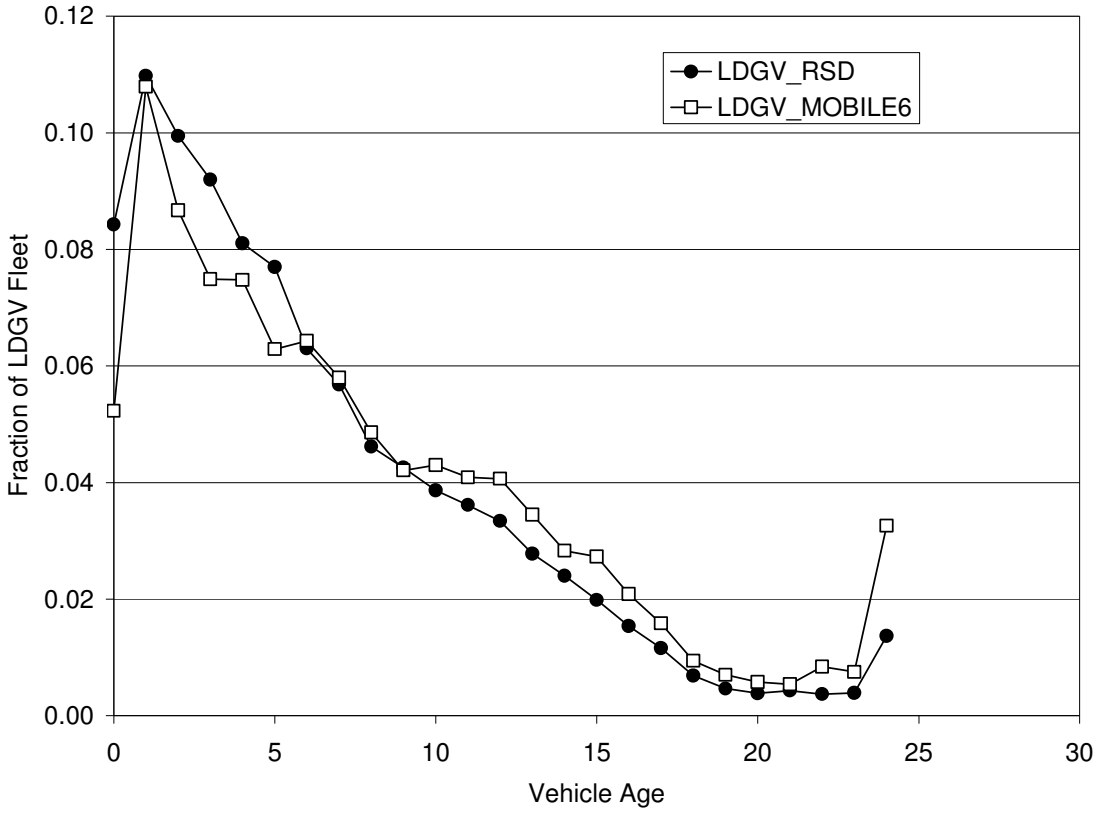

Figure 5-5. Comparison of LDGV fleet distribution as measured by RSD and the registration fleet distribution used as input in the MOBILE6 emissions model.

MOBILE6 parameters were selected for conditions that approximately corresponded to those of the on road measurements. These took place during the months of April, May, July, and August. April temperatures in the Las Vegas Valley have an average minimum of 48 deg F and an average maximum of 81 deg F. July is the hottest month with an average minimum temperature of 71 deg F and an average maximum temperature of 105 deg F. MOBILE6 estimates were made for a daytime low temperature of 57 deg F and a daytime high temperature of 90 deg F to represent a mid point between the range of temperatures associated with the on road tests. The input temperatures affect evaporative HC emissions vehicles that are not quantified in the on road tests and are excluded from the comparison.

MOBILE6 generates emission factors for a variety of speeds and road types (i.e. freeways, onramp's, local streets, and arterials). The average speed for the on road tests was ~60 kph (37.5 mph) and the average acceleration was 1 kph/s (0.6 mph/s). MOBILE6 emission factors were selected for vehicles traveling at 40 mph (the closest speed at 5 mph intervals).

MOBILE6 uses different driving cycles for different road types. It assumes a hard acceleration on freeway onramps to permit merging into the higher speed traffic flow. The freeway driving cycle assumes a constant cruising speed. Mileage based emission factors for freeway onramps are higher than freeway emission factors because the vehicle is assumed to be in the command enrichment mode at the onramp. MOBILE6 outputs fuel economy data for each vehicle classification and age so that distance-based emission factors can be converted to fuel based factors. MOBILE6, however, does not consider changes in fuel economy that occur under different driving cycles. The MOBILE6 fuel economy of a vehicle under load is the same as that for constant-speed operation, whereas in reality the fuel economy is substantially lower during acceleration. This causes MOBILE6 to overestimate g/kg fuel for freeway on ramps as it underestimates the amount of fuel needed for a given distance during acceleration.

Figure 5-6 compares LDGV fuel-based CO, NO, and HC exhaust emissions for MOBILE6 and the average on road measurements from this study for increasing vehicle ages. Similar comparisons for other vehicle categories are more uncertain owing to the smaller number of on road tests results for HDGV, LDDV, and HDDV. MOBILE6 emission factors for both freeway onramps and freeways are shown, although the on road tests correspond to on ramp operations.

The upper panel of Figure 5-6 shows the CO on road emissions to be similar to the MOBILE6 freeway emissions for new vehicles. For vehicles 1 to 14 years old, MOBILE6 CO emissions are higher than the on road measurements by up to a factor of 3. MOBILE6 and on road CO emissions converge for vehicles 15 years and older. MOBILE6 freeway on ramp emissions are consistently higher than the on road emissions for all vehicle ages. This is consistent with higher fuel economy assumed for the on ramp acceleration as well as with the relatively low VSP measured for most vehicles in these tests.

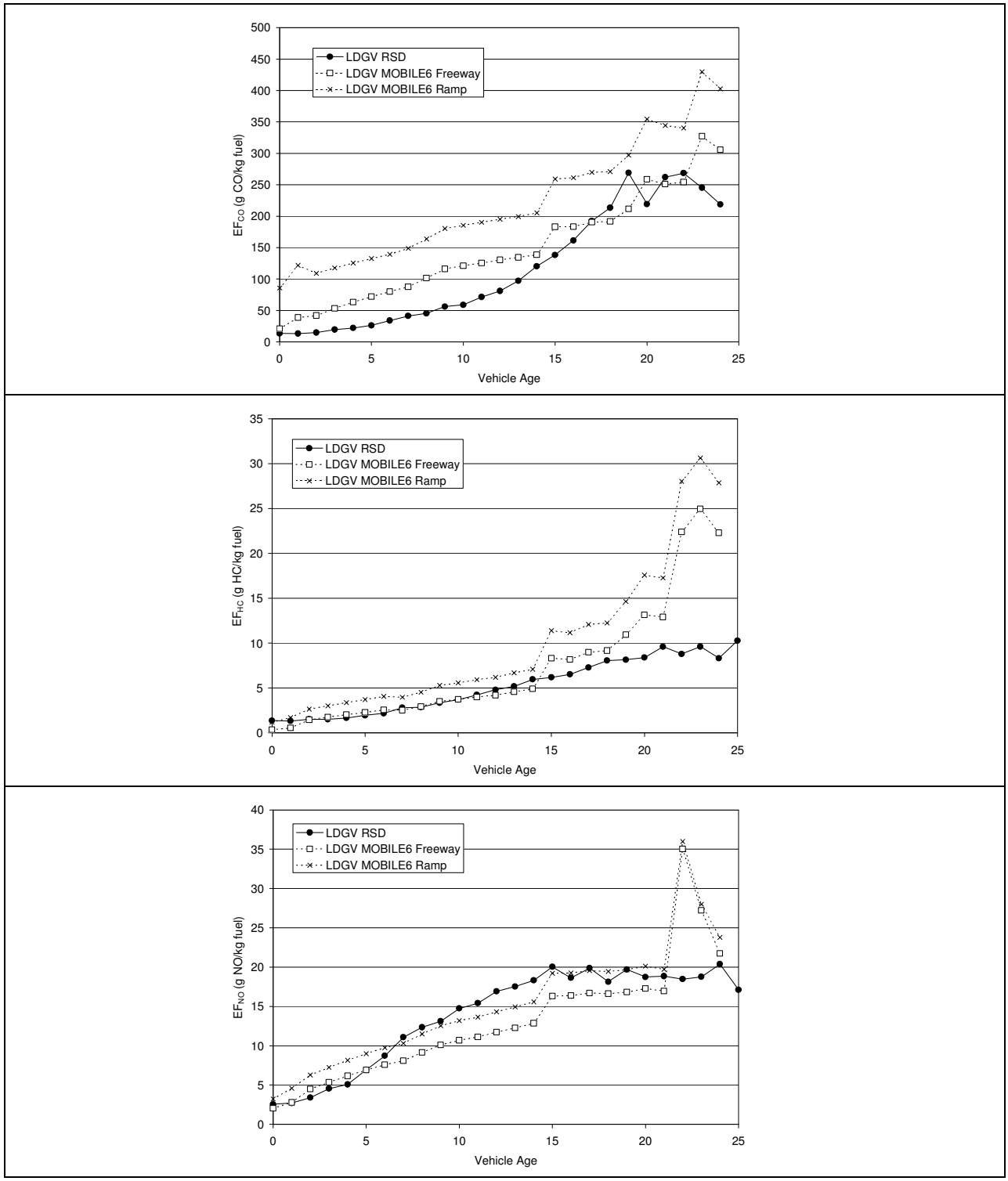

Figure 5-6. Comparison of remotely sensed emission factors for CO, HC, and NO with MOBILE6 output for both freeway and onramp facilities.

HC and NO emissions are more consistent between MOBILE6 estimates and on road measurements. For HC (the middle panel in Figure 5-6), measured and modeled freeway emissions are in good agreement for vehicles less than 14 years old. For older vehicles, MOBILE6 estimates HC emissions higher than those measured. Similarly, NO emissions from MOBILE6 are in good agreement with measurements for vehicles less than five years old. For older vehicles, the MOBILE6 NO emissions are lower than the on road measurements.

Figure 5-5 shows the vehicle ages for which MOBILE6 and on road emissions estimates differ. Fleet wide emission factors for each of the four vehicle classifications are calculated by multiplying the aged based emission factors by the fraction of registered vehicles of that age and summing the results over all vehicle ages. These are compared in Table 5-3. An additional class "Large Trucks with Trailers" is shown in the table, corresponding to large tractor trailers identified by the license plate readers and flagged during data reduction. These vehicles may correspond to HDDV but their registration could not be checked because the license plate corresponded to the trailer being pulled rather than the tractor. This class of vehicle is shown here for comparison with known HDDV to evaluate the accuracy of this labeling.

For CO, MOBILE6 gasoline vehicle emissions exceed the on road measurements by 102% and 78% for LDGV and HDGV, respectively. In contrast, MOBILE6 emissions are 26% to 54% lower than on road measurements for diesels. With the exception of LDDV, MOBILE6 freeway HC emissions are 19% and 38% higher than the on road emissions. MOBILE6 LDDV HC emissions are 180% higher the on road values. MOBILE6 NO emissions for LDGV are similar to the on road measurements, but they are higher for the other vehicle categories, with heavy-duty vehicles between 78% and 84% larger than the on road measurements.

PART5 does not consider vehicle age distributions to estimate exhaust PM emissions. PART5 emission factors are based on tunnel studies and dynamometer tests with PM being quantified on filters that are weighed prior to and after sampling. On road PM emissions measurements are based on optical measurements that only approximately correspond to the gravimetric mass. Even with this difference in measurement principles and basic data bases (none of the PART5 tests were performed in Nevada), agreement between the two approaches is reasonable. PART 5 estimates 27% to 30% percent more PM emissions from LDGV and LDDV compared to the on road averages. On road light-duty and heavy-duty diesel emissions are similar at 1.5 g/kg fuel. PART5 HDDV PM emissions are 45% lower than LDDV emissions. As a result, PART5 HDDV emissions are 33% lower than the on road values. The largest discrepancy is for HDGV, for which PART5 emissions are more than 2.5 times those measured in the on road tests.

PM emissions from large tractor/trailers are more similar to gasoline vehicles than they are to HDDV, even though they should be in the HDDV category. These vehicles often had elevated exhaust pipes on the tractor. The remote sensing beam did not directly cross the dense plume, but measured a more diluted exhaust wake after the trailer. This dilution probably lowers the PM concentrations below instrument detection limits, thereby negatively biasing the average.

Table 5-3. Comparison of fleet averaged emission factors measured by RSD and LIDAR with modeled MOBILE6 and PART5 output.

	$EF_{CO}\left(\frac{g\,CO}{kg\ fuel}\right)$			$EF_{HC}\left(\frac{g\,HC}{kg\ fuel}\right)$			$EF_{NO}\left(\frac{g\,NO}{kg\ fuel}\right)$			$EF_{PM}\left(\frac{g\,PM}{kg\ fuel}\right)$		
Vehicle Type	**RSD**	**MOBILE6**	**% diff**	**RSD**	**MOBILE6**	**% diff**	**RSD**	**MOBILE6**	**% diff**	**LIDAR**	**PART5**	**% diff**
LDGV	49	99	***+102***	2.9	4.0	***+37***	8.8	8.8	***0***	0.10	0.13	***+30***
LDDV	19	8.7	***-54***	2.3	6.5	***+183***	15.2	19	***+25***	1.5	1.9	***+27***
HDGV	56	100	***+78***	2.6	3.6	***+38***	10.3	19	***+84***	0.07	0.25	***+257***
HDDV	10	7.4	***-26***	1.6	1.9	***+19***	19.9	35.5	***+78***	1.5	1.0	***-33***
Large Trucks w/Trailers (from License Plate picture)	79			7.8			12.7			0.20		

5.3.1 Implications for Emissions Inventories

The results from this section have important implications for the development of emissions inventories based on the MOBILE6/PART5 models. Modeled and measured emissions appear to be in reasonable agreement (±50%) for CO from HDDV, HC from LDGV, HDGV, and HDDV, NO from LDGV and LDDV, and PM from LDGV, LDDV, and HDDV. This consistency does not prove that MOBILE6/PART5 estimates truly represent reality, but it does add confidence to their use for planning purposes as the on-road measurements are completely independent of the data used in the emissions models.

The most important discrepancy is that for CO emissions from LDGV, for which MOBILE6 estimates emissions twice those of the on road tests. Differences in assumptions about actual fuel economy and the degree of power enrichment indicate that MOBILE6 may overestimate emissions for the on road testing conditions. This comparison does not invalidate the MOBILE6 CO estimates, but it does suggest that further examination of the model input data and assumptions is warranted. MOBILE6 sensitivity tests should be performed using a variety of the input conditions that might represent Las Vegas driving conditions. Different fuel economies and VSPs would be among the parameters varied. As Figure 5-5 demonstrates, the roadway (i.e. freeway/onramp/local/arterial) is an important variable that affects CO emissions. The assumption that a freeway driving cycle represents the on road measurements does not appear to be valid. On road tests that represent other driving conditions (e.g., residential, cold start, cruising, congestion) need to be included in future experiments.

5.4 Comparison of LV Remote Sensing Emissions with Similar Studies from Other Cities

The Coordinating Research Council (CRC, 2002) is conducting multiyear on road CO, HC, and NO emissions studies in Los Angeles, CA, Denver, CO, Chicago, IL, and Phoenix, AZ (CRC, 2002) to establish baseline emissions and to quantify the reductions due to new emissions control technologies. Table 5-4 compares exhaust emissions factors from these tests with those from Clark County, NV. Both diesel and gasoline vehicle emissions are included in the totals. The skewness of the pollutant distributions are represented by the fraction of total pollutant attributable to the 10% highest emitting vehicles.

Table 5-4. Comparison of on road emissions from Clark County, NV with emissions in Denver, CO, Phoenix, AZ, Los Angeles, CA, and Chicago IL for valid samples paired with vehicle registrations.

Variable	*Clark Co, NV April-May 2002*	*Clark Co, NV August 2001*	*Clark Co, NV April-July 2000*	*Denver January-February, 1999 (CRC, 2002)*	*Phoenix November 1998 (CRC 2002)*	*Los Angeles June-July, 1999 (CRC 2002)*	*Chicago September 1999 (CRC 2002)*
Avg. Fleet Age	1995.3	1994.0	1993.9	1992.4	1993.3	1992.4	1994.3
Attempted Measurements	24,115	12,324	22,837	34,613	32,789	26,001	28,925
Mean CO (g CO/kg fuel)	42	58	53	58	37	70	45
Percent of total CO from Dirtiest 10% of Fleet (%)	79.3	75.7	76.3	66.3	70.7	69.6	63.0
Mean HC (g HC/kg fuel)*	5.7	6.0	5.5	5.3	7.8	8.0	7.3
Percent of total HC from Dirtiest 10% of Fleet (%)	42.2	47.6	50.3	63.7	65.5	52.8	47.3
Mean NO (g NO/kg fuel)	8.5	8.7	9.1	8.3	5.0	5.1	5.3
Percent of total NO_x from Dirtiest 10% of Fleet (%)	47.4	47.1	45.1	44.6	56.0	51.1	51.1

*Adjusted by a factor of 2 to adjust for differences between NDIR and FID detection of HC as propane (Singer, 1999).

Clark County CO emissions are within the range of measurements from the other cities. The CO contribution from the highest emitting 10% of registered vehicles is larger in Clark County in the other cities. This implies that Clark County could benefit most from a program that targets high CO emitters.

Average HC exhaust emissions in Clark County also fall within the range measured in the other cities. Unlike CO, HC emissions are more evenly distributed across the vehicle population in Clark County than in other cities. The highest emitting 10% HC emissions in Clark County account for 42.2% to 50.3% of the total HC while the top 10% accounts for 63.7% and 65.5% of HC emissions in Denver and Phoenix, respectively.

Average Clark County NO emissions are comparable to those of wintertime Denver, CO, but higher than those in the other cities by nearly a factor of two. NO exhaust concentrations are more evenly distributed across the fleet in Clark County. Only 45.1% to 47.4% of NO exhaust concentrations are attributable to the highest emitting 10% of vehicles.

HC emissions in Phoenix, Los Angeles, and Chicago are ~37% higher than the average emissions for Clark County and Denver while the NO emissions in Phoenix, Los Angeles, and Chicago are 40% lower than NO exhaust concentrations in Clark County and Denver. NO is typically higher when CO and HC are lower owing to different air/fuel ratios and operating

temperatures. The results in Table 5-4 are consistent with this trade-off with respect to Las Vegas/Denver comparisons with Los Angeles/Chicago/Phoenix tests results. This may have to do with the locations and times of the tests as well as to differences in fuels and local tuning of the vehicles. Differences in the mixture of diesel and gasoline vehicles in the on road tests could also be a cause of these differences.

It is difficult to compare the fleet average mobile emissions for different cities based solely on the fleet average on road emissions tests. Vehicle age and vehicle specific power can have a large influence on the measured emission factors. It is likely that other variables such as vehicle repair history, weather conditions, elevation, fuel composition, and smog reduction programs can also influence emission factors. Also the use of different instruments and calibration systems can make these types of comparisons difficult to interpret unambiguously.

6. CONCLUSIONS AND RECOMMENDATIONS

6.1 Summary

The exhaust emissions from nearly 150,000 vehicles in the Las Vegas Valley were measured using optical remote sensing over the period from April 2000 to May 2002. Established techniques to measure CO, HC, and NO emissions were applied at 10 different locations distributed across the valley. In addition, a new technique developed at DRI and using an ultraviolet LIDAR was used to measure PM emissions from vehicles. This report documents the first large-scale application of the LIDAR technique for measuring particle emissions from on road vehicles.

Vehicle exhaust remote sensing involves deploying monitoring equipment on both sides of a single lane road to optically interrogate engine exhaust after a vehicle passes through an analytical beam. Unlike conventional inspection and maintenance smog check programs, the technique is a nonintrusive method of measuring the emissions from a large number of vehicles operating in real world conditions. Data from vehicle remote sensing can be used in four ways: (1) *clean screening* to exempt low emitting vehicles from smog testing; (2) *enforcement* to require high emitting vehicles to be tested and repaired prior to their annual smog check; (3) *emissions inventory development* using the measured emissions factors to estimate area wide emissions based on fuel sales; and (4) *vehicle profiling* to target emissions control strategies to the highest emitting segment of the on road vehicle fleet. The results of the study have several implications for each of these applications of remote sensing.

- Clean screening is the remote sensing application in which vehicles determined to be in compliance with emissions regulations (based on remote sensing data) are exempt from periodic inspection and maintenance testing. Owners of clean vehicles are not inconvenienced with vehicle inspection and have the option of the standard I/M test. Effective clean screening emphasizes the accurate identification of low emitting vehicles. High emitting vehicles that pass clean screening will stay on the road and emit more pollutants over time. For NO, vehicles passing the test area with a Vehicle Specific Power (VSP) less than 4 kW/Mg are more likely to show low NO emissions compared with vehicles passing the test section under a heavier load. Validation criteria should be applied to clean screening remote sensing measurements to ensure that vehicles are exempted from I/M testing only when VSP is greater than 4 kW/Mg. These criteria would reduce the number of "false negative" designations.
- Remote sensing enforcement programs notify vehicle owners of excessive emissions that were remotely sensed and request that additional testing be performed at an I/M test facility for additional testing. This may inconvenience the owner if the vehicle is operating properly. Attempts to design and implement this type of program have been hampered by the lack of a reliable method to screen out the occasional high emissions of properly functioning vehicles (i.e. vehicles with "false positive" readings). The measured relationship between VSP and CO indicates that "commanded enrichment" will cause properly functioning vehicles to emit more CO when VSP is greater than 20 kW/Mg. Criteria should be applied to remote sensing data used for enforcement purposes to prevent high

emissions notification to drivers passing through the test section with a VSP greater than 20 kW/Mg.

- The goal of emissions inventory development is to determine actual emissions for the vehicle fleet, fuels, and operating conditions. A representative sample of these variables is needed for an air quality control region, and remote sensing is suited to this purpose because it can test thousands of vehicles in a single day. Emissions per unit of fuel consumed are expected to vary from test to test, but random variations are attenuated by the large number of tests. The times and locations of on-road tests need to be selected to include the full range of vehicle types, fuels, and operations.
- Modeled and measured emissions appear to be in reasonable agreement (±50%) for CO from HDDV, HC from LDGV, HDGV, and HDDV, NO from LDGV and LDDV, and PM from LDGV, LDDV, and HDDV. This consistency does not prove that MOBILE6/PART5 estimates truly represent reality, but it does add confidence to their use for planning purposes as the on-road measurements are completely independent of the data used in the emissions models. The most important discrepancy is that for CO emissions from LDGV, for which MOBILE6 estimates emissions twice those of the on road tests. Differences in assumptions about actual fuel economy and the degree of power enrichment indicate that MOBILE6 may overestimate emissions for the on road testing conditions. This comparison does not invalidate the MOBILE6 CO estimates, but it does suggest that further examination of the model input data and assumptions is warranted to ensure that modeled data can be reconciled with measurements.
- The increase of emissions with vehicle age is a well-known feature of on road vehicle emissions tests. New vehicles are often exempted from annual I/M testing because they are unlikely to be high emitters; the first Nevada smog-test is required when a vehicle is three years old. Scrapping high emitting vehicles or banning them from operation within a polluted airshed are policies that can achieve reduction in fleet emissions. Based on the CO, HC, and PM emissions distributions for LDGV with vehicle age, many vehicles older than fifteen to twenty years (i.e. model year 1987 and older) should be candidates for fleet removal.

Remote sensing data in Clark County was compared with results from recent remote sensing studies in Los Angeles CA, Denver CO, Chicago IL, and Phoenix AZ. Emissions factors in Las Vegas were in general agreement with the emissions factors measured in at least one of the other cities. It is noteworthy that NO emissions in Clark County are nearly equivalent to those measured in Denver CO, but are ~80 percent higher than NO emissions factors and Phoenix, Los Angeles, and Chicago. Conversely, HC emissions factors in Clark County and Denver were ~40 lower than those measured in the other cities.

6.2 Recommendations

The results of the study have prompted several recommendations that should be applied to reduce the uncertainty in the estimation of emissions from mobile sources:

- The discrepancy between the remotely sensed gas measurements and the MOBILE6 emissions factors needs to be explored in more detail. Observed differences between the measurements and the model may be due to variations in the distribution of vehicle specific power as measured at the remote sensing test sites and as assumed in the road facility type used as input to the MOBILE6 model. Sensitivity tests should also be run on other input variables (i.e. temperature, fuel type, I/M effectiveness, etc.) for the MOBILE6 model to gain a better understanding of what factors have the strongest influence on modeled emissions.
- Based on the distribution of vehicle emissions factors with vehicle specific power, fleet averaged emissions factors should be scaled to represent the distribution of VSP used in emissions factors models such as MOBILE6. This emissions factors scaling should also be applied to remote sensing measurements from a variety of urban areas to empirically evaluate the effectiveness of different emissions control strategies.
- Additional remote sensing experiments should focus on portions of the fleet underrepresented by the freeway onramp tests. These vehicles include heavy-duty gasoline vehicles (HDGV), light-duty diesel vehicles (LDDV), and heavy-duty diesel vehicles (HDDV). Tests should be conducted in areas with a large population of these different vehicle types (i.e. landfill entrance areas, diesel fueling stations, etc.).
- The LIDAR particle emissions factor measurement provided useful information about the distribution of particle emissions factors with vehicle age and by vehicle class. At present, the minimum detectable limit (MDL) of the instrument is insufficient to resolve particle emissions factors on the majority of individual vehicles tested. Enhancements to the design of the instrument are needed to reduce the uncertainty of the measurement to resolve particle emissions from a larger fraction of the fleet.
- The LIDAR particle measurement system has been calibrated only using theoretical assumptions about the size and optical properties of the exhaust aerosol. Collocated tests using the LIDAR and other proven particle and gas measurement systems will provide an experimental basis for the calibration of the LIDAR. These tests will improve confidence in the interpretation of the LIDAR results.

7. REFERENCES

An F. and Scora G. (1997) Characterization and Modeling of Vehicular Unburned Hydrocarbon Emissions.

Ashbaugh L. L. et al. (1992) (ed. J. C. Chow and D. M. Ono). pp. 885-898. Air & Waste Management Association.

Barber, P.W. and S.C. Hill (1990), Light Scattering by Particles – Computational Methods, World Scientific, Singapore.

Bessagnet B. and Roset R. (2001) Fractal modeling of carbonaceous aerosols – application to car exhaust plumes. Atmospheric Environment 35, 4751-4762.

Bishop, G. A., J.R. Starkey, A. Ihlenfeldt, W.J. Williams, and D.H. Stedman (1989) IR Long-Path Photometry: A Remote Sensing Tool for Automotive Emissions. *Anal. Chem.* **61**:671A-677A.

Cadle, S.H., P Mulawa, J. Ball, C. Donase, A. Weibel, J.C. Sagebiel, K.T. Knapp, and R. Snow (1997) Particulate emission rates from in-use high-emitting vehicles recruited in Orange County, California. *Environ. Sci. Technol.,* **31**:3405-3412.

CRC (2002) Coordinating Research Council Inc. Webpage (http://www.crcao.com/reports/recentstudies00-02/recent_reports_and_study_results.htm) Accessed 07/21/2002.

Fujita, E, R.E. Keislar, J. Bowen, W. Goliff, E. Uberna, L. Sheetz. M. Keith, J. Sagabiel, and B. Zielinska (1999). 1998 Central Texas On-Road Hydrocarbon Study. Draft final report. Prepared for the Texas Department of Transportation, Austin, TX. Prepared by Desert Research Institute, April, 1999.

Horvath, H. (1993) Atmospheric light absorption – a review, Atmospheric Environment 27A, 293-317.

Jimenez J. L. (1999) Understanding and Quantifying Motor Vehicle Emissions with Vehicle Specific Power and TILDAS Remote Sensing. Ph.D. Massachusetts Institute of Technology.

Jimenez J. L. et al. (1999) Vehicle Specific Power: A Useful Parameter for Remote Sensing and Emissions Studies. Presentation for the 9th CRC Conference, San Diego, CA.

Keislar, R.E., H. Moosmüller, H. Kuhns, E. Fujita, and J. Watson (1999) Measurement of On-Road Particulate Matter Emissions by Lidar. Presented at the Ninth CRC On-Road Vehicle Emissions Workshop, San Diego, CA, April 19-21, 1999.

Kittelson D. B. (1998) Engines and nanoparticles: A review. J.Aerosol Sci. 29[5/6], 575-588.

Knapp, K. (1992) Dynamometer Testing of On-Road Vehicles from the Los Angeles In-Use Emissions Study. In *Transactions: PM10 Standards and Nontraditional Particulate Source Controls.* J.C. Chow and D.M. Ono, Eds. Air & Waste Management Association, Pittsburgh PA, pg. 871-884.

Lawson, D.R., P.J. Groblicki, D.H. Stedman, G.A. Bishop, and P.L. Guenther (1990) Emissions from in-use vehicles in Los Angeles: A pilot study of remote sensing and the inspection and maintenance program. *J. Air Waste Manage. Assoc.,* **40**:1096.

Li Z. (2002) Clark County Department of Comprehensive Planning, personal communications.

Martins J. V., Artaxo P., Liousse C., Reid J. S., Hobbs P. V., and Kaufman Y. J. (1998) Effects of black carbon content, particle size, and mixing on light absorption by aerosols from biomass burning in Brazil. Journal of Geophysical Research 103[D24], 32041-32050.

Martins, J., P. Artaxo, C. Liousse, J. Reid, P. Hobbs, and Y. Kaufman (1998) Effects of black carbon content, particle size, and mixing on light absorption by aerosols from biomass burning in Brazil. Journal of Geophysical Research 103, 32,041-32,050.

McClintock, P. (1999) "Remote Sensing of Real World High Exhaust Emitters, CRC Project Number E-23 – Interim Report." Prepared for Coordinating Research Council, Inc. and the Colorado Department of Public Health and Environment. Prepared by Applied Analysis, Inc., Tiburon, CA, March 12, 1999.

Measures, R.M. (1992), Laser Remote Sensing, Kreiger, Malabar, Florida.

Popp, P. J., Bishop, G. A., and Stedman, D. H. (1998) On-Road Remote Sensing of Automobile Emissions in the Chicago Area: Year 1. Report prepared by Department of Chemistry and Biochemistry, University of Denver, CRC E-23-4, Denver, CO.

Schwartz, J. (1998) Remote Sensing of Vehicle Emissions: State of the Technology, Potential Applications, Cost Estimates, and Recommendations. Prepared by the California Inspection and Maintenance Review Committee, September 9, 1998.

Shi J. P., Mark D., and Harrison R. M. (2000) Characterization of particles from a current technology heavy-duty diesel engine. Environmental Science and Technology 34[5], 748-755.

Singer B. C., Harley R. A., Littlejohn D., Ho J., and Vo T. (1998) Scaling of infrared remote sensor hydrocarbon measurements for motor vehicle emission inventory calculations. Environmental Science and Technology 32[21], 3241-3248.

Singer B. C., Kirchstetter T. W., Harley R. A., Kendall G. R., and Hesson J. M. (1999) A fuel-based approach to estimating motor vehicle cold-start emissions. Journal of the Air & Waste Management Association 49[2], 125-135.

Stedman, D. (2002) University of Denver. Personal communications.

Stedman, D.H. and G.A. Bishop (1990) An analysis of on-road remote sensing as a tool for automotive emissions control. Final report to the Illinois Department of Energy and Natural Resources. ILENR/RE-AQ-90/05.

Stephens, R.D., M.T. Giles, P.J. Groblicki, R.A. Gorse, K.J. McAlinden, D.B. Hoffman, R. James, and S. Smith (1994) Real World Emissions Variability as Measured by Remote Sensors, SAE Technical Paper Series # 940582. Presented at International Congress and Exposition, Detroit MI, February 28 –March 3, 1994.

Völger P., J. Bösenberg, and I. Schult (1996), Scattering properties of selected model aerosols calculated at UV-wavelengths: implications for DIAL measurements of tropospheric ozone, Beitr. Phys. Atmosph. 69, 177-187.

Zhang, Y., G.A. Bishop, and D.H. Stedman (1994). Automobile emissions are statistically γ-distributed. *Environ. Sci. Technol.*. **28**:1370-1374.

A. APPENDIX

A.1 Site Descriptions

The following figures are the traffic control plans for each of the remote sensing site surveyed as part of this study. Records for the GOWAN, MEAD515, and CHRL515 site could not be located at the time or writing, but traffic control permits were obtained for these sites.

A.1.1 MEADI15

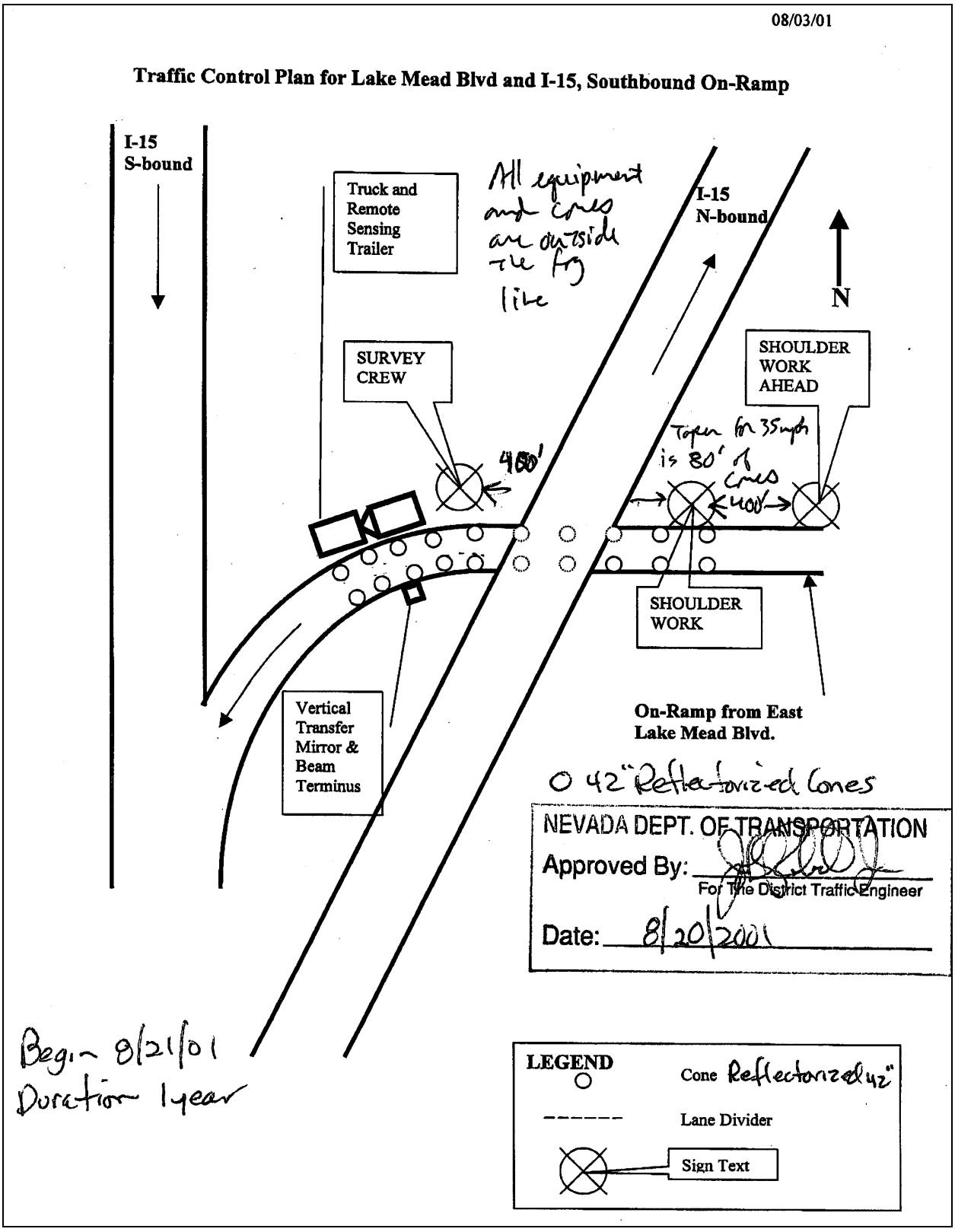

Figure A-1. Traffic control plan for the Lake Mead and I-15 site (MEADI15).

A.1.2 EASTERN

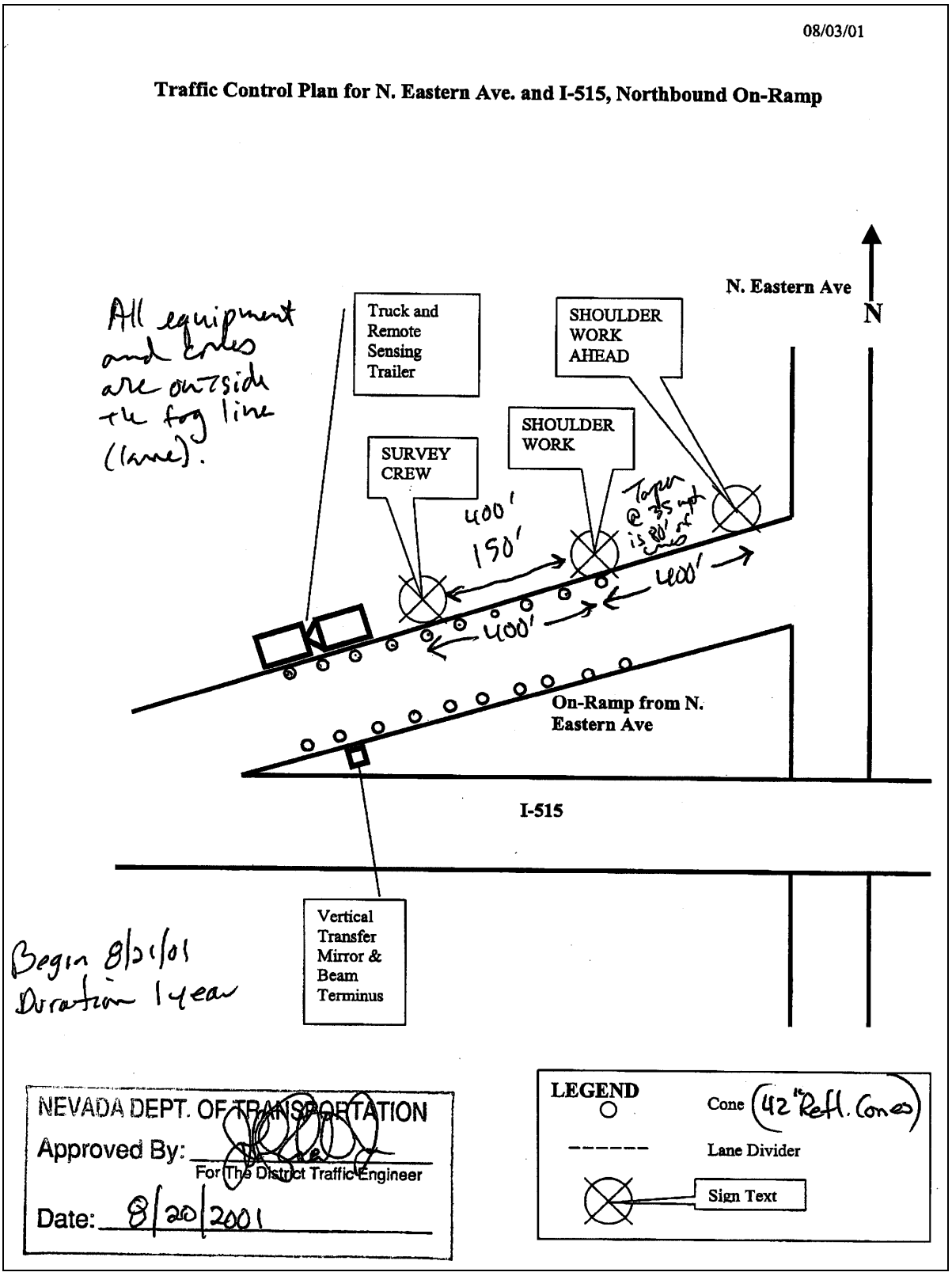

Figure A-2. Traffic control plan for the Eastern and I-515 site (EASTERN).

A.1.3 CRAIG95

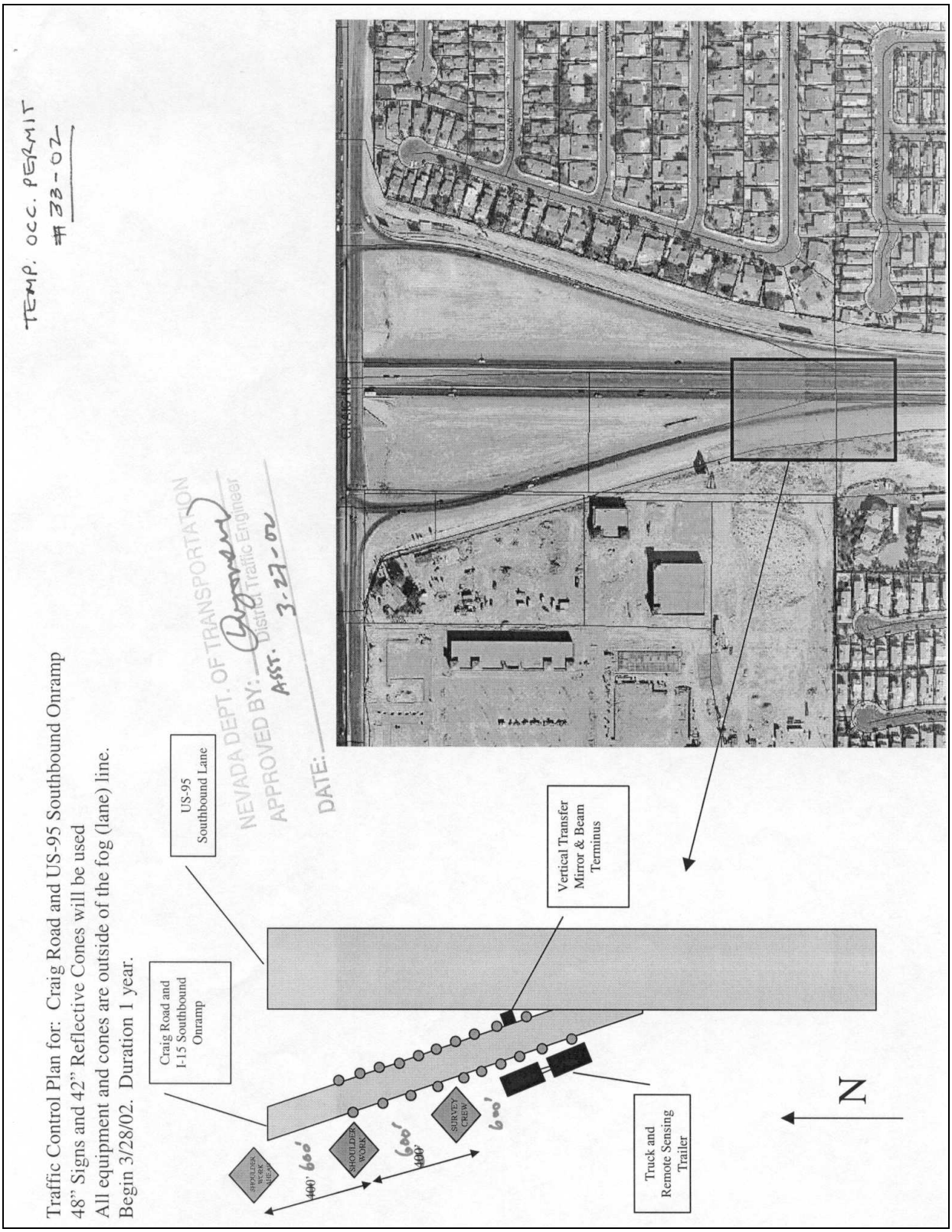

Figure A-3. Traffic control plan for the Craig and US95 site (CRAIG95).

A.1.4 GV215

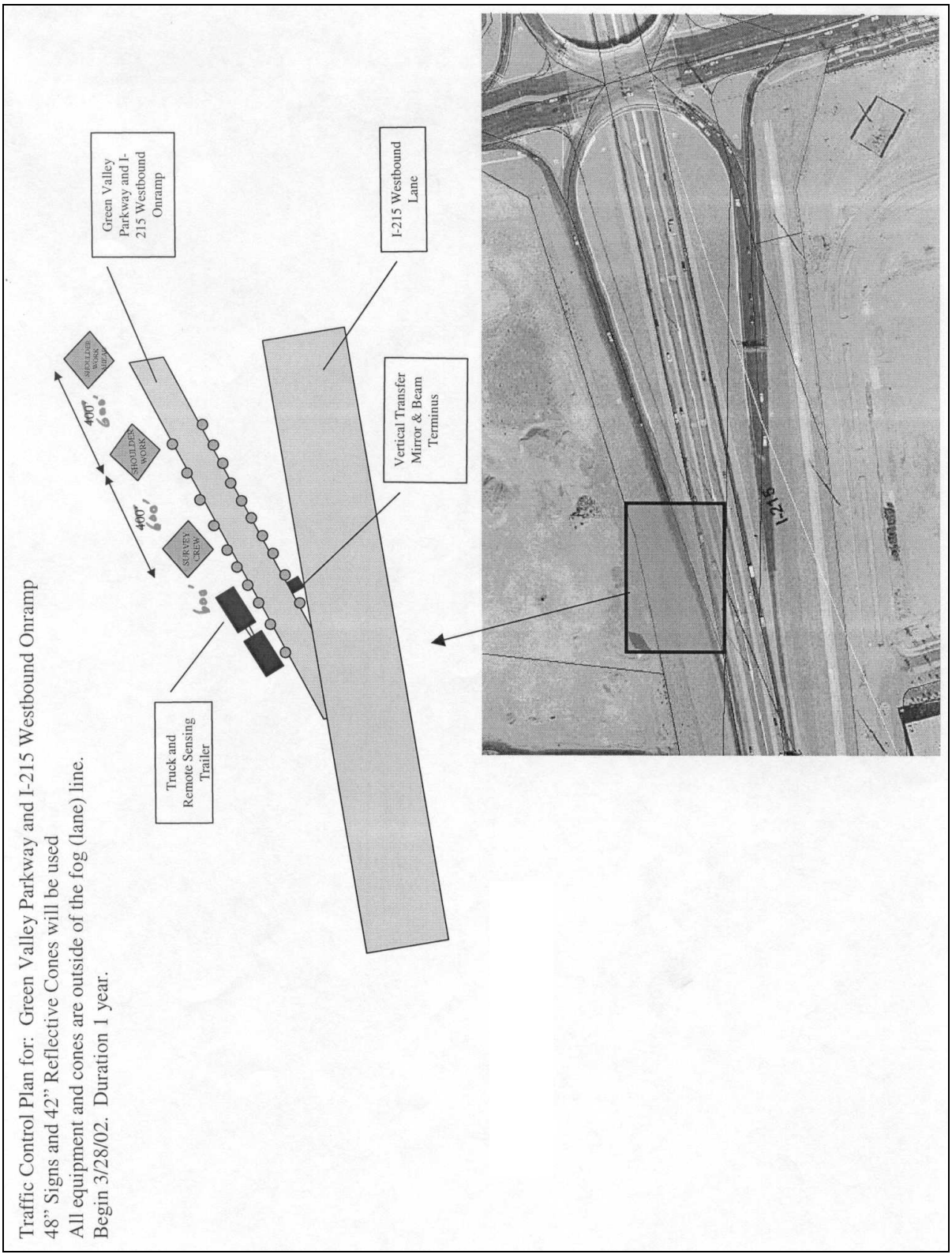

Figure A-4. Traffic control plan for the Green Valley and I215 (GV215).

A.1.5 CRAIGI15

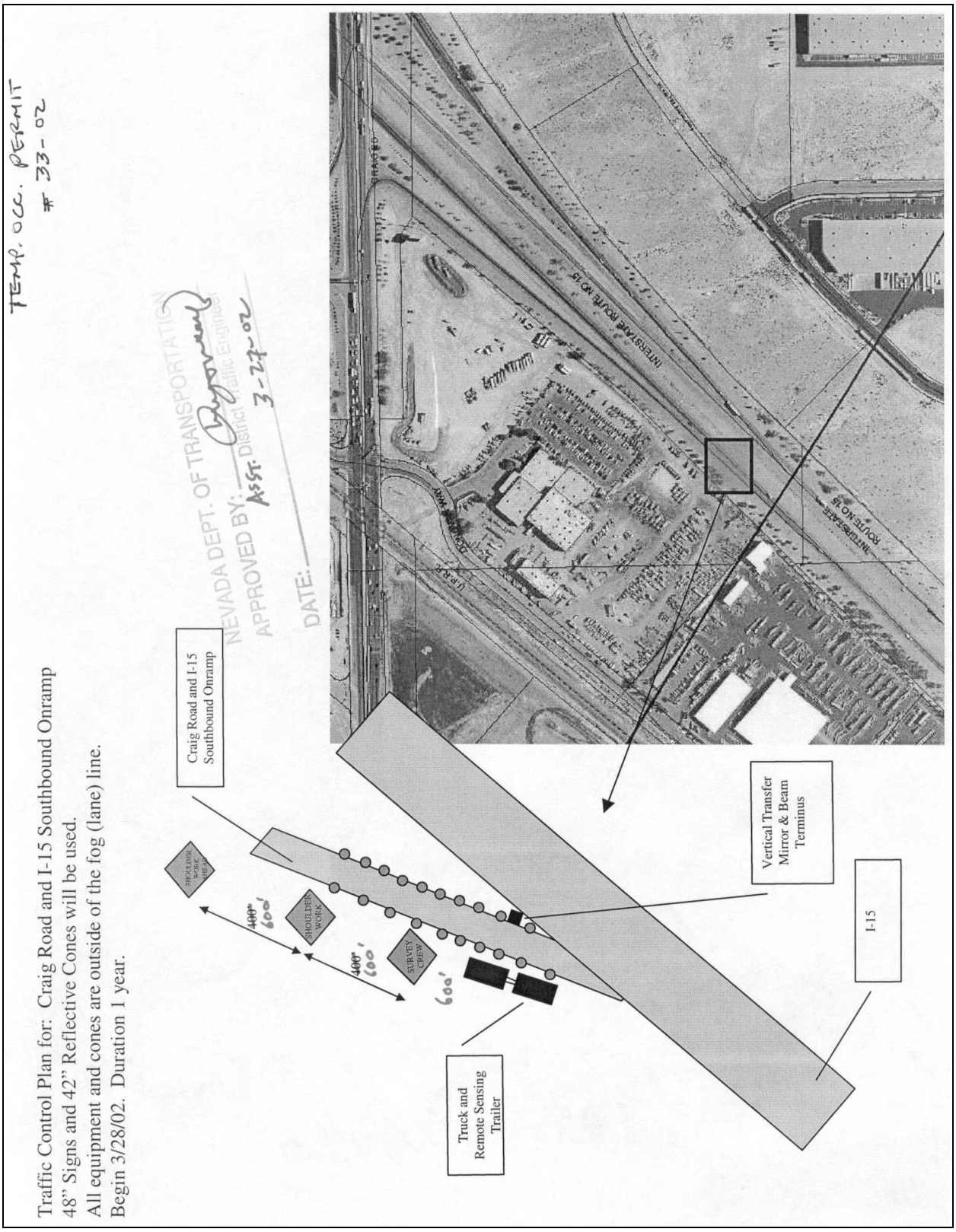

Figure A-5. Traffic control plan for the Craig and I15 (CRAIGI15).

A.1.6 SUMMRAM

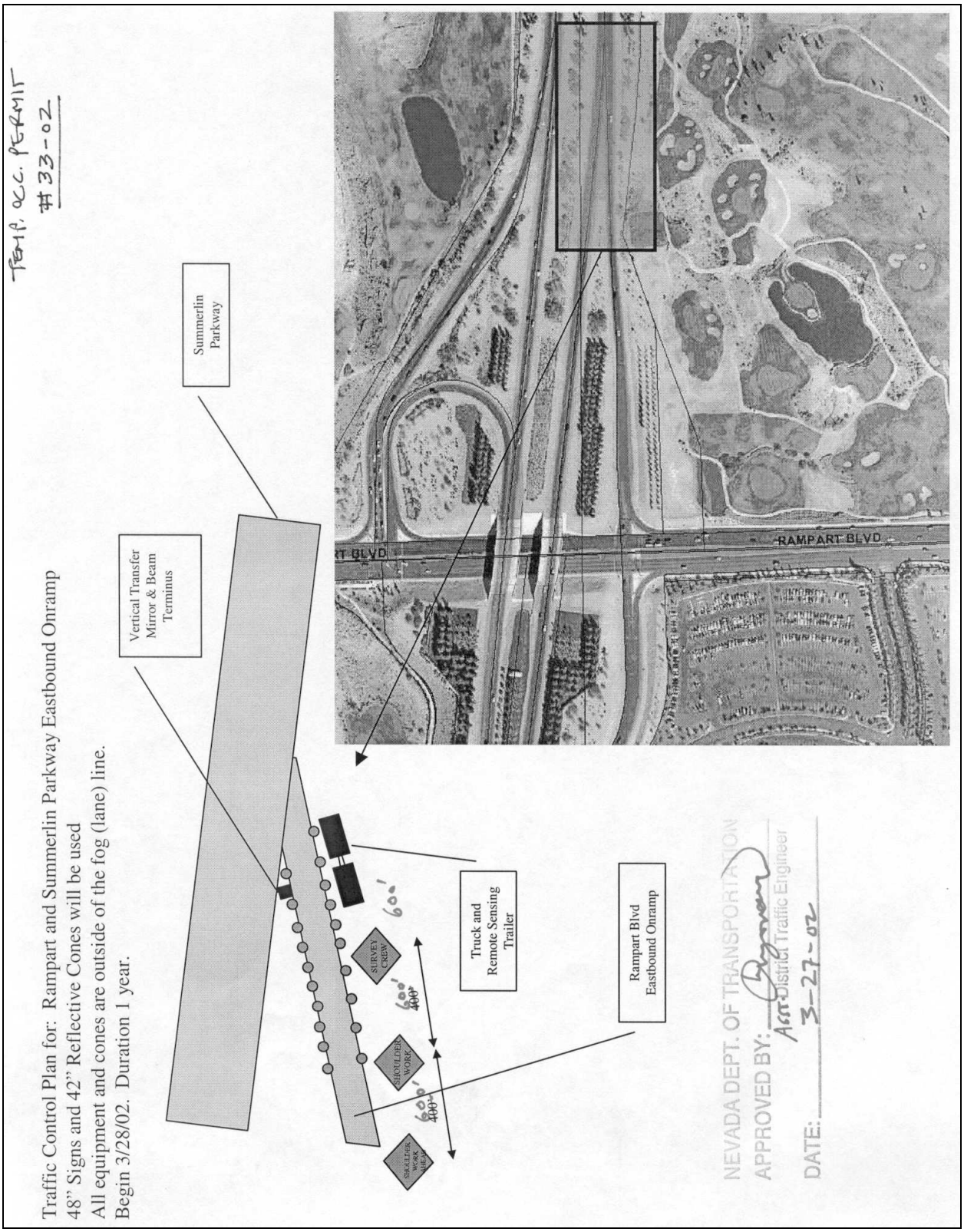

Figure A-6. Traffic control plan for the Summerlin Parkway and Rampart (CRAIGI15).

B. INSTRUCTIONS FOR MS ACCESS DATA PROCESSING TOOL

Lorax data processing begins with reading the ASCII files produced by the LORAX and RSD data acquisition systems into an Access database. Four database tables are constructed and populated by this process, LoraxFileNames, LoraxRawData, RSDVehicles, and RSDRawData. These tables reflect the input ASCII files with two exceptions.

1. Usually the first Lorax ambient data record has a time stamp of a few milliseconds, but occasionally ambient data immediately preceding a vehicle are not available. If the first ambient data record has a time stamp between 350 msecs and 10 mins., then all ambient records for that vehicle are flagged "Old ambient data" in the warning flag field. Any Lorax ambient data record with a time stamp of greater than 10 minutes is flagged "Bad ambient data" in the error flag field. Records flagged "Old ambient data" are used in subsequent data processing. Records flagged "Bad ambient data" are not used in subsequent data processing.
2. RSD ambient data records are subjected to a three-sigma filter to flag spikes caused by vehicle block. Flagged records are not used in subsequent data processing.

Raw data are read into the database by use of form ReadRawData.

The browse buttons are used to select Lorax and RSD data sets and processing is begun by use of the Go button. Text box Info is provided to track processing completion.

At the next stage LORAX VID's are matched with RSD VID's. This is accomplished, at present, through a graphical procedure. A plot of Lorax VID's and RSD VID's is presented and the operator populates a database table giving beginning and ending pairs of matching VID's. This database table is used in subsequent processing to match Lorax data to RSD data.

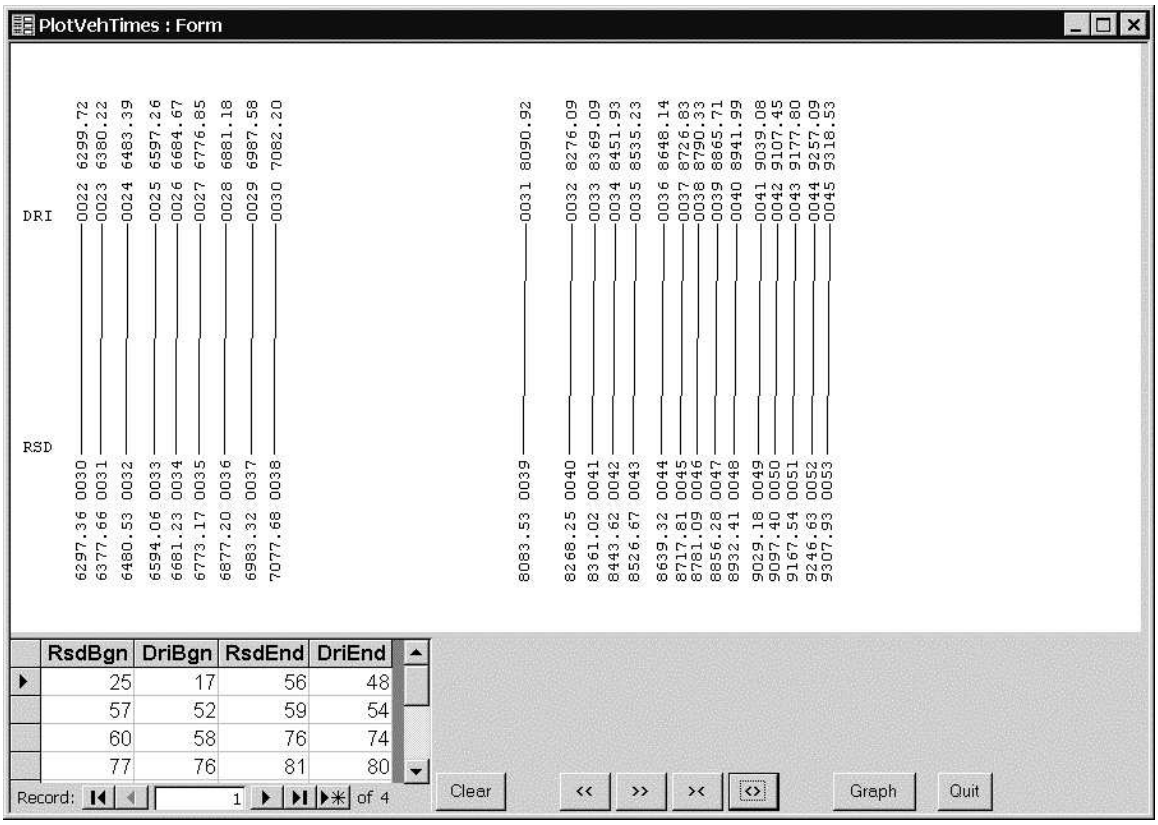

Improvements in matching vehicles during data acquisition will obviate the need for this step in future Lorax data processing.

The final stage of data processing is accomplished by use of form Results.

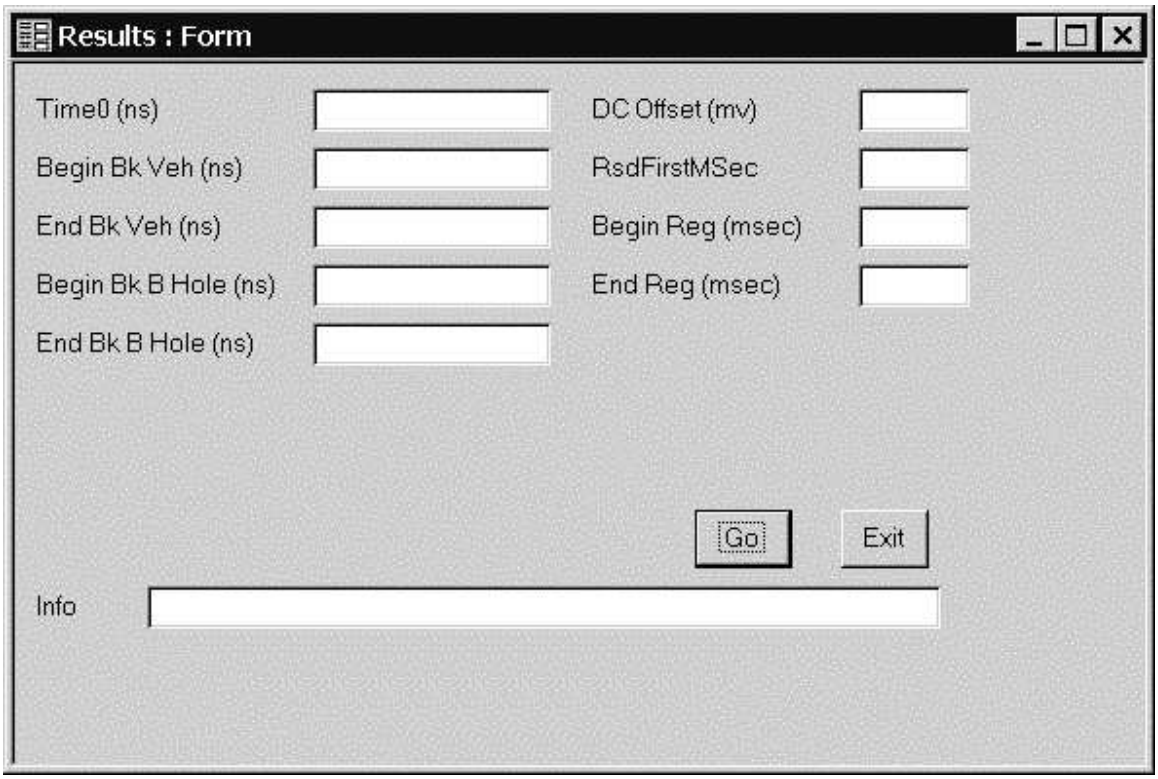

The input fields to form Results are:

Time0. Time, for each Lorax shot, is measured in nanoseconds. Time0 is the beginning time for which the range correction factors are applied.

BeginBkVeh. The beginning time in nanoseconds for the backscatter integral.

EndBkVeh. The end time in nanoseconds for the backscatter integral.

BeginBkBHole. The beginning time in nanoseconds for the black hole integral.

EndBkBHole. The end time in nanoseconds for the black hole integral.

DCOffset. The value in millivolts of the dc offset. A form, TraceAverage, is provided for estimating the dc offset. This is discussed further below.

RSDFirstMSec. Time for each vehicle data acquisition period is measured in milliseconds acquired from the Lorax ASCII files. RSDFirstMSec is the time in milliseconds to associate with the first RSD data record. This is a nominal value of 20 msecs.

BeginReg. Beginning time in milliseconds for the interval over which regression statistics are calculated.

EndReg. End time in milliseconds for the interval over which regression statistics are calculated.

After the input data boxes are filled, clicking on the Go button causes the following to happen.

1. Database table RsdShots is created and populated from the RSD data. This database table contains RSD shot data. It has one record per shot. Its fields are:

RsdShotsID	Record ID.
Msecs	Time in milliseconds of shot.
RsdFlag	Flag set by data processing. See RSD Flags table below.
CO2F	CO_2 flag read from RSD ASCII data file.
RefAmb	Average of ambient reference signal.
RSDVID	RSD VID.
PT_CO	Transmittance of CO plume capture.
PT_CO2	Transmittance of CO_2 plume capture.
PT_HC	Transmittance of HC plume capture.
PT_REF	Transmittance of reference plume capture.
Opc	Opacity.
CO	CO molecular density measure.
CO2	CO_2 molecular density measure.
HC	HC molecular density measure.
SMK	Smoke density.

The processing done in filling database table RsdShots is adapted from proprietary RSD software and will not be described. The data processing software follows the RSD software with the exception that only ambient data records passing the three-sigma filter test are used. Typically one or two records from the ambient data set of 20 records are dropped.

In database table RsdShots, transmittance of plume capture for CO_2 is defined for each shot as the ratio of CO_2 plume signal to the reference plume signal. Similar definitions hold for CO and HC. Transmittance of plume capture for the reference signal is defined for each shot as the ratio of the reference plume signal to the average ambient reference signal. Opacity is defined as one minus transmittance of reference plume capture. Smoke density is defined as the natural logarithm of one divided by the transmittance of reference plume capture. For transmittance of reference plume capture close to one, these two measures are approximately equal.

2. Database table LoraxShots is created and populated from the Lorax data. This database table contains Lorax shot integrals. It has one record per shot. Its fields are:

ShotsID	Record ID
LorRawID	Key into Lorax raw data database table.
DRIVID	Lorax VID.
ShotType	Flags shot type (0=ambient, 1=vehicle).
DatTim	Date and time associated with vehicle, excluding seconds.
Secs	Seconds associated with the DatTim field. Time is treated with two fields, because the built in database Date type does not treat fractions of a second.
Msecs	Time in milliseconds of shot
DriErrF	Lorax error flag set by software. See Lorax Error Flags table below.

DriWarnF	Lorax warning flag set by software. See Lorax Warning Flags table below.
TrFlag	Trace flag. This will be discussed subsequently.
TrAvg	Trace average. This will be discussed subsequently.
Bk	Back scatter integral.
Bh	Black hole integral.

Processing steps for populating database table LoraxShots follow.

1. Integrals are computed using the trapezoidal rule. Integrations are done on all Lorax data records. Error flags and/or warning flags set during the raw data processing are retained in database table LoraxShots. The integration limits used are those set in the Results form, and the DC offset is subtracted from data values before further processing.
2. Black hole integrals are computed first. Occasionally flat traces occur because of beam block. These are recognized by examining the black hole integral value. If the integral is over 20 nanosecond-millivolts the trace is accepted as valid and flag TrFlag is set to 0. If the integral is under 20 nanosecond-millivolts and all data points fall between 5 and –10 millivolts the trace is accepted as a valid flat trace and flag TrFlag is set to 1. Otherwise, flag TrFlag is set to 2. No range correction factors are applied to black hole integrals, and they are retained in database table LoraxShots with units of nanosecond-millivolts. Traces with TrFlag = 1 may be used to compute an average DC offset. Form TraceAverage, mentioned above, provides this capability.
3. For Lorax traces with TrFlag = 0, the back-scatter integral is calculated. Again, DC offset is first subtracted from each data value. At this point, however, for the back-scatter integral, range corrections are applied to each data point. Range corrections are needed because the signal strength depends not only on intensity of back scatter, but also on the geometry of the signal path, and the spread of the telescope field of view. The range corrected data points are then summed as part of the integration process. After integration and dividing out nanosecond units the result is back-scatter in units of Rayleighs. Back-scatter integrals are retained with these units in the database.
4. For all Lorax data records the average of all uncorrected data points is stored in field TrAvg.

3. Database table Results is created and populated for vehicle pairs. This database table contains the statistics calculated for data analysis, and the parameters used in the calculations. It has one record per matching vehicle pair. Its fields are:

ResID	Record ID.
DriErrF	Lorax error flag.
DriWarnF	Lorax warning flag.
RSDFlag	RSD Flag.

DRIVID	Lorax VID.
RSDVID	RSD VID.
DatTim	Date and time associated with vehicle, excluding seconds.
Secs	Seconds associated with the DatTim field. See discussion of database table Lorax Shots.
BkLeftB	Back-scatter integral left boundary in nanoseconds.
BkRightB	Back-scatter integral right boundary in nanoseconds.
BhLeftB	Black hole integral left boundary in nanoseconds.
BhRightB	Black hole integral right boundary in nanoseconds.
RegBegin	Beginning of interval (milliseconds) over which regression statistics are calculated.
RegEnd	End of interval (milliseconds) over which regression statistics are calculated.
TimeZero	Beginning of interval (nanoseconds) over which range correction factors are applied.
DCOff	DC offset.
RsdFirstMSec	Time in milliseconds associated with first RSD data record.
NumBkAmb	Number of valid ambient back-scatter data records. Valid records have fields DRIErrFlag and TrFlag in database table LoraxShots set to 0.
BkAmbAvg	Average of valid ambient back-scatter integrals.
NumBhAmb	Number of valid ambient black hole data records. Valid records have fields DRIErrFlag and TrFlag in database table LoraxShots set to 0.
BhAmbAvg	Average of valid ambient black hole integrals.
NumBkExh	Number of valid vehicle plume back-scatter data records. Valid records have fields DRIErrFlag and TrFlag in database table LoraxShots set to 0.
BkExhAvg	Average of valid vehicle plume back-scatter integrals.
NumBhExh	Number of valid vehicle plume black hole data records. Valid records have fields DRIErrFlag and TrFlag in database table LoraxShots set to 0.
BhExhAvg	Average of valid vehicle plume black hole integrals.
BkAmbCV	Coefficient of variation of valid ambient back-scatter integrals.
BkRatio	Ratio of valid vehicle plume back-scatter maximum to average of valid ambient back-scatter (BkAmbAvg).
CO2ExhAvg	Average CO2 for vehicle exhaust plume.
CO2ExhMax	Maximum CO2 for vehicle exhaust plume.
T_RefExhAvg	Average transmittance of reference exhaust plume capture. This is the average of PT_REF defined in the discussion of Database table RsdShots.
OpcExhAvg	Average opacity of exhaust plume.
OpcExhMax	Maximum opacity of exhaust plume.
SmkExhAvg	Average smoke density of exhaust plume.
SmkExhMax	Maximum smoke density of exhaust plume.
Bk_CO2Exh100	Ratio of average back-scatter minus ambient average to average CO2 for exhaust plume over all data points.
Bk_CO2Exh50	Ratio of average back-scatter minus ambient average to average CO2 for exhaust plume over data points lying within the middle 50% of the time period defined by the RSD data records.

Bk_CO2Exh20	Ratio of average back-scatter minus ambient average to average CO2 for exhaust plume over data points lying within the middle 20% of the time period defined by the RSD data records.
Bk_CO2ExhF40	Ratio of average back-scatter minus ambient average to average CO2 for exhaust plume over data points lying within the first 40% of the time period defined by the RSD data records.
Bk_CO2ExhL60	Ratio of average back-scatter minus ambient average to average CO2 for exhaust plume over data points lying within the last 60% of the time period defined by the RSD data records.
numBkCO2	Number of data points in back-scatter minus ambient average vs CO2 regression.
BkCO2M	Slope of back-scatter minus ambient average vs CO2 regression.
BkCO2B	Intercept of back-scatter minus ambient average vs CO2 regression.
BkCO2R	Correlation coefficient of back-scatter minus ambient average vs CO2 regression.
BkCO2R2	R-Square of back-scatter minus ambient average vs CO2 regression.
SE_BkCO2R	Standard error of residuals of back-scatter minus ambient average vs CO2 regression.
SE_BkCO2M	Standard error of slope of back-scatter minus ambient average vs CO2 regression.
SE_BkCO2B	Standard error of intercept of back-scatter minus ambient average vs CO2 regression.
numBkSmk	Number of data points in back-scatter minus ambient average vs smoke density regression.
BkSmkM	Slope of back-scatter minus ambient average vs smoke density regression.
BkSmkB	Intercept of back-scatter minus ambient average vs smoke density regression.
BkSmkR	Correlation coefficient of back-scatter minus ambient average vs smoke density regression.
BkSmkR2	R-Square of back-scatter minus ambient average vs smoke density regression.
SE_BkSmkR	Standard error of residuals of back-scatter minus ambient average vs smoke density regression.
SE_BkSmkM	Standard error of slope of back-scatter minus ambient average vs smoke density regression.
SE_BkSmkB	Standard error of intercept of back-scatter minus ambient average vs smoke density regression.
numSmCO2	Number of data points in smoke density vs CO2 regression.
SmCO2M	Slope of smoke density vs CO2 regression.
SmCO2B	Intercept of smoke density vs CO2 regression.
SmCO2R	Correlation coefficient of smoke density vs CO2 regression.
SmCO2R2	R-Square of smoke density vs CO2 regression.
SE_SmCO2R	Standard error of residuals of smoke density vs CO2 regression.
SE_SmCO2M	Standard error of slope of smoke density vs CO2 regression.
SE_SmCO2B	Standard error of intercept of smoke density vs CO2 regression.
numCOCO2	Number of data points in CO vs CO2 regression.

COCO2M	Slope of CO vs CO2 regression.
COCO2B	Intercept of CO vs CO2 regression.
COCO2R	Correlation coefficient of CO vs CO2 regression.
COCO2R2	R-square of CO vs CO2 regression.
SE_COCO2R	Standard error of residuals of CO vs CO2 regression.
SE_COCO2M	Standard error of slope of CO vs CO2 regression.
SE_CoCO2B	Standard error of intercept of CO vs CO2 regression.
numHCCO2	Number of data points in HC vs CO2 regression.
HCCO2M	Slope of HC vs CO2 regression.
HCCO2B	Intercept of HC vs CO2 regression.
HCCO2R	Correlation coefficient of HC vs CO2 regression.
HCCO2R2	R-square of HC vs CO2 regression.
SE_HCCO2R	Standard error of residuals of HC vs CO2 regression.
SE_HCCO2M	Standard error of slope of HC vs CO2 regression.
SE_HCCO2B	Standard error of intercept of HC vs CO2 regression.

Plotting routines

Several plotting routines are provided for data analysis. They are accessed through the following forms.

PlotData

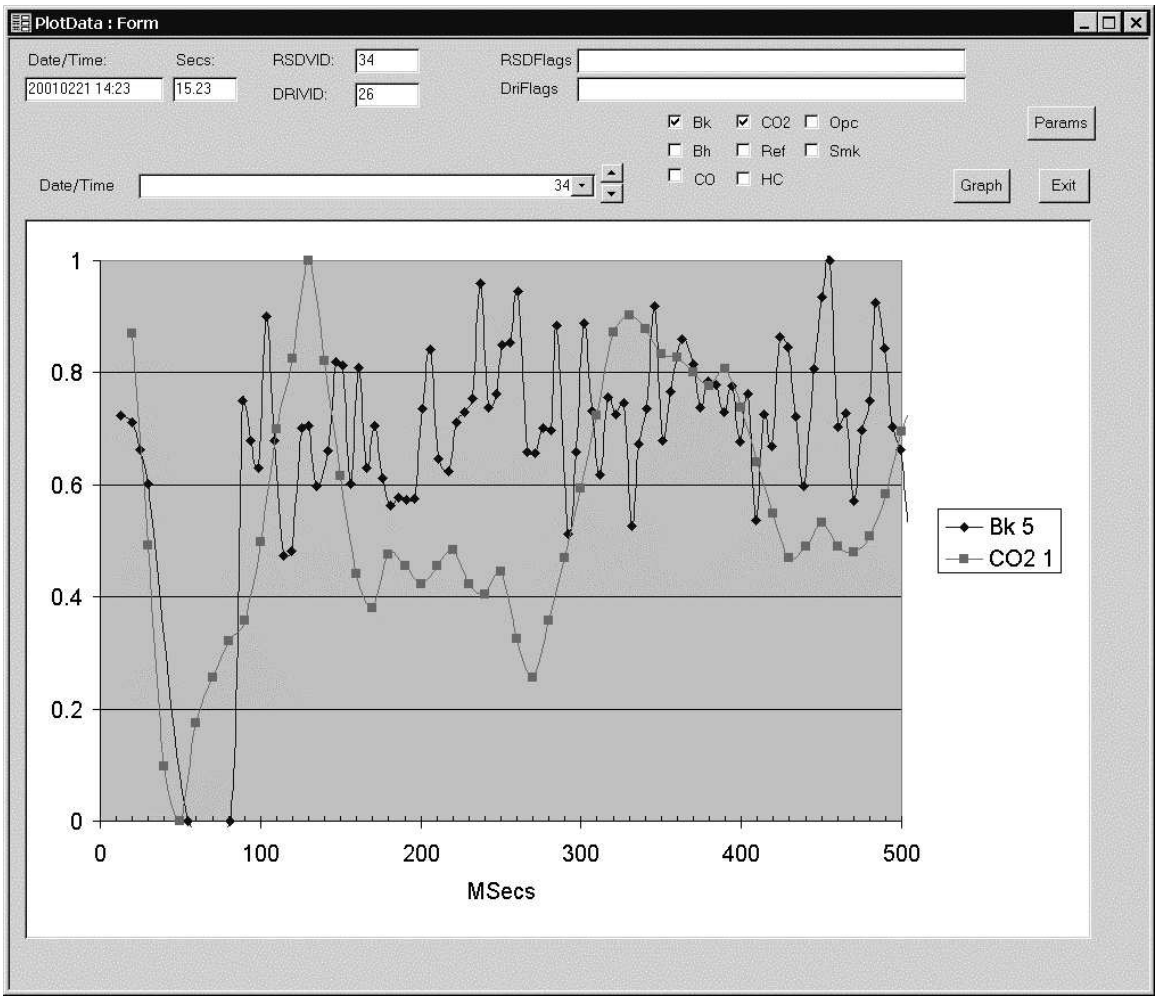

PlotData presents time series plots of any or all of plume back-scatter integrals minus average ambient back-scatter integrals (Bk), black hole integrals (Bh), CO, CO2, transmittance of reference plume capture (Ref), HC, opacity (Opc), and smoke density (Smk) for match vehicle pairs. Matched vehicle pairs are selected with the Date/Time combo box just above the graph, and parameters to be plotted are selected with the check boxes. Along with indicating the plotted parameters, the graph label box gives the scales of the plots. The other text boxes display information pertinent to the selected vehicle pair. The Graph button causes the plot to be drawn. Clicking the Params button brings up the parameters window.

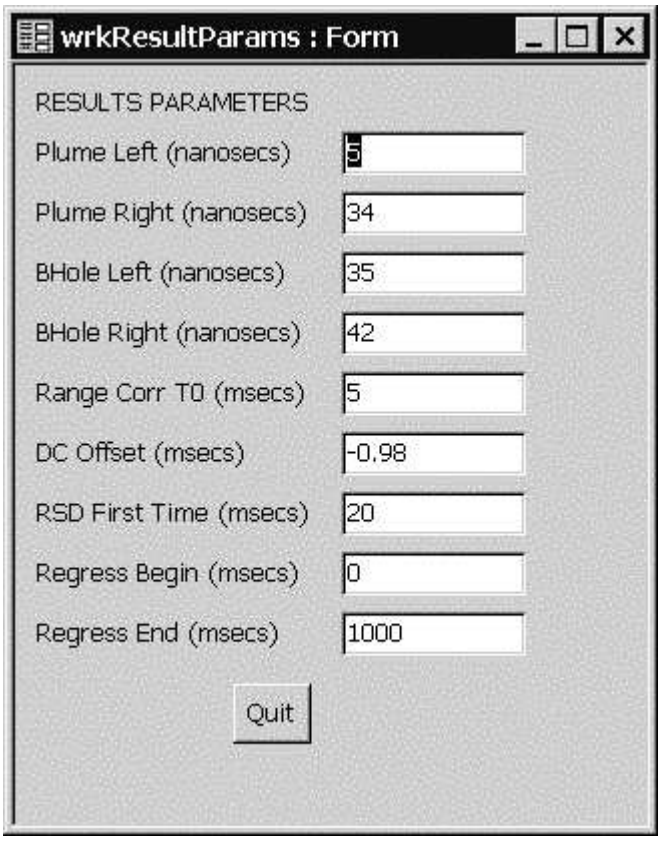

This form is preloaded with the parameter values read from the Results table. The plot, however, does not use the Results table, but performs calculations on the raw data using parameters specified in the parameters window. These may be changed prior to drawing the plot to study the effect of changing parameters on the calculated values.

PlotLoraxShots

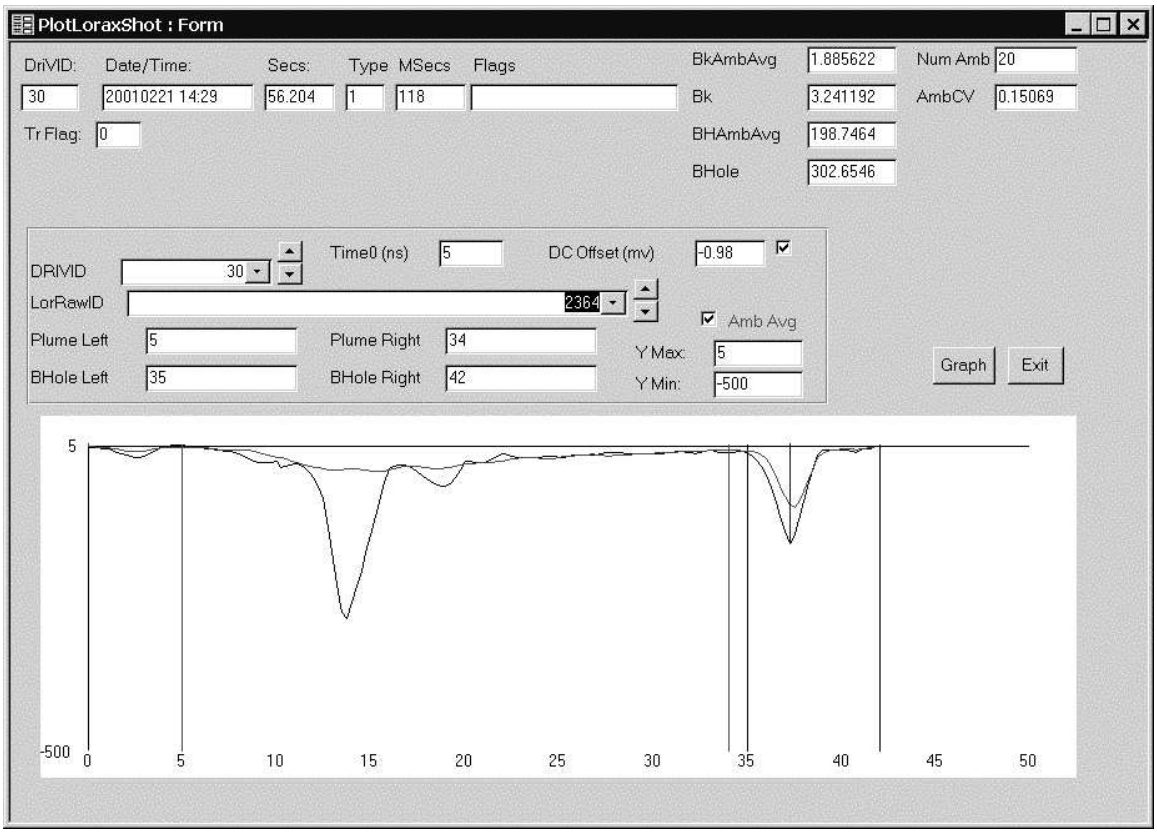

PlotLoraxShots plots individual LORAX shots. The panel box above the graph contains an input combo box, a check box, and several input text boxes. The shot to be plotted is selected by use of the combo box. Use of the DRIVID combo box plots the first shot for that VID. Integrals are calculated using values in the Plume and BHole text boxes, the Time0 text box, and the DC Offset text box. The boxes are preloaded with values taken from the Results table, but may be changed prior to ploting. Checking or unchecking the AmbAvg check box causes the ambient Bk average plot to be presented or hidden. Numerical results of the calculations are presented in the text boxes in the upper right of the form, and information pertinent to the particular shot is presented in the text boxes in the upper left of the form.

PlotRegress

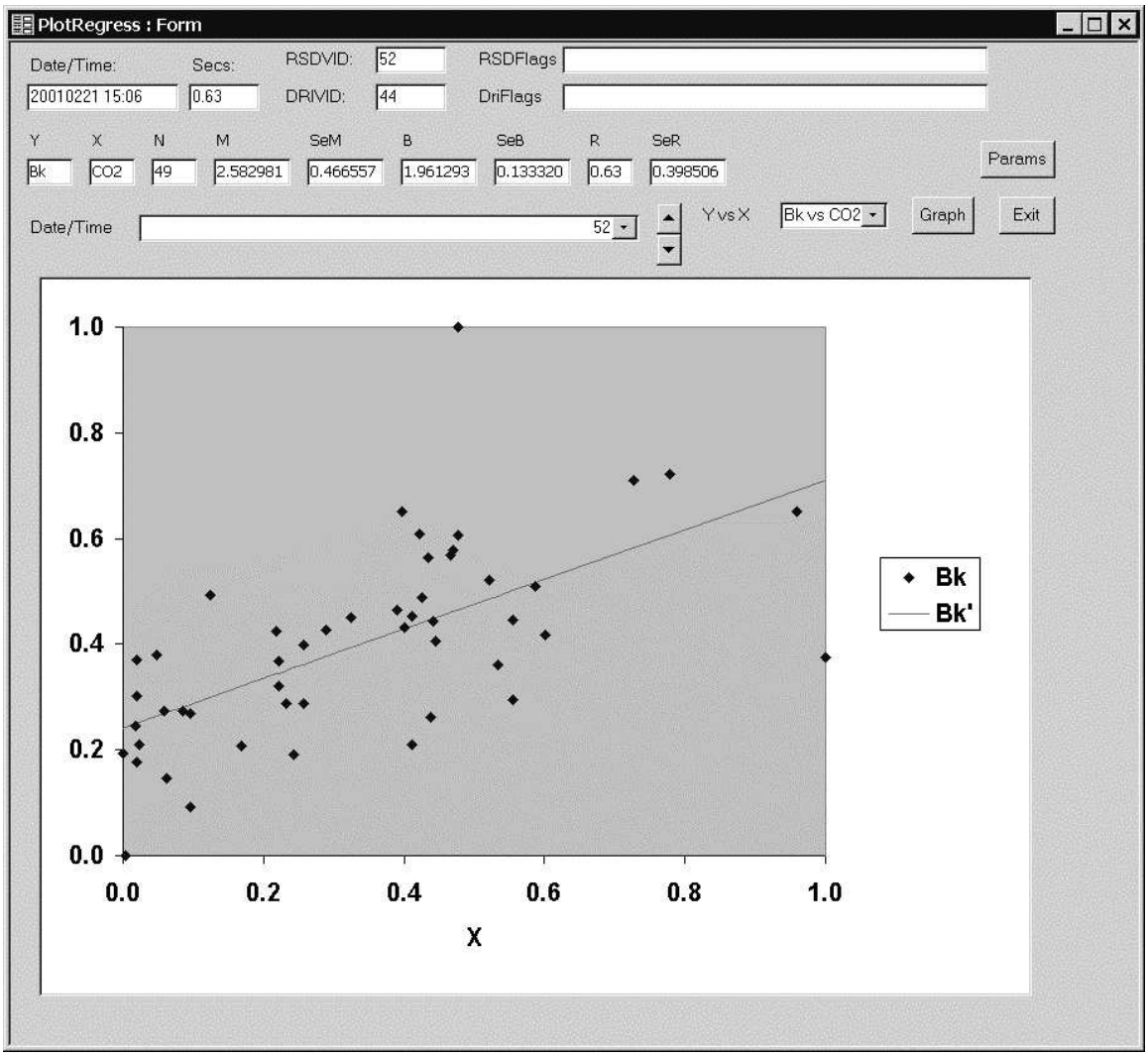

PlotRegress presents regression results for matched vehicle pairs. The vehicle pair is selected with the Date/Time combo box and the parameters to be regressed are selected in the Y vs X combo box.

Regression statistics are presented in the text boxes immediately above the Date/Time combo box, and information pertinent to the particular vehicle pair is presented in the text boxes in the upper left of the form. As in form PlotData, the plot presents the results of calculations done on data from the raw data tables using input parameters accessible from the parameters window.

Tables

RSD Flags

Flag	Meaning
1	Invalid or suspect data
2	Bad # of ambient records
3	Bad # of plume records
4	Bad ambient ref
5	Bad plume ref
6	Bad time sync VIDs
7	VID not found
8	Failed 3 sigma

Lorax Error Flags

Flag	Meaning
1	DRI VID not found
2	Bad Shot Data
3	Bad ambient data
4	Bad plume data
5	Maximum plume recs exceeded
6	Can't match VIDs
7	Too few regress pts
8	Regression failed
9	Bad data file
10	Bad black hole data

Lorax Warning Flags

Flag	Meaning
1	Old Ambient Data
2	Bad Ambient Data
3	Quadrature failed

C. CONVERSION OF EXHAUST CONTENT TO FUEL BASED EMISSIONS FACTOR

This derivation was prepared by Gary Bishop of the University of Denver in 2002.

FEAT Equations for CO, HC and NO.

ASSUMPTIONS:

Fuel C:H ratio is 2 and non-oxygenated.
Fuel density is 0.726 g/ml and is approximated with a mix of Octane and Benzene that averages the molecular formula of CH_2.
Fuel out tailpipe is similar (to make the math simpler we have chosen for the exhaust HC to be a multiple of the input HC) to calibration gas which is propane.
Concentrations are calculated on a dry basis and corrected for any excess air not involved in combustion (these equations are correct for diesel vehicles, and the ratios are correct for diesel vehicles. However, if remote sensing data are to be compared to a direct tailpipe measurement, that measurement comparison either must consider only the ratios, or must be corrected for the considerable excess oxygen not involved in typical diesel combustion).
Equal amount of seen HC's and unseen HC's in the exhaust (Singer & Harley et al, Environ. Sci Technol. 1998, 32, 3241-3248)

$$CH_2 + m(0.21O_2 + 0.79N_2) \rightarrow aCO + bH_2O + c(C_3H_6 + inv\ C_3H_6) + dCO_2 + eNO + (0.79m - \frac{e}{2})N_2$$

$$Q = \frac{CO}{CO_2} = \frac{a}{d} \qquad Q' = \frac{HC}{CO_2} = \frac{c}{d} \qquad Q'' = \frac{NO}{CO_2} = \frac{e}{d}$$

by Carbon balance : a + 6c + d = 1

by Hydrogen balance: 2b + 12c = 2

by Oxygen balance: a + b + 2d + e= 0.42m

Eliminate a: a = dQ and c = dQ'

a + 6c + d = 1; dQ + 6dQ' + d = 1

$$d = \frac{1}{Q + 6Q' + 1}$$

Eliminate b: 2b + 12dQ' = 2 ; b = 1 - 6dQ'

dQ + b + 2d + e= 0.42m; dQ + 1 - 6dQ' +2d + e= 0.42m

substituting d from above:

$$0.42\ \frac{m}{d} = Q+\frac{1}{d}-6Q'+2+Q'' = Q+Q+6Q'+1-6Q'+2+Q'' = 2Q+3+Q''$$

From the combustion equation the mole fraction of CO_2 is:

$$fCO_2 = \frac{d}{a + 2c + d + e + 0.79m - \frac{e}{2}}$$

divide numerator and denominator by d:

$$fCO_2 = \frac{1}{\frac{a}{d} + 2\frac{c}{d} + 1 + 0.5\frac{e}{d} + 0.79\frac{m}{d}}$$

substituting from above for a/d, c/d and e/d to get:

$$fCO_2 = \frac{1}{Q + 2Q' + 1 + 0.5Q'' + 0.79\frac{m}{d}}$$

multiply numerator and denominator by 0.42:

$$fCO_2 = \frac{0.42}{0.42Q + 0.84Q' + 0.42 + 0.21Q'' + (0.79)(0.42\frac{m}{d})}$$

substituting from above (0.42 m/d = 2Q + 3 + Q") leads to:

$$fCO_2 = \frac{0.42}{2.79 + 2Q + 0.84Q' + Q''}$$

from which follows:

$$\%CO_2 = \frac{42}{2.79 + 2Q + 0.84Q' + Q''} = \frac{100}{6.64 + 4.76Q + 2Q' + 2.38Q''}$$

$$\%CO = Q*\%CO_2 \qquad \%HC = Q'*\%CO_2 \qquad \%NO = Q''*\%CO_2$$

Some useful conversions are:

For grams/gallon assume fuel density of 726 g/l, a fuel carbon fraction of 86%, 3.79 l/gallon and for CO 28g/mole; for HC (propane, C_3H_8) 44g/mole for NO 30g/mole; for C 12g/mole:

$$\frac{gmCO}{gal} = \frac{28*Q*0.86*726*3.79}{(1+Q+6Q')*12}$$

$$\frac{gmHC}{gal} = \frac{2*44*Q'*0.86*726*3.79}{(1+Q+6Q')*12}$$

$$\frac{gmNO}{gal} = \frac{30*Q''*0.86*726*3.79}{(1+Q+6Q')*12}$$

We now prefer to use grams of pollutant/kg of fuel because it requires no assumption about the fuel density:

$$\frac{gmCO}{kg} = \frac{28*Q*860}{(1+Q+6Q')*12}$$

$$\frac{gmHC}{kg} = \frac{2*44*Q'*860}{(1+Q+6Q')*12}$$

$$\frac{gmNO}{kg} = \frac{30*Q''*860}{(1+Q+6Q')*12}$$

If you want to express the measured ratios in the units of other molecules, for example $gmNO_2/kg$ since all emitted NO will eventually oxidize in the atmosphere to NO_2, you only have to change the molecular weight of the species in the appropriate equation.

D. PART 5 MODEL OUTPUT (BY2002 CLARK COUNTY NV)

Veh. Type:	LDGV	LDGT1	LDGT2	HDGV	MC	LDDV	LDDT	2BHDDV	LHDDV	MHDDV	HHDDV	BUSES	All Veh.
Total Idle (g/hr) :	*	*	*	*	*	*	*	1.208	0.000	1.449	1.355	1.286	*
Gas. SO2: (g/mi) :	0.078	0.104	0.106	0.175	0.033	0.102	0.127	0.206	0.000	0.405	0.482	0.461	0.099

* Missing Data
User supplied veh miles traveled mixture , veh registration distributions.
Ramps :scene name
Particle Size Cutoff 10.00 Microns Altitude: 500. Ft. Driving: Transient RFG:No
Cal. Year: 2002 I/M Program: Yes Region: Low

Veh. Type:	LDGV	LDGT1	LDGT2	HDGV	MC	LDDV	LDDT	2BHDDV	LHDDV	MHDDV	HHDDV	BUSES	All Veh.
Veh. Speeds:	40.0	40.0	40.0	40.0	40.0	40.0	40.0	40.0	40.0	40.0	40.0	40.0	40.0
VMT Mix:	0.5450	0.3870	0.0250	0.0020	0.0030	0.0080	0.0010	0.0054	0.0000	0.0071	0.0154	0.0011	
Composite Emission Factors (g/mi)													
Lead:	0.000	0.000	0.000	0.000	0.000	0.000	0.000	0.000	0.000	0.000	0.000	0.000	0.000
SOF:	-	-	-	-	-	0.037	0.092	0.052	0.000	0.146	0.092	0.107	-
RCP:	-	-	-	-	-	0.131	0.064	0.050	0.000	0.186	0.292	0.136	-
Direct SO4:	0.008	0.012	0.011	0.011	0.001	0.005	0.007	0.014	0.000	0.028	0.034	0.032	0.010
Exhaust PM:	0.013	0.017	0.027	0.069	0.020	0.174	0.162	0.116	0.000	0.361	0.418	0.274	0.026
Indir. SO4:	0.023	0.030	0.030	0.050	0.009	0.029	0.036	0.059	0.000	0.117	0.139	0.133	0.028
Sulfate PM:	0.031	0.042	0.041	0.061	0.010	0.035	0.043	0.074	0.000	0.145	0.172	0.165	0.039
Brake:	0.013	0.013	0.013	0.013	0.013	0.013	0.013	0.013	0.000	0.013	0.013	0.013	0.013
Tire:	0.008	0.008	0.008	0.012	0.004	0.008	0.008	0.008	0.000	0.012	0.036	0.008	0.008
Total PM:	0.056	0.067	0.078	0.144	0.046	0.224	0.219	0.196	0.000	0.502	0.606	0.427	0.075

Fugitive Dust: Unpaved Roads Fleet Average 1600.14 g/mi (as calculated in AP42 Vol 1 9/88)*
Paved Roads Fleet Average 4.22 g/mi (as calculated in draft AP42 Vol 1 3/93)*
Unpaved Roads Fleet Average 1599.94 g/mi (as calculated in AP42 Vol 1 9/88, minus tailpipe and tire-wear emissions)**
Paved Roads Fleet Average 4.01 g/mi (as calculated in draft AP42 Vol 1 3/93, minus tailpipe and tire-wear emissions)**

* Includes fleet average tailpipe, tire-wear and brake-wear emissions.
** Includes fleet average brake-wear emissions.

Paved Road Silt: 0.86 (g/m^2) Fleet average vehicle weight: 6000
Unpaved Silt: 16.0% Fleet average number of wheels: 4
Precipitation Days: 24 >0.01 in. (per year)